이학박사 학위논문

효소 활성 측정과 생물 영상화를 위한 반응기반 탐침의 개발

Reaction-based probe for enzyme activity assay and bioimaging

2017 년 8 월

서울대학교 대학원

화학부 유기화학전공

윤 혜 영

효소 활성 측정과 생물 영상화를 위한 반응기반 탐침의 개발

Reaction-based probe for enzyme activity assay and bioimaging

지도 교수 홍 종 인

이 논문을 이학박사 학위논문으로 제출함

2017 년 8 월

서울대학교 대학원

화학부 유기화학전공

윤 혜 영

윤혜영의 이학박사 학위논문을 인준함

2017 년 8 월

위 원 장 _____ (인)

부위원장 _____ (인)

위 원 _____ (인)

위 원 _____ (인)

위 원 _____ (인)

Abstract

Reaction-based probe for enzyme activity assay and bioimaging

Hey Young Yoon

Major in Organic Chemistry

Department of Chemistry

Graduate School

Seoul National University

The detection of enzyme activity provides many clues to the nature of living systems and the interaction between biomolecules. Enzyme reaction triggers chemical transformation of substrate to regulate its function relating to many biological events. The most general approach for enzyme activity assay is a reaction-based strategy using the chemical transformation of substrates. Numerous probes have been developed based on the enzymatic reaction. However, only a few strategies to control a signal have been developed, and most of them have not been applied practically. Herein, several probes based on two basic strategies are proposed.

The chemical transformation of a probe by enzymatic reaction triggers intramolecular cyclization to form fluorescent N-methylisoindole, which is a basic strategy to detect the enzyme activity.

Sulfatases catalyze the hydrolysis of sulfate esters that are present in a range of biomolecules. We have developed a new activity-based sulfatase probe (probe 1) that generates a fluorescent N-methylisoindole upon hydrolysis by sulfatase. Because of the autoxidation of N-methylisoindole, the sulfatase activity was also tested under reducing conditions containing either glutathione (GSH) or tris(2-carboxyethyl)phosphine (TCEP), which exhibited little change in the kinetic parameters, but a stronger emission than non-reducing conditions. Probe 1 also showed stronger intensity upon treatment with sulfatase under neutral conditions than acidic conditions, but it still has limitations in the selectivity of a specific sulfatase. Nevertheless, the fluorescent signal of the released N-methylisoindole provides a new assay for measuring sulfatase activity that could be applied for high-throughput screening (HTS).

Bacterial arylsulfatases are crucial to biosynthesis in many microorganisms, as they cleave aromatic sulfate esters for use as a sulfur source. They are associated with pathogenesis and are applied in many areas, such as industry and agriculture. The hydrolysis of probe 1 by sulfatases induced fluorescence intensity enhancement and the generation of colored precipitates through the polymerization of N-methylisoindole, which enabled the monitoring of bacterial arylsulfatase activity and the discrimination of periplasmic sulfatases from cytosolic sulfatases through liquid- and solid-phase colony-based assays.

For imaging analysis, the fluorescence of N-methylisoindole, the product of

probe 1 from the cleavage upon sulfatase activity emitted a signal at the shorter wavelength. To overcome this limitation, fluorescence resonance energy transfer (FRET), aggregation-induced emission (AIE), and the excimer formation process were introduced. The FRET-based probe showed no fluorescence changes upon the treatment of sulfatase because the distance between N-methylisoindole and naphthalimide, an FRET acceptor, was 6.6 Å, which was out of range of the Förster distance. The AIE-based probe exhibited decreasing fluorescence and color changes, meaning that N-methylisoindole generation and polymerization did not intensify the AIE process. The excimer formation-based probe showed decreasing excimer emission, but increasing monomer and N-methylisoindole emissions. It also generated colored precipitates. When the probe was applied to bacteria species, the tendency of the emission was different from that in the results of the test in the homogenous condition, but precipitates were still formed. Thus, the excimer formation-based probe was only applicable to staining periplasmic sulfatase-expressing bacteria.

The next strategy to design a probe was based on intramolecular charge transfer (ICT). The basic scaffold was 2-dicyanomethylene-3-cyano-2,5-dihydrofuran (DCDHF) unit conjugated to a modified electron-donating group.

Leucine aminopeptidases (LAPs) are widely distributed in organisms, from bacteria to humans, and play crucial roles in cell maintenance and growth. Thus, assays for LAP are necessary for measuring its activity and inhibitor potency. In this paper, we report a small-molecule probe, DCDHF conjugated to a leucine residue, which exhibits colorimetric and fluorogenic changes according to LAP activity.

Human steroid sulfatase (STS) plays a pivotal role in the regulation of biologically active steroid to bind to the estrogen receptor (ER), which is related to hormone-dependent diseases. DCDHF conjugated with phenyl sulfate ester exhibits pH-dependent emission, which was appropriate for discriminating STS, whose optimal pH is 7; other arylsulfatases usually exhibit the maximal activity at pH 5. DCDHF conjugated with phenyl sulfate interposing a self-immolative spacer between them is a ratiometric probe that could detect and monitor sulfatase activity in a complex cellular context.

Keywords: bioimaging, reaction-based probe, fluorescence, optical properties enzyme activity assay, spectral responses

Table of Contents

Abstract i

Table of Contents v

I. Introduction

1. Enzyme activity assays 2

2. Bioimaging 9

3. Fluorescent probe for detecting enzyme activity 16

4. Design strategy of fluorescent probe 21

II. Probes inducing signal changes by intramolecular cyclization upon the treatment of enzyme

1. Sulfatase activated probe generating N-methyl isoindole in buffer containing reducing agents

1.1. Introduction 36

1.2. Results and Discussion 38

1.3. Experiments 44

2. Detection of bacterial sulfatase activity and discrimination of periplasmic sulfatase activity through liquid- and solid-phase colony-based assays

2.1. Introduction 60

2.2. Results and Discussion 64

2.3. Experiments 75

3. Efforts for improvement of probe 1 using diverse signal generation strategies

3.1. Introduction 87

3.2. Results and Discussion 90

3.3. Experiments 98

III. Probes inducing fluorescence changes by intramolecular charge transfer process upon the treatment of enzyme

1. Small-molecule probe using dual signals to monitor leucine aminopeptidase activity

1.1. Introduction 118

1.2. Results and Discussion 119

1.3. Experiments 125

2. Selectvie detection of Steroide sulfatase (STS) and ratiometric detection of sulfatase activity in living cells

1.1. Introduction 132

1.2. Results and Discussion 135

1.3. Experiments 145

References 156

국문 초록 (Abstract in Korean) 174

I.

Introduction

1. Enzyme activity assays

To understand the nature of living systems composed of complex interactions with diverse cellular components, such as biopolymers, ions, and metabolites, each function of the components should be clarified preferentially. Bioassays, which are defined as “an analytical procedure measuring a biological activity of a test substance based on a specific, functional, biological response of a test system,” have contributed to the elucidation of the characteristics and functions of biomolecules [1]. In particular, enzyme assays have contributed to the analysis and understanding of enzyme reaction mechanisms and the chemical properties of substrates and products. Enzyme assays are based on the interactions of enzymes and their substrates, which enable the detection of enzyme activity and generation of “fingerprint” profiles of enzymes based upon their substrate preference. Such analysis clarifies the types of chemical compounds as the potential substrates of the enzyme to understand its catalytic mechanism and properties. In contrast, a generated reaction pattern of unknown enzymes with a set of various substrates may possibly reveal their identity. Additionally, enzyme assays are indispensable tools for the research of biological processes and useful for medical diagnosis and the development of potential inhibitors. In a biological context, enzymes specifically and greatly enhance the chemical transformation rate of biomolecules during biosynthesis, modification, and degradation [2], and enzyme specificity for a substrate is essential for maintaining most cellular processes; thus, enzymes can act as a disease marker and drug target. Insights into the substrate preference of an enzyme under different assay conditions could identify physiological substrates to help in the dissection of complex biological pathways and provide valuable information in the design of potent, selective

inhibitors.

Enzyme assays play a central role in the context of microbial screening and directed evolution experiments [3]. Microbial enzymes are very meaningful in microbial pathogenesis research and many industries, such as biocatalysts. Some microbial enzymes, including hyaluronidase and phospholipase, are reported to have a relationship with bacterial pathogenicity, and bacterial peroxidase and cellulase have been used in waste treatments, textiles, and the detergency industry [4, 5]. Microorganisms are a source of enzymes because they can be cultured in large quantities in a short time for bulk production [6]. In addition, the directed evolution of enzymes to change or reinforce their properties in a targeted manner has rapidly become established as a powerful strategy. For medicinal and industrial purposes, methods for screening or selecting variants of interest that possess the desired characteristics are significant. The methods should show a significant catalysis signal, which will be the criteria to determine the selection and isolation of microbial colonies with desirable catalytic properties.

To measure an enzyme's catalytic activity, it is essential to identify the chemical changes of substrates to form products. The incredible variety of enzymes can be typically classified according to the types of chemical reactions they catalyze (e.g., oxidation-reduction, group transfers, elimination, isomerizations, rearrangements) Furthermore, the same types of reactions are mechanistically similar even though their substrates are small molecules, proteins, or nucleic acids. In any case, the enzymatic assay is designed based on distinguishing a given substrate and a given product in a quantifiable manner.

HTS is typically defined as a process to identify the compounds in a large set that have desired biological activity for validation in biological or pharmacological research. Ultimately, the goal of HTS is to generate chemical structures that will contribute to drug discovery and development based on a therapeutics setting or that will be used as probes to address biological questions in basic research [7]. As well as the pharmaceutical industry, HTS is applied in many areas, including the discovery of biopharmaceuticals, catalysts, plant science, pesticide research, cosmetics, and toxicity. The basic premise of screening is that biological assays should be performed with simple and optimized techniques that are effective, for which the results will be biologically relevant [8]. Moreover, the HTS assay protocol should be sufficiently sensitive to be able to identify candidates with low potency and efficiency. The reproducibility and stability of the biological response, which reduces false positive signals, are required. Economic feasibility should also be considered [9].

Enzyme assays are based on enzyme-catalyzed chemical transformations that are advantageous in terms of sensitivity and very important for HTS. The screening of enzymes on the basis of their catalytic activities allows for intrinsic signal amplification due to multiple turnovers of enzymes, leading to extremely high detection sensitivity. Numerous ways to detect the conversion of a substrate into a product with an observable signal have been developed. Enzyme activity might lead to thermal changes, an insoluble polymer product, or turnover using standard analytical methods, such as chromatography (affinity chromatography, GC, or HPLC), mass spectrometry, radioligand assays, or spectroscopic techniques.

According to the manual for the quenching steps of enzyme reactions, various assay strategies are able to distinguish discontinuous and continuous assay methods. Discontinuous assays involve a step to manually stop and quench the enzymatic reaction at different times. The stopped and quenched sample separates the products from the substrate to measure the concentration changes of the substrate or products. These methods are valuable when a given substrate–product pair exhibits either similar or no spectroscopic properties. In these procedures, to determine the initial velocity of the enzyme reaction, the reaction at designated time points should be efficiently stopped or quenched and a large amount of untreated substrate should be separated from a very small amount of formed product and measured by HPLC, MS, or radiometric analysis [2]. HPLC or radiometric analysis provide the highest degree of sensitivity, as well as exhibit a degree of broad-scale utility. Nonetheless, most discontinuous methods only serve as endpoint probes, but laborious steps are inappropriate in HTS; in particular, radioactive techniques need a long exposure time and have waste disposal and safety issues.

Continuous assays are defined as continuously monitoring either the disappearance or appearance of a given substrate or product, and they often use spectroscopic techniques, such as ultraviolet-visible absorption and fluorescence emission. Ultraviolet-visible absorption and fluorescence spectroscopies are convenient for continuous monitoring and accurate with respect to determining concentration changes. Additionally, fluorescence spectroscopy is more sensitive than UV/Vis absorption in most cases.

Because of their operational simplicity, reliability, and greater sensitivity for low enzyme turnover reactions, colorimetric and fluorometric assay methods

are the largest group of enzyme assays. The simplest approach relies on the designed chromogenic or fluorogenic substrates to induce spectral responses through specific enzymatic reactions. The most common chromogenic and fluorogenic substrates for assaying hydrolase activity are *p*-nitrophenyl and 7-hydroxylcoumarin derivatives (Fig. 1a and 1b). In each case, these substrates mimic the natural substrate of the hydrolase by linking p-nitrophenyl or 7-hydroxycoumarin at the cleavage site of the substrates. Other common chromogenic substrates are resorufin or 1-naphtol derivatives. Resorufin analogs have been previously used to spectrophotometrically monitor the activity of enzymes, including galactosidase, lipase, protease, and glucuronidase, and are particularly useful for detecting activity at low enzyme concentrations due to their intense fluorescence (Fig. 1c). Naphthol derivatives are used for the activity staining of gels. Hydrolysis yields 1-naphthol, which reacts with a diazo compound to yield a red-brown insoluble precipitate (Fig. 1d).

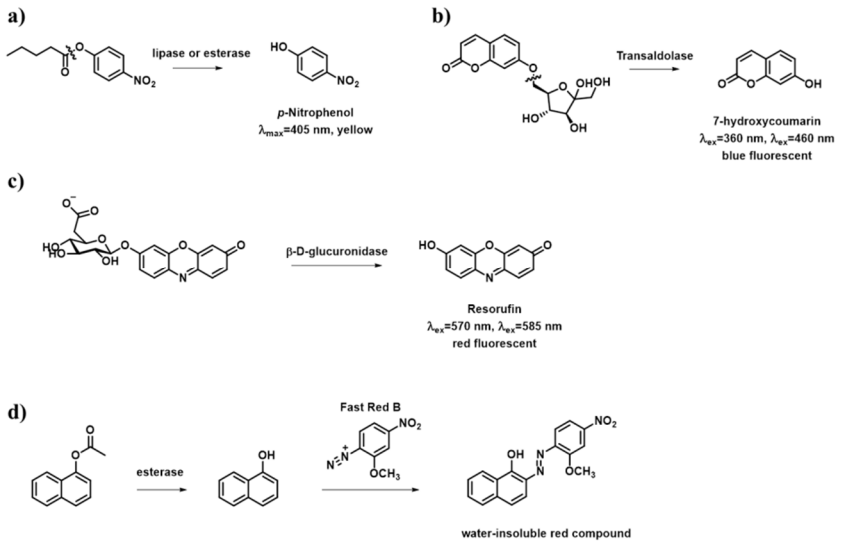

Figure **1.** Examples of chromogenic and fluorogenic probes [3, 10].

UV/Vis-based assays are able to visualize prescreening for enzyme activity on microtiter plates. Fluorescence-based assays have a high degree of sensitivity, which allows the use of very dilute substrate concentrations and extremely small amounts of catalysts. Moreover, these spectral assays can be used for the real-time monitoring of enzyme activity by providing a direct correlation between enzyme activity and the signal. However, chromogenic and fluorogenic substrates are limited by the needs of built-in chromophores and fluorophores to mimic the true substrate of interest and it is never certain whether the true substrates will behave the same way as the chromogenic and fluorogenic mimics. Nevertheless, spectral-based methods provide a high signal-to-noise ratio and are compatible with standard microarray scanners. Thus, UV/Vis absorption and fluorescence spectroscopies are most suitable for use in high-throughput platforms utilized for screening very large numbers of compounds for effects on enzyme activity [2, 10].

Historically, screening assays have been usually performed on purified proteins involving receptors and enzymes. Recently, the target sets have been spread out on cell-based or organism-based high-content screening (HCS), which analyzes biological events at a subcellular resolution [7, 11]. According to the target sets, three types of assays are available. One is a protein-based assay that utilizes the radioligand, affinity selection chromatography, mass spectroscopy, and optical techniques to detect protein–small-molecule interactions. This type of assay is often direct and specific to the target of interest with less variability due to the homogeneous nature of a reaction and might not elicit the same response in a cellular context because of membrane permeability, off-target effects, and cytotoxicity, among others. Cell-based assays containing enzyme-linked immunosorbent assay and expression

reporter gene assays to monitor cellular response, such as the translational level, are usually combined with optical readout. These are able to examine entire pathways of interest and select compounds showing desirable activity in cellular environments. Organism-based assays to monitor phenotypic changes generally use fluorescence imaging techniques [7, 11].

Unicellular organisms, such as yeast and bacteria, are readily adapted to microbial assays and HTS. The development of novel analytical tools and protocols for finding desirable microbial strains and allowing the high-throughput assessment of variants is an active research area. Random screening is used to examine each variant of the library to check for a particular characteristic without any prior evaluation of the library. It is necessary to subject the picked clones from an agar plate to analysis via liquid chromatography/mass spectrometry (LC/MS) or gas chromatography/mass spectrometry (GC/MS). This type of test is a laborious process and severely limits the size of libraries that can be practically screened [3]. In contrast, facilitated screening significantly reduces the candidates to be screened through colorimetric or fluorescent changes of desired characteristics. Facilitates screening of colonies on agar plates or microplates is most effectively and reasonably high throughput, allowing several hundred thousand clones to be screened and an individual microbe containing active enzyme or enzyme-producing genes to be picked manually from agar or microtiter plates or the use of fluorescence-activated cell sorting. Industries are looking for new microbial strains to produce different enzymes to fulfill the current enzyme requirements.

In contrast to unicellular organisms, multicellular organisms have more

complex biological networks with intact cell–cell interactions and multidimensional tissue organization. Thus, organism-based assays can provide an additional level of physiological relevance beyond that of cell-based assays, but their adaption to HTS is still challengeable. These cell-based and organism-based high-content screenings can detect multiple phenotypic responses, such as translocation, reporter internalization, intracellular trafficking, neurite outgrowth, and toxicity, using microscopes. Low-resolution microscopy can visualize and analyze a cell population that has desirable activity, whereas high-resolution analysis of a single cell can visualize cellular structures and intracellular translocations. In addition, improved highly sensitive detection and imaging methods allow real-time analysis of the HCS assay.

As a result, the improvement of various assay methods and cell-imaging technologies are rapidly expanding into research on cell content and the characterization of cell behavior for understanding aspects of cells, such as physiological state, differentiation, disease, and metabolism.

2. Bioimaging

After the completion of several genome sequences, one of the great challenges is to identify the biological significance of intracellular molecules directly in living systems. Then, the identified molecular function of proteins or cellular regulating molecules must be clarified in biological systems and in the development of disease. Through molecular imaging, many biological processes at the cellular and molecular level can be observed and the

spatiotemporal distribution of molecular or cellular processes can be monitored, as well. The information from molecular imaging can potentially facilitate the discovery of informative biomarkers that can be used for the earliest detection of disease and the creation of new classes of drugs directed at new therapeutic targets.

Our understanding of biological systems is increasingly dependent on our ability to visualize and quantify signaling molecules and events with high spatial and temporal resolution in the cellular context. Historically, imaging methods have largely relied on imaging gross anatomy, and diseases or treatment effects were mostly detected as structural abnormalities.

The conventional imaging methods are magnetic resonance imaging (MRI), nuclear imaging, and X-ray computed tomography (CT), and optical methods have been used recently.

MRI is an imaging technique that exploits the spin properties of the water proton (^{1}H) usually being ubiquitous in the body in a magnetic field to obtain information on its location in three-dimensional space. A contrast agent, such as Gd^{3+} chelates and iron oxide nanoparticles, can increase or decrease the signal by influencing the relaxation time of surrounding water protons, and this can provide increased or decreased image intensity at the agent accumulation site [12]. MRI probes where the contrast agents are conjugated to targeting ligands can provide a selective image of target receptors, but the sensitivity of contrast MR imaging is usually low and a millimolar concentration range of the contrast agent is typically required.

Nuclear imaging, including single-photon emission tomography (SPET) and

positron emission tomography (PET), is based on the detection of the decay of radioactive isotopes contained in probes that are able to administer to the target [13]. SPECT uses ^{123}I and ^{99m}Tc as nuclides considered to have a longer half-life than PET isotopes, ^{18}F, ^{11}C, and ^{124}I, which allows for a longer radiosynthesis time, thus making them more practical. In contrast, the short half-life of PET isotopes limits the availability of PET imaging, which often requires an on-site cyclotron. Compared with MR imaging, nuclear imaging offers both high sensitivity and tomographic capability, but has poor spatial resolution (1–2 mm) [14]. However, the contrast agents used in MRI and radioactive isotopes in PET continuously emit signals and are thus "always on" [15]. Because the "always-on" probes always emit signals regardless of their proximity to or interaction with target tissues or cells, they are limited to investigating structural abnormalities, and the background signal should be considered. To investigate biological events or the functions of biomolecules beyond structural abnormalities, molecular imaging probes need to emit signals with a high target-to-background ratio (TBR). For the improvement of the TBR, which means improving the sensitivity and specificity for the detection of diseases with imaging, molecular imaging probes must be designed to maximize the signal from the target and minimize the signal from the background [16]. Recently, molecular probes introducing signal off-on or ratiometric signal changes by biomolecules have been advanced to improve TBRs. The activatable probes emit a signal through conformational changes after target binding, acidification, enzymatic reactions, or chemical reactions with metal, reactive oxygene species (ROS), and reactive nitrogene species (RNS).

Optical imaging with fluorescent probes is a relatively new medical imaging

technique [17]. High-resolution light imaging devices at reasonable cost and high sensitivities with real-time capabilities are the advantages of optical imaging and have led to widespread luminescence imaging analytical techniques. Low-resolution microscopy can analyze a cell population or determine the effects of external stimuli or small molecules in a biological system. High-resolution microscope technology will be invaluable in assessing various molecule interactions with biological pathways in living cells and organisms. Optical imaging is more sensitive than radionuclide imaging and can be "targeted" if the fluorophore is conjugated to a targeting ligand. In addition, fluorescent probes can be activatable optical probes, which is a unique feature in molecular imaging, because these probes remain undetectable unless they are turned on only in specific environments. Activatable fluorescence probes can maximize the target signal and minimize the background signal, resulting in higher TBRs compared with conventional "always-on" imaging agents. Finally, optical imaging with activatable probes emit low-to-no background signal and generate a signal only in desirable environments, which allows more sensitive detection of small targets against a dark background [18]. However, several disadvantages, including the lack of quantitation with optical imaging due to unpredictable light scattering and absorption and the restriction of the object of interest in deep tissue, should be resolved. Despite the fact that the limited depth of light penetration in tissue is an issue that needs to be solved in fluorescence optical imaging, optical imaging is of particular value for mapping specific molecular events in living systems and for tracking target cells by virtue of its high sensitivity and specificity, low background signal, ease of quantitative analysis, and the possibility of localize (labeling) and quantify the light emission of targets.

Advances in molecular biology, organic chemistry, and materials science have recently led to the creation several new classes of fluorescent probes for imaging in cell biology [19]. To design a successful molecular imaging probe, several characteristics should be considered, including wavelength, brightness, stability, and interactions between targets and probes. Excitation at a short wavelength (ultraviolet to green) of the fluorophore can damage tissues or cells, and its poor tissue penetration is applicable only to superficial structures. In contrast, excitation at a longer wavelength (approximately 600 nm to near-infrared) can heat tissues or cause the autofluorescence of hemoglobin. The optimal excitation wavelength of a fluorophore would be in the deep red or near-infrared range because of the combined virtues of good tissue penetration and low autofluorescence [18, 20]. The brighter the probes, the greater the penetration depth expected. Increased brightness often comes at the cost of increased size, which can be implicated in the interaction with targets and is difficult to image with the exogenous injection of probes. Many organic fluorophores lose their fluorescence due to cellular environments or photobleaching. For longitudinal observation, the stability of the probes should be considered. Most small-molecule fluorophores conjugated to targeting moieties may alter the interaction with targets and be implicated in the kinetics of target probes, leading to rapid liver accumulation before successful targeting.

2.1. Fluorophores

For the purposes of discussion, fluorophores can be divided into small synthetic fluorophores, genetically encoded proteins that are often naturally occurring fluorophores produced within cells, and nanoparticles characterized

by large molecular diameters and high quantum yields.

2.1.1. Small-molecule fluorophores

Small synthetic fluorophores have molecular weights ranging from 300 to 2000 Da and span the emission spectrum from blue to NIR. In particular, fluorophores based on fluorescein, BODIPY, rhodamine, and cyanine as core structures are easily available from commercial providers. Generally, they can be modified for better brightness, longer wavelength emission, hydrophilicity, and introduction to various targeting ligands. They can also be controlled for fluorescence intensity by various strategies, such as self-quenching, ICT, and Förster resonance energy transfer (FRET). These properties of small molecular fluorophores and their small sizes allow the imaging to target versatile biomolecules, including metals, ROS, RNS, and many proteins, through the exogenous injection of probes.

2.1.2. Fluorescent proteins

Genetically encoded fluorescent proteins (FPs), such as green fluorescent protein (GFP), are found in a wide range of animals in nature. The expression of FP alone or genetic fusions with other proteins induce quite bright fluorescence without any cofactors, which facilitates *in vivo* imaging for visualizing deep objects. Mutation can either increase the photostability or generate fluorescent proteins (FPs) that are photoswitchable, which is useful for monitoring protein diffusion, trafficking, and age. The fluorescence of FPs is normally stable in the biochemical environment except under acidic conditions, but they have been improved by genetic engineering. These fluorophores can be used to monitor a variety of biological events and signals by the quantification of expressed protein levels targeting subcellular

compartments, tissues, and intact organisms and very rarely cause photodynamic toxicity [21]. However, they must be genetically encoded and transfected within the genome of host cells. They are also very large at 25–50 kDa and difficult to conjugate, which limits their use as an injectable target-specific fluorescent protein probe; thus, they are feasible only in the context of gene therapy [22].

Bioluminescence imaging has been extensively applied for genetically engineered luminescent microorganisms and cells used to evaluate the spatial distribution of a given target molecule and biological process by whole-body imaging in live animals. It takes advantage of emissions without external excitation to decrease the background signal for sensitive and selective detection. However, like FPs, luciferase needs genetic encoding for a proper exogenous injection study.

2.1.3. Fluorescent Nanocrystals

Numerous nanocrystals, developing materials, have been used as a signal reporter in bioassay and bioimaging, and some have unique optical properties. Quantum dots (QD) are characterized by a broad excitation range, narrow emission peak, resistance to photobleaching, various emission wavelengths, and ultrahigh brightness [23, 24]. Recently, using these materials as a fluorophore or conjugated system with other fluorophores, such as luciferase and small-molecule fluorophores, has achieved selective and bright bioimaging. However, the toxicity of the nanomaterials needs to be considered. For instance, QDs contain heavy metals, such as cadmium and selenium, in their core and are generally too large to accumulate in cells [25].

3. Fluorescent probes for detecting enzyme activity

Enzymes play substantial roles in many biological and physiological processes and function as critical biomarkers for various diseases. Enzymes catalyze biochemical transformations, which is different from the role of a protein receptor. The imaging and assay of enzyme activity in living subjects provides a powerful and widely applicable tool for elucidation of the enzyme function and mechanism in biology and disease diagnostics, but the complexity and dynamics of enzymatic reactions in living systems present unique challenges for probe design. For the imaging of receptor proteins, a fluorescent probe generally involves a signaling fluorophore and guest species that are bound to the target receptor. After binding to the target receptor of the probe, the photophysical characteristics of the fluorophore are changed, and such a change provides a signal that indicates guest binding. Compared with imaging the protein receptor using the probes, in which the signal is generally induced by conformational or environmental changes upon their binding [26-28], a fluorescent probe for imaging enzyme activity usually triggers optical responses by enzymatic reaction, which is called a reaction-based probe. Enzymes are classified into six categories based on the chemical reaction types: oxidoreductases, transferases, hydrolases, lysases, isomerases, and ligases. Although they catalyze a large number of chemical transformations, the same type of reaction occurs through a similar mechanism even though their substrates are different. Thus, the enzyme reaction-based probe should be designed based on the distinguishable signal generation of the chemical transformation of a given substrate. For distinguishable signal generation, enzyme reaction-based probes utilize various molecular scaffolds, including small molecules, nanoparticles, and genetically encoded proteins, as

molecular imaging modalities.

3.1. Probes with fluorescent proteins

Fluorescent proteins (FPs) have been improved by genetic engineering to possess different emission spectra and better brightness and are extensively applied to observe gene expression and protein–protein interactions [29, 30]. Recently, they have also been applied to monitor enzyme activity in cells using the FRET strategy. Many probes containing FPs to detect protease activity have been developed, which were composed of two FPs linked through a cleavable peptide by protease (Fig.). For example, a probe incorporating FPs as fluorophores w linked with the peptide substrate of caspase was used to monitor apoptosis [31]. During programmed cell death, caspase activity is increased for the proteolysis of cellular proteins and is a critical event that should be observed to monitor apoptosis. The probe emits YFP fluorescence (em 528 nm) with the excitation wavelength of CFP (433 nm) due to FRET. However, caspase cleaves the substrate peptide linker, and the probe exhibits CFP emission with the same excitation wavelength (Fig. 2a). These fluorescence wavelength changes of caspase activity enable apoptosis to be observed, which provides information for the design of strategies to regulate the caspase activity during apoptosis. A FRET-based FP probe was also reported to detect changes in kinase and phosphatase activity within cells. A reported kinase and phosphatase activity probe was composed of CFP and YFP linked with kinase substrate and a specific phosphopeptide-binding domain (Fig. 2b). The FRET occurred due to the proximity between YFP and CFP by binding the phosphorylated substrate to the phosphotyrosine-binding domain. On the other hand, the dephosphorylation created a long

distance between the two FPs and the probe emitted only CFP fluorescence (476 nm). These responses of the probe were able to monitor kinase activity and phosphatase activity in living cells [32]. However, engineered FPs, such as CFP and YFP, exhibit relatively weak fluorescence compared with wild-type GFP. Additionally, the major drawback of FRET-based FP probes is their large size, which interrupts the interaction between the target enzyme and probe, and the genetic encoding process is an obstacle for targeting various enzymes.

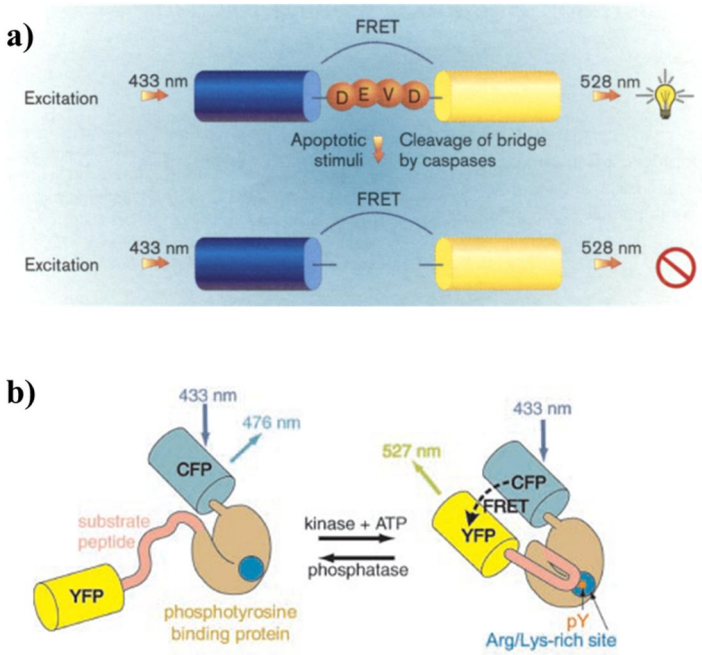

Figure 2. Strategies to detect caspase activity (a) and kinase activity (b) using FPs.

3.2. Bioluminescence imaging reporter probes

Most recently, the bioluminescent firefly protein, luciferase, has been utilized to monitor enzyme activity. The main advantage of using bioluminescence reporters is their high sensitivity and minimal background due to unnecessary

external excitation. A recombinant luciferase-based probe was investigated as a novel molecular-based reporter to detect caspase-3 activity for the noninvasive imaging of apoptosis [33]. Monitoring the apoptosis, which is a physiologic process in normal development, and homeostasis of multicellular organisms would enable the evaluation of therapeutic agents. The luciferase reporter fused to two ER regulatory domains through caspase-3 substrate peptide attenuated their activity because of steric inhibition. The caspase peptide substrate between the luciferase and ER regulatory domains was cleaved by caspase, and then the luciferase activity was recovered to generate the bioluminescence of luciferin. The probe exhibited a 10-fold luminescence increase and was used for the real-time imaging of caspase activity in mice (Fig. 3a). The ability to image caspase-3 activation noninvasively provides a unique tool for the evaluation of the therapeutic efficacy of experimental therapeutic agents as well as for studies on the role of apoptosis in various disease processes. In another study, modified luciferin containing nitroreductase (NTR) substrate was used as a probe to detect NTR activity instead of recombinant luciferase [34]. Bacterial NTRs have been widely applied in the development of novel antibiotics, cancer therapeutic agents, and degradation agents. Using the developed probe based on caged luciferin by NTR substrate, sensitive and non-invasive NTR imaging could be performed. The reduction of substrate by NTR induced the elimination of the linker on the hydroxyl moiety of luciferin and generation of uncaged luciferin to emit bioluminescence (Fig. 3b). This strategy enabled the monitoring of NTR activity *in vivo* and could contribute to the application of NTR in many areas.

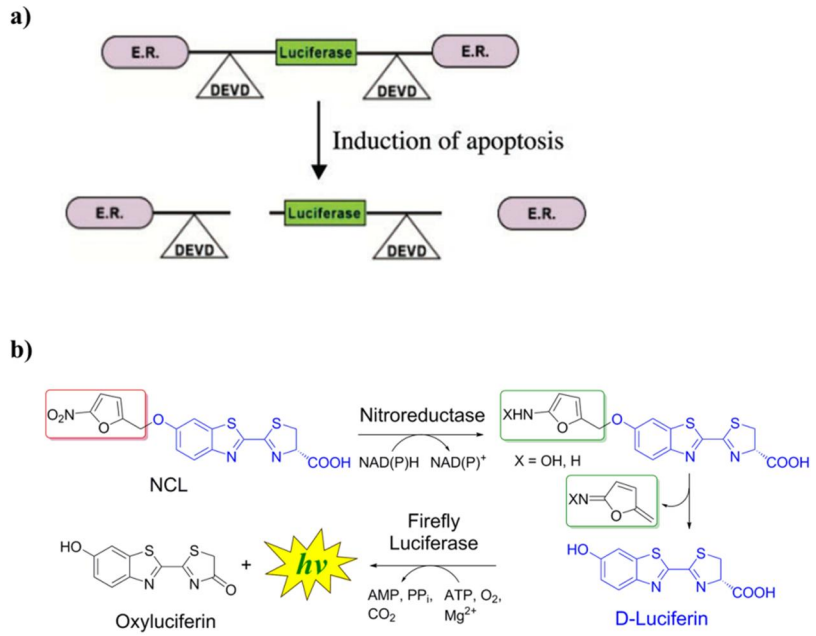

Figure 3. Schemes for detection of caspase activity using modified luciferase (a) and detection of nitroreductase activity using modified luciferin (b).

However, probes using GFP or the luciferin–luciferase pair as a signal reporter still have limitations in size, injection, and off-on strategy design.

3.3. Small-molecule substrate reporters of enzymatic activity

Probes comprised of small-molecule fluorophores as reporters to detect enzyme activity have been widely used for screening substrates or inhibitors, enzyme kinetics, and functions in cellular contexts, cellular stains, and the visualization of biological events [11]. A key advantage of these probes over other fluorophore types is their use of chemical synthesis to mimic various substrate or inhibitor candidates and modulate the optical properties in a biological experiment [35]. The strategy of these probes is generally based on the enzymatic conversion of substrates to elicit optical signal changes. The chemical activation of fluorophores by enzymatic catalysis enables advanced

imaging experiments to be achieved where a distinct subset of fluorophores can be visualized against unactivated fluorophores. Recently, many fluorogenic probes of kinases, phosphatases, and proteases have been developed and successfully applied to living cells [35].

4. Design strategy of Fluorescent probe

There are several ways to design activatable fluorescent probes. Enzymatic reactions entail chemical transformation, and chromogenic and fluorogenic probes are regarded as reagents that can be catalyzed by enzymes accompanied by changes of their spectroscopic properties. The activatable probes being conjugated with enzyme substrate are generally silent until the release of the transformation of the substrate by enzyme activity. Then, the reactions lead to the generation of signal changes; thus, the enzyme activity can be determined.

Typically, these probes are comprised of a reporter moiety, reaction moiety, and linker. The properties of a reporter moiety, generally spectroscopic moiety, are changed upon reaction with the enzyme of interest. The reaction moiety, such as the substrate mimic or recognition moiety, is responsible for the selective reaction with the target enzyme. A suitable pacer or linker connects the reporter moiety and reaction moiety, but sometimes the two moieties are integrated without any linker [36].

The exploration of new mechanisms to control the properties of the signal reporting units according to the interaction with reaction moieties is an important issue for designing new fluorescent probes. Numerous new and

well-organized probes have been designed using fundamental photophysical mechanisms at the molecular level and the principles of supramolecular chemistry [37]. The most widely used conventional signaling mechanisms for optical detection include ICT, twisted ICT and FRET, photoinduced electron transfer (PET), and other approaches, such as excimer formation and precipitations.

4.1. Intramolecular charge transfer (ICT)

Many probes utilizing the ICT process employ push-pull chromophores, which contain electron donor and acceptor units separated by a π-electron-rich conjugated linker [38]. The enhancement or suppression of this ICT process leads to signal changes; increases in donor and acceptor strength induce red-shifted absorption and fluorescence changes. The easiest approach for designing an ICT-based probe is using push-pull fluorophores that are masked with enzyme-labile groups [37]. Numerous probes have been reported. Resorufin is the most useful fluorophore for detection and imaging analysis because of its small size and long wavelength emission. In a report, a probe for detecting nitroreductase (NTR) activity and imaging hypoxia was developed according to the basis of resorufin introducing 5-nitrofuran as a mask and substrate [39]. Hypoxia is caused by an inadequate oxygen supply; under this condition, intracellular reductases are involved in the selective activation of specific functional compounds. The nitro group in the probe was reduced by the catalysis of NTR to the hydroxylamine or amino group, then 1,6-rearrangement and elimination occurred to release resorufin, increasing the fluorescence intensity to 585 nm. This probe could also image and differentiate HeLa and A549 cells under normoxic and hypoxic conditions. As

a result, the fluorescence enhancement by nitroreductase activity under hypoxic conditions enabled the establishment of a sensitive and selective fluorescence method for imaging the hypoxic status of tumor cells (Fig. 4a).

Another example is an activatable fluorescent probe for detecting γ- glutamyl transpeptidase (γGT), which was comprised of indocyanine as a signaling reporter and gamma glutamic acid as a substrate, with a cleavable linker interposed between them [40]. γGT is known as a tumor-related enzyme, and the level of γGT in serum is an important factor of cancer. The indocyanine of the probe was conjugated with a cleavable linker to block ICT quenching fluorescence. The hydrolysis of the probe by γGT and subsequently occurring cleavage-induced dramatic fluorescence enhancement recovered the ICT. The properties of the probe enabled the imaging of γGT in the mouse model of colon cancer to be achieved (Fig. 4b).

Leucine aminopeptidase (LAP), which cleaves N-terminal leucine residues from substrates, is implicated in many pathological disorders as a well-defined biomarker. For the quantitative detection of LAP distribution and dynamic ranges, a near-infrared fluorescent ratiometric probe was developed [41]. While the probe conjugated with leucine residue through an amide bond exhibited weak emission at a shorter wavelength (535 nm) because of the weak ICT, the hydrolysis by LAP to release the free aniline moiety of the probe induced strong emission at 660 nm because of the strong ICT. The high contrast on the ratiometric NIR fluorescence signal was capable of the quantification of endogenous LAP activity in various types of living cells and three-dimensional imaging, which enables the observation of the intracellular LAP distribution (Fig. 4c).

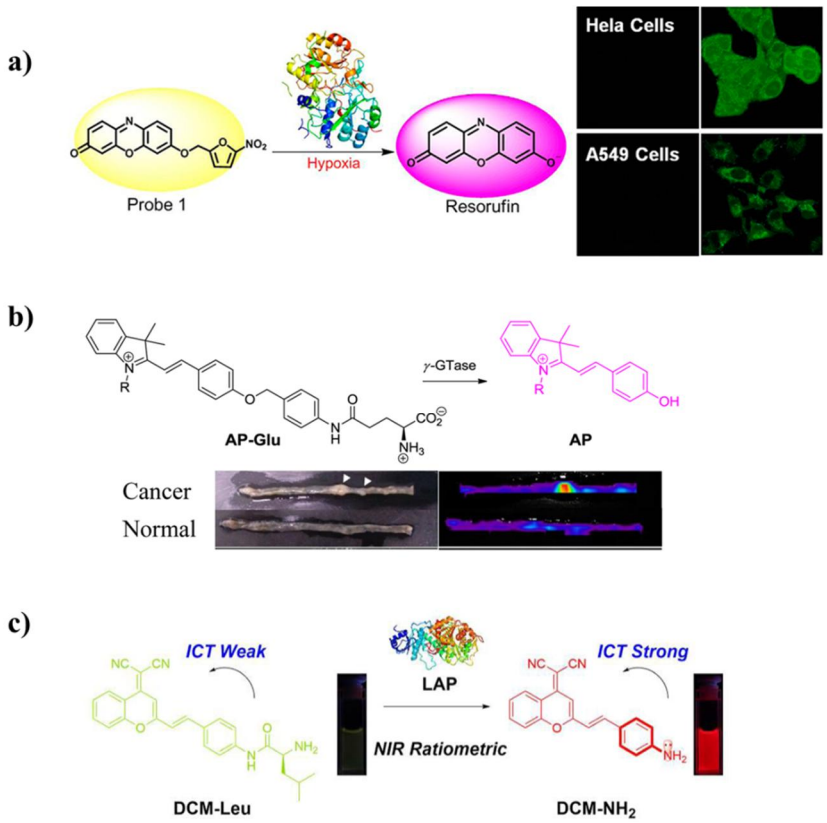

Figure 4. a) ICT-based resorufin probe of nitroreductase, b) indocyanine probe of γGT, and c) DCM probe of LAP. These pictures were adapted from references 40, 41, and 42, respectively.

4.2. Fluorescence resonance energy transfer (FRET)

FRET is the most broadly used strategy for designing enzyme-activatable probes. For efficient FRET, the emission spectrum of the donor and absorption spectrum of the acceptor should overlap and the distance between the donor and acceptor should be in the range of 10 to 100 Å.

A ratiometric fluorescent probe for detecting phosphodiesterase activity based on FRET has been reported [42]. Coumarin, a FRET donor, was conjugated to

fluorescein, a FRET acceptor, with two phenyl linkers with the phosphodiester moiety placed between them. When the probe was excited at 370 nm, the fluorescence of the coumarin of the probe was quenched and only the emission of fluorescein was observed. The cleavage of phosphodiester moiety in the probe by phosphodiesterase activity resulted in the fluorescent enhancement of coumarin and decrease of fluorescein emission at the excitation of 370 nm (Fig. 5a).

Matrix metalloproteinase 12 (MMP12) is a proteolytic enzyme mainly secreted by macrophages and implicated in inflammation and could be a drug target. For the detection of MMP12 activity, a membrane-targeted reporter (LaRee1) was designed consisting of coumarin343 as a donor, peptide sequences as a substrate of MMP12, and TAMRA as an acceptor [43]. In addition, palmitic acid was incorporated in the probe for linkage to the membrane. The cleavage of the substrate peptide in the probe by MMP12 induced the loss of FRET, and the cleaved hydrophobic part containing coumarin343 was internalized in the cell. LaRee1 was achieved to detect and monitor MMP12 activity *in vitro* and *in vivo* (Fig. 5b).

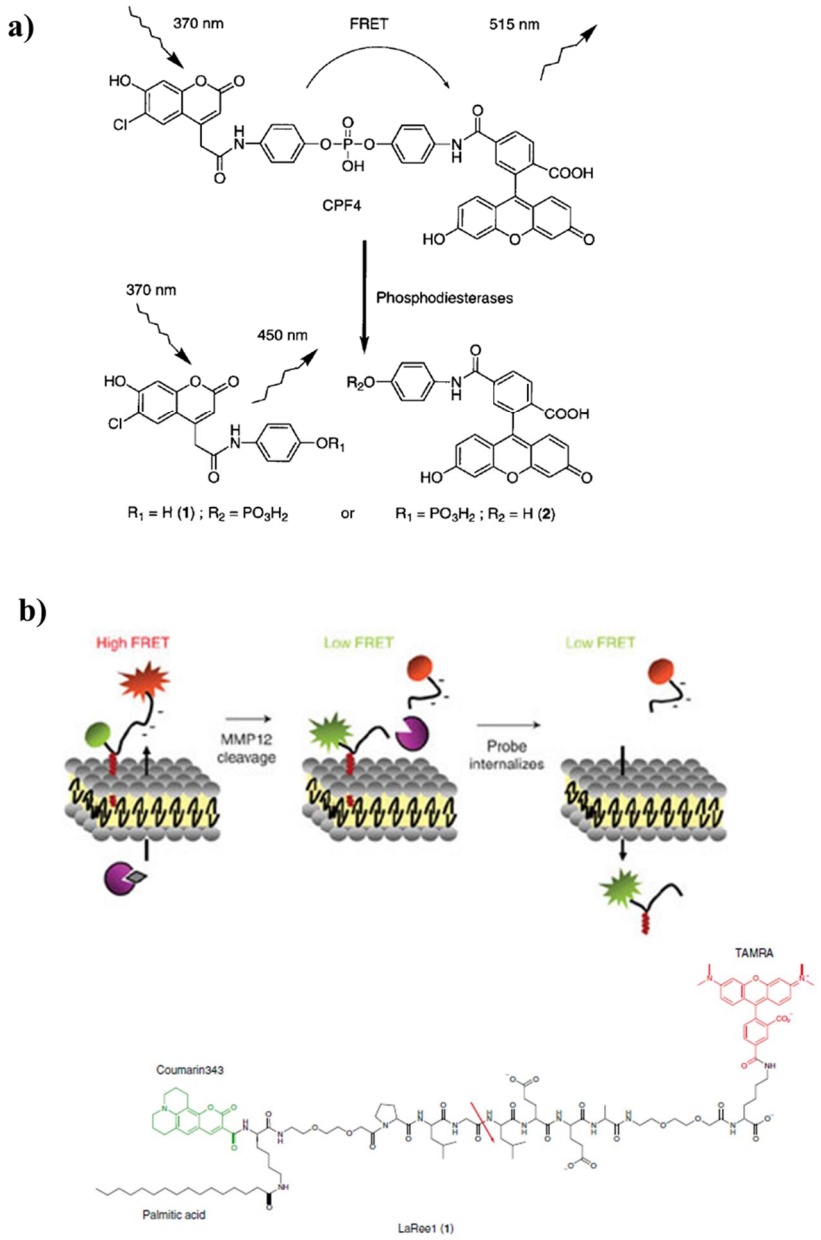

Figure 5. a) FRET-based probe of phosphodiesterase and b) FRET-based probe of MMP12. The pictures are adapted from ref. 42 and 43.

4.3. Photoinduced electron transfer (PET)

PET has been widely used for the detection of biomolecules and enzyme activity. A PET-based probe generally consists of an electron donor unit and an acceptor unit. Upon excitation, the unoccupied orbital of the acceptor becomes fully occupied by electron transfer from the donor, the release of the excited electron is blocked, and emission is quenched.

A PET probe for the detection of Arylamine N-acetyltransferases (NATs, EC 2.3.1.5), which catalyze the transfer of an acetyl group from acetyl CoA to aromatic amines, has been developed [44]. NATs are known as drug-metabolizing enzymes that influence drug efficacy and adverse effects. A long-lived luminescent lanthanide complex as a probe for NAT was quenched by PET from an aniline of the probe, and the acetylation of the aniline by NAT triggered a 100-fold increase of luminescence. This probe was applied for the sensitive and rapid detection of NAT activity of a recombinant enzyme or cell lysate, which is expected to be useful for drug discovery and clinical diagnosis (Fig. 6a).

This example probe used the d-PET mechanism. The near-infrared fluorescent probe for NTR employed cyanine dyes with the introduction of a nitro aromatic group as a substrate [45]. Because the nitro aromatic group is strongly electron-withdrawing, the fluorescence of the probe was quenched by d-PET, unlike in the former example. After NTR catalyzed the reduction of the nitro group of the probe to amine and d-PET was inhibited, the fluorescence of the cyanine dye was increased. Because NTR is overexpressed in hypoxic tumors, the probe enabled the detection and monitoring of tumor hypoxia through the fluorescence enhancement from

NTR activity in cells and *in vivo* (Fig. 6b).

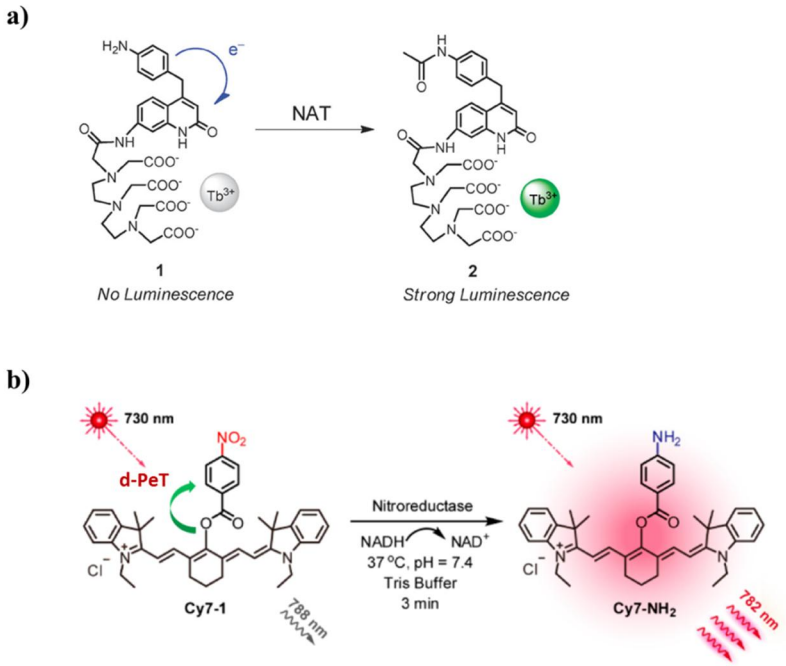

Figure 6. a) PeT-based probe of NAT and b) peT-based probe of nitroreductase. The figures are adapted from ref. 44 and 45.

4.4. Excited-state intramolecular proton transfer (ESIPT)

In the ESIPT system, protons in the excited state transfer a molecule in a range of picoseconds. The chromophores in the excited-state hiring ESIPT process absorb similar wavelengths to those in the ground state, but their fluorescence is significantly different to having a large Stokes shift.

A commercially available ESIPT fluorophore, 2-(2'-hydroxyphenyl) benzothiazole (HBT), was phosphorylated for the selective and sensitive detection of PTP activity [46]. Protein tyrosine phosphatases (PTPs) and protein tyrosine kinases (PTKs) play crucial roles in cellular regulation and signal transduction pathways. Upon selective enzymatic hydrolysis, the enol

form was converted to the excited-state keto form to emit stronger fluorescence with a large Stokes shift (Fig.7).

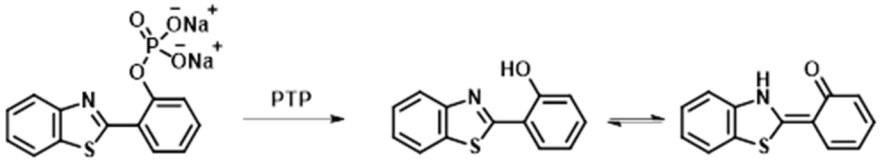

Figure 7. ESIPT-based probe of protein tyrosine phosphatase. (ref. 48)

4.5. Covalent bond formation

The formation of covalent bonds has been applied to develop activatable chromogenic and fluorogenic probes for various analytes. In particular, the cyclization of the probes by target enzymatic reaction could induce dramatic signal changes. This is because such probes have only reactive moieties to generate new scaffolds by enzymatic reactions compared with most probes, which employ other strategies to retain fluorophore scaffolds to be released by enzymatic reaction. There are several examples using the probes that are based on the formation of covalent bonds for the selective detection of target enzymes.

Monoamine oxidases (MAO, EC 1.4.3.4), which catalyze the aerobic oxidation of amine, play a substantial role in the central neuro system, and the MAO activity level are related to neurological diseases. An amine substrate of MAO was oxidized to the corresponding imines, which was followed by hydrolysis to the aldehyde. The strategy of the probe for the detection of MAO activity was based on the oxidation of amine substrate forming aldehyde to be attacked by the aniline of the probe and cyclized to increase fluorescence intensity (Fig. 8a) [47].

The phosphate groups of the non-fluorescent probes in Figure **8** were cleaved by alkaline phosphatase (ALP) activity [48], and the generated phenolic oxygen attacked the nitrile group and intramolecularly cyclized, resulting in highly emissive iminocoumarin-benzothiazoles (Fig. 8b). With these probes, the real-time imaging of endogenous ALP activity was performed in living cells.

a)

b)

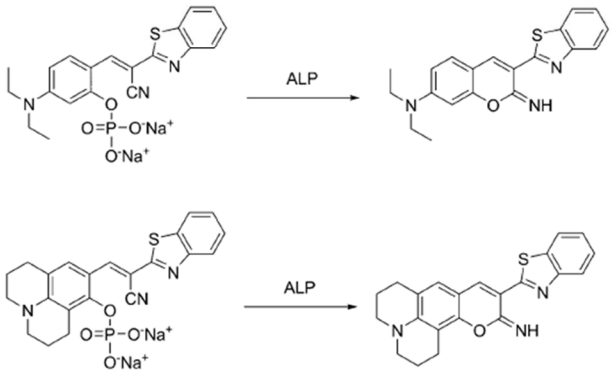

Figure 8. a) the probe to be cyclized by MAO activity b) the probe to be cyclized by ALP. The figures are adapted from ref.47 and 48.

4.6. Excimer formation

An excimer is defined as a complex formed by the interaction of a fluorophore in the excited state and the same fluorophore in the ground state. The emission spectrum of the excimer is exhibited at a longer wavelength

than that of the monomer, and, in most cases, both the emission of the excimer and monomer are observed. The emission wavelength changes of a probe by excimer formation and rupture upon the target enzyme enable the detection and monitoring of enzyme activity.

The excimer pyrene has a particular property according to which the aggregation of pyrene monomer produces an excimer to emit a longer wavelength (450–550 nm). The strategy of a probe to detect acetylcholinesterase (AChE, EC 3.1.1.7) activity employed this particular property [49]. Acetylcholinesterase catalyzes the hydrolysis of acetylcholine to choline and acetate. It is known to be related to the nervous system, and its inhibitors are used for the treatment of neuromuscular disorders. For the detection of AChE activity, the probe consisted of pyrene butyric acid linked with choline by an ester bond and poly(vinylsulfonate) (PVS), which induced the aggregation of the probe. When cationic choline-labeled pyrene existed with anionic PVS, the probe aggregated to exhibit excimer fluorescence (Fig. 9a). In contrast, hydrolysis of the probe by AChE generated an anionic pyrene butyrate fragment to release the monomer emitting at approximately 400 nm. This strategy was shown to be applicable to real-time ACHE activity monitoring and inhibitor screening.

4.7. Polymerization and self-assembly

Enzyme-triggered self-assembly or the polymerization of small molecules into hydrogels or precipitates has been applied for enzyme inhibitor screening and drug delivery as well as activity assays. Hydrogel formation or the polymerization of optical probes needs a large number of probes and could induce self-quenching effects for the fluorophore, which are improper for

sensitive detection and optical imaging. Nevertheless, polymerization and self-assembly can be used as imaging methods to confirm the location of target enzymes because they are formed in the vicinity of the enzyme activity site [13]. An example is the probe for the detection of furin activity, which was designed on the basis of the last step to synthesize luciferin, a condensation reaction between 2-cyanobenzothiazole and 1,2-aminothiol (cysteine) in buffer at pH 7.4 [50]. 1,2-aminothiol could be modified with the target substrate, which was able to react with the target enzyme to release 1,2-aminothiol and cause condensation (Fig. 9b). Upon furin activity, the probe was cleaved and formed condensation products, which were subsequently polymerized to decrease their basic emission. This intracellular condensation process enabled the imaging of the proteolytic activity of furin.

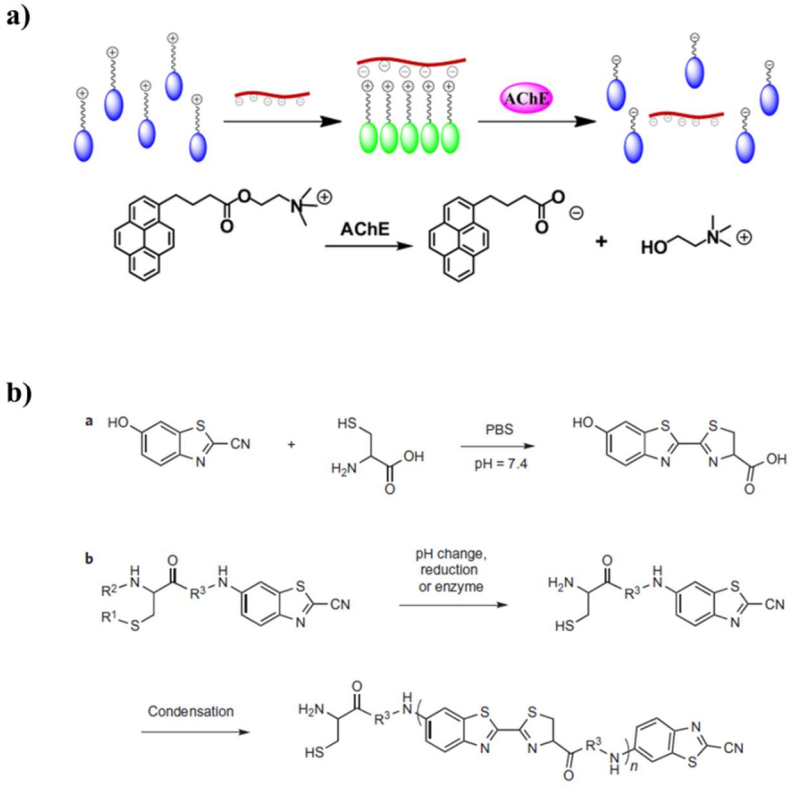

Figure 9 a) excimer formation based probe for AChE and b) self-assembly formation based probe of protease furin. The figures are adpated from ref. 49 and 5.

II.

Probes inducing signal changes by intramolecular cyclization upon the treatment of enzyme

Section 1.
Sulfatase activated probe generating N-methyl isoindole in buffer containing reducing agents

1.1. Introduction

In many biological systems, the sulfation state of biomolecules is important in determining their function. Sulfation state is regulated by sulfatases (EC 3.1.5.6) which catalyze the cleavage of sulfate esters present in biomolecules such as carbohydrates, steroids, and proteins [51-53]. Human sulfatases are broadly classified based on their subcellular location. The three classes are, lysosomal sulfatases, non-lysosomal sulfatases, and extracellular sulfatases. Sulfatases in each subcellular location play important roles in many biological processes including cellular degradation, hormone regulation, and cell signaling. In breast carcinoma cells, for example, it has been reported that the mRNA level the mRNA level is increased but the activity of steroid sulfatases is decreased [54, 55]. In order to deepen our understanding of sulfatase biology, the development of probes capable of measuring sulfatase activity is required.

Optical probes have proven to be powerful tools for measuring sulfatase activity and these assays have contributed to the diagnosis and treatment of sulfatase-related diseases.

In general, sulfatase activity assays have been performed using *p*-nitrophenyl sulfate (*p*-NPS) or 4-methylumbelliferyl sulfate (4-MUS). However, these sulfatase substrates have slow reaction rates and lack sensitivity [56-58]. Several other activity-based sulfatase probes have been reported. These are comprised of luminophores and a sulfate group, and they exhibit an optical change after cleavage of the sulfate ester by sulfatases [59-63]. These probes have better kinetics and increased sensitivity compared to *p*-NPS and 4-MUS [8-12], and they were able to discriminate mycobacterium strains through individual sulfatase activity patterns [12].

Here, we introduce a new activity-based probe for measuring sulfatase activity assay using the formation of fluorescent *N*-methylisoindole [64]. Based on the ability of sulfatase to cleave sulfate groups, we designed a pro-fluorescent probe (probe **1**) which consists of a phenyl sulfate moiety as a substrate and 2-formyl benzylcarbamate moiety as a signaling unit. When the sulfate group of probe **1** is cleaved by sulfatase, self-immolation and intramolecular cyclization occur, resulting in the generation of a fluorescent *N*-methylisoindole (Scheme1). Isoindole derivatives has been reported to be unstable and decompose easily, resulting in reduced fluorescence intensity [65, 66]. To avoid this reduction in fluorescence intensity, we also examined sulfate ester hydrolysis under reducing conditions, namely in the presence of glutathione (GSH) or tris(2-carboxyethyl)phosphine (TCEP).

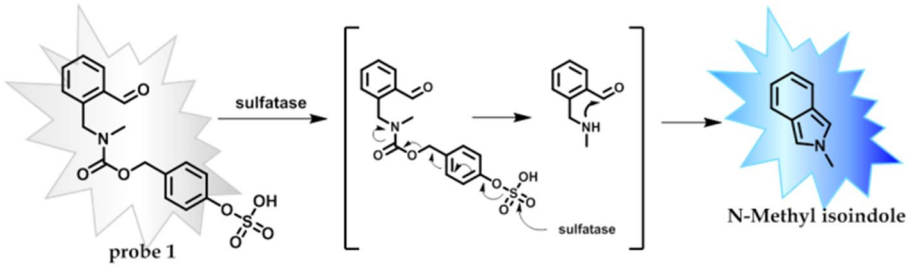

Scheme 1 probe **1** for sulfatase activity assay

1.2. Results and Discussion

To examine the fluorescence changes upon treatment with sulfatases, we measured the fluorescence intensity of probe **1** in the absence and presence of sulfatases. When excited at 325 nm, probe **1** was non-fluorescent in the absence of sulfatase, but in the presence of sulfatase, the fluorescence of probe **1** was enhanced in a time-dependent manner (Figure 10a). After 60 min incubation of the probe with sulfatase, the fluorescence intensity at 415 nm increased up to 8-fold and became saturated (Figure 10a). The fluorescent signal arose from the *N*-methylisoindole generated as a result of sulfatase activity. To confirm the generation of *N*-methylisoindole, a Diels-Alder reaction using *N*-phenylmaleimide was carried out to trap isoindoles [67], and mass spectrometric analysis was also performed. The peak of the Diels-Alder adduct was observed at m/z 304 which corresponds to the calculated molecular weight of the adduct (Figure S2a). These results confirmed that enzymatic cleavage of the sulfate group in the probe triggered the generation of a fluorescent *N*-methylisoindole.

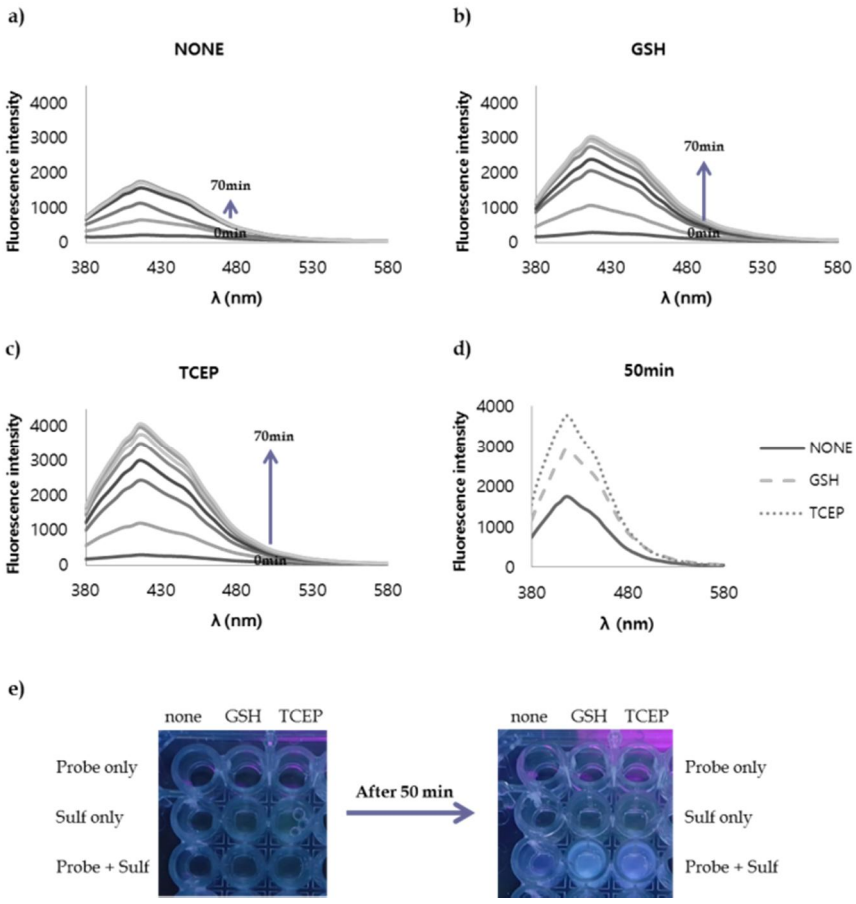

Figure 10. Time-dependent fluorescence changes of probe 1 (20μM) with sulfatase (0.25mg/ml) at 37℃, a) in 50mM Tris buffer at pH 7.4, b) in 50mM Tris buffer containing 1mM GSH, c) in 50mM Tris buffer containing 1mM TCEP. d) Fluorescence intensities of probe 1 in three different buffers after 50min in cubation with sulfatase at 37℃, and e) fluorescence changes of probe 1 under UV light.

However, *N*-methylisoindoles are known to be unstable and readily autoxidize in air and water [68-70]. Such autoxidation will attenuate the fluorescence intensity of *N*-methylisoindole and reduce the utility of this molecular probe. In order to reduce the autoxidation rate of *N*-methylisoindole, we used two different buffers that contained 1 mM of GSH or 1 mM of TCEP as reducing

agents. GSH was used as a representative physiological reducing agent and TCEP was used since it is a common reducing agent in many enzyme activity assays and inhibitor screens. As shown in Figures 1b and 1c, the fluorescence intensity at saturation was increased 10-fold in GSH buffer and 14-fold in TCEP buffer compared to the intensity in absence of sulfatase. Moreover, after 50 min of incubation, the fluorescence intensities of *N*-methylisoindole in buffers containing 1 mM GSH or 1 mM TCEP were 1.7 times and 2 times stronger compared to those under 50 mM Tris buffer without reducing agents, respectively (Figure 10d). In addition, the increase in fluorescence intensity was dependent on the concentrations of GSH and TCEP (Figure S1), which confirmed that the stronger fluorescence emission was due to the reducing agents. To identify the products of the enzymatic reaction in GSH- or TCEP-containing buffer, a Diels-Alder reaction using *N*-phenylmaleimide was also carried out. Mass spectrometry showed the presence of a peak at m/z 304, indicating formation of the same Diels-Alder adduct as was obtained without reducing agents (Figure S2b and S2c). Therefore, the stronger fluorescence intensity in GSH- or TCEP-containing buffer solutions could be attributed to inhibition of *N*-methylisoindole autoxidation by the reducing agents.

The optimal pH of most human sulfatases including arylsulfatase A, B, and galactosamine-6-sulfatase was reported to be around 5, while the optimal pH of arylsulfatase C (steroid sulfatase) and endo sulfatases is 7 [53]. To confirm the utility of probe **1** under neutral and acidic conditions, the fluorescence changes of probe **1** with the treatment of sulfatase were monitored in acidic buffer (pH 5.0) and 1 mM GSH- or 1 mM TCEP-containing acidic buffer (Fig 11 and Fig. S3). Compared to the fluorescence intensity of probe **1** in neutral buffer solutions, the fluorescence intensity of probe **1** with the treatment of

sulfatase in acidic buffer was considerably weak. Given that sulfatase from *Helix pomatia* also showed proper activity at acidic pH [56, 61], these phenomena would be caused by more rapid decomposition of *N*-methylisoindole in acidic conditions [65, 67-70]. This result indicates that probe **1** would be more feasible to detect sulfatase activity at neutral pH.

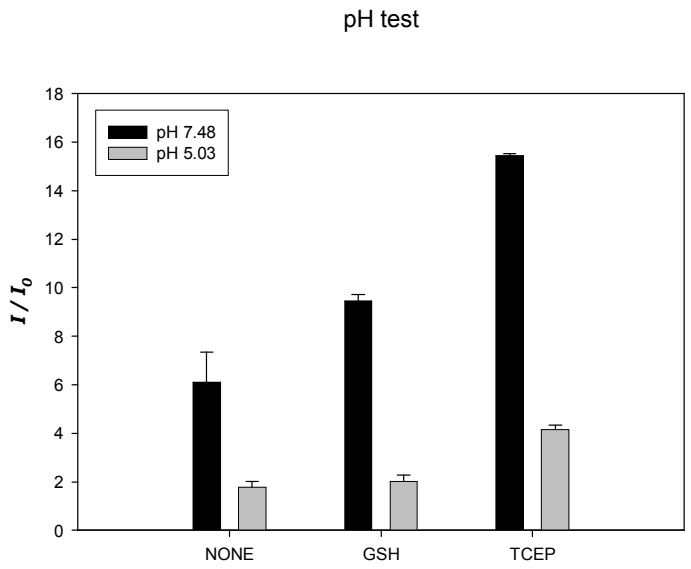

Figure 11. Relative fluorescence intensity of probe 1 after 30 min incubation with sulfatase in neutral and acidic conditions with and without reducing agents.

To analyze the kinetic parameters of sulfatases, we measured the reaction rates over a range of probe concentration. Concentrations of probe **1** from 0.5 μM to 100 μM, and 0.25 mg/mL of sulfatase in 50 mM Tris buffer at pH 7.4 were used and the same experiments were performed in two different buffers containing 1 mM GSH and 1 mM TCEP, respectively. From the enzyme experiments, the K_m and V_{max} values were obtained by plotting enzyme reaction rates as a function of probe concentration (Table 1 and Figure S4). Compared to previous reported kinetic values obtained using 4-NPS

(K_m=1.85±0.32 mM, V_{max}=33.8±4.8 μM/min) [62], the calculated K_m and V_{max} values of probe **1** indicated a slower reaction rate with sulfatase but a higher affinity for sulfatase. In addition, despite using different reducing agents in enzyme reactions, we observed similar K_m and V_{max} values, which indicated that the interaction between probe **1** and sulfatase was not affected by the reducing agents.

Table 1. Kinetic parameters

	Probe 1			***p-nitrophenyl sulfate (p-NPS)***[a]	***3-O-methylfluorescein-sulfate (MFS)***[b]
	none	GSH	TCEP		
K_m (μM)	203 ± 57	204 ± 59	206 ± 73	1850 ± 320	24.8 ± 2.2
V_{max} (μM/min)	0.27 ± 0.06	0.21 ± 0.04	0.17 ± 0.04	33.8 ± 4.8	0.00041 ± 0.00001

[a] Assay was carried out with sulfatase from *Helix pomatia* in 100 mM Tris buffer (pH 7.43) at 30℃ [11].

[b] Assay was carried out with sulfatase from *Helix pomatia* in 100 mM potassium acetate buffer (pH 5.0) at 37℃ [12].

High-throughput screening for the identification of drugs has become widely used and many probes have been developed for such screening. To investigate whether the probe was appropriate for inhibitor screening, we measured the IC_{50} values of estrone 3-O-sulfamate (EMATE) which is a known inhibitor of human steroid sulfatase [71, 72] using a range of EMATE concentrations and 0.25 mg/mL sulfatase and 20 μM probe **1**. The IC_{50} values determined by the Hill plots are shown in Table 2 and Figure S5. Although these values were larger than the reported IC_{50} value of EMATE (80 nM) measured using placental microsomes [73, 74], considering the large amount of sulfatase used,

the IC_{50} values are acceptable. The inhibition potency in TCEP-containing buffer was greater than the other IC_{50} values in Tris buffer with and without GSH. Despite the fact that reducing agents are commonly used in enzyme assays and inhibitor screens, they can generate false positive hits [75]. These data implied that TCEP could interrupt the interaction between EMATE and sulfatases, resulting in a greater IC_{50} value. Therefore, it is recommended probe **1** be used in the presence of Tris buffer, or Tris-buffer containing GSH, for any potential high-throughput sulfatase inhibitor screen.

Table 2. Inhibitory potency

	Probe 1			***[H³]estrone sulfate***	
	none	GSH	TCEP		
IC_{50} (nM)	324.3± 182.3	317.6 ± 86.4	1076.5±1338.5	6.5×10^{-7} [a]	80 [b]

[a] The measurement was performed with [H^3] estrone sulfate and MCF-7 cell [25]

[b] The measurement was performed with [H^3] estrone sulfate and placental microsome [26]

1.3. Conclusion

We have developed an activity-based sulfatase probe that generates fluorescent *N*-methylisoindole after cleavage by sulfatases. The reduced fluorescence intensity resulting from the autoxidation of *N*-methylisoindoles was improved by using reducing agents, such as GSH and TCEP, causing a 2-fold increase in the fluorescence intensity compared to the fluorescence intensity in the buffer with no additives. We also demonstrated that this probe had reasonable kinetic parameters under three different assay conditions,

among which Tris buffer and Tris buffer containing GSH appeared to be feasible for potent inhibitor screening. Therefore, probe **1** provides a new assay for measuring sulfatase activity that could be applied to high throughput screening.

1.4. Experiments

1.4.1. General

^{1}H and ^{13}C NMR spectra were collected on a Bruker Advance DPX-300. Fast atom bombardment mass spectrometry (FAB-MS) data were obtained using a JEOL JMS-AX505WA mass spectrometer with m-nitrobenzyl alcohol (NBA) as a matrix and the data were reported in units of mass to charge (m/z). Analytical thin layer chromatography was performed using Kieselgel 60F-254 plates from Merck. Column chromatography was carried out on Merck silica gel 60 (70-230 mesh). UV/vis spectra were collected on a Beckman DU-800 and fluorescent spectra were measured on a Jasco FP-6500 and SpectraMax M2 spectrophotometer. All chemical reagents and Sulfatase from Helix pomatia, (S9626 Sigma) were purchased from either Sigma-Aldrich or TCI and used without any further purification.

1.4.2. Chemical synthesis

We synthesized probe **1** as follows [60, 61, 76, 77].

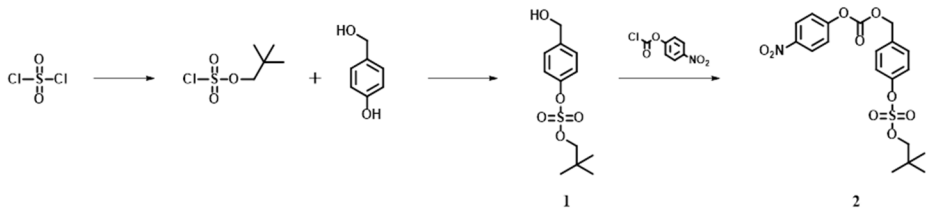

Scheme S 1. Synthesis of sulfatase substrate intermediate (compound **2**)

A solution of sulfuryl chloride (1.62 ml, 20 mmol) in Et_2O was cooled to -75℃ under nitrogen. A solution of neopentyl alcohol (1.76 g, 1 equiv.) and pyridine (1.62 ml, 1 equiv.) in Et_2O was added dropwise to the cooled solution for 1 h. The resulting mixture was warmed to room temperature and stirred for an additional 2 h. The resulting white precipitates were filtered off and the filtrate was concentrated in vacuo. The product was used for a next synthesis step without further purification.

Compound 1: Compound **1** was prepared according to a published procedure [76]. To a solution of 4-hydroxybenzylalcohol (1.7 g, 1 equiv.) in anhydrous THF, sodium hydride (437 mg, 1.1 equiv.) was slowly added at 0℃. After 10 min, the crude neopentyl chlorosulfate was added to the reaction mixture. Then, the reaction mixture was warmed to room temperature, and stirred overnight. Upon completion, sodium hydride in the reaction mixture was quenched with water and THF was removed in vacuo. Ethyl acetate was added to the residue and the organic layer was washed with brine, then dried over Na_2SO_4 and concentrated in vacuo. The crude product was purified by silica gel chromatography (chloroform:acetone = 50:1) to give compound **1** (970 mg, 17% yield). ^{1}H NMR (300 MHz, $CDCl_3$) δ 1.02 (9H, s), 4.10 (2H, s),

4.74 (2H, s), 7.31 (2H, d, *J* = 8.7 Hz), 7.44 (2H, d, *J* = 8.5 Hz).

Compound 2: To a solution of 4-nitrophenyl chloroformate (640 mg, 1.1 equiv.) in anhydrous THF was added pyridine (257 µL, 1 equiv.) at 0°C. After stirring for 20 min, a solution of compound **1** (970 mg, 3.54 mmol) in anhydrous THF was added dropwise over a 10-min period, and the mixture was allowed to warm up to room temperature [77]. Stirring was continued at room temperature for 16 h and then the solvent was removed *in vacuo*. The residue was dissolved in ethyl acetate and washed with saturated aqueous NH_4Cl solution several times and concentrated *in vacuo*. The crude product was purified by silica gel column chromatography (chloroform:acetone = 100:1) to yield compound **2** (784 mg, 1.78 mmol, 50% yield). ^{1}H NMR (300 MHz, $CDCl_3$) δ 1.03 (9H, s), 4.13 (2H, s), 5.32 (2H, s), 7.38 (2H, d, J = 8.5 Hz), 7.41 (2H, d, J = 9.0 Hz), 7.52 (2H, d, J = 8.6 Hz), 8.30 (2H, d, J = 8.5 Hz); ^{13}C NMR (75 MHz, $CDCl_3$) δ 25.86, 31.90, 69.75, 83.69, 115.331, 121.43, 121.81, 125.28, 125.46, 130.30, 133.64, 145.39, 150.48, 155.45; HRMS (FAB): m/z calcd. for $[C_{19}H_{21}NO_9S+Na^+]$ 462.0835, found 462.0838.

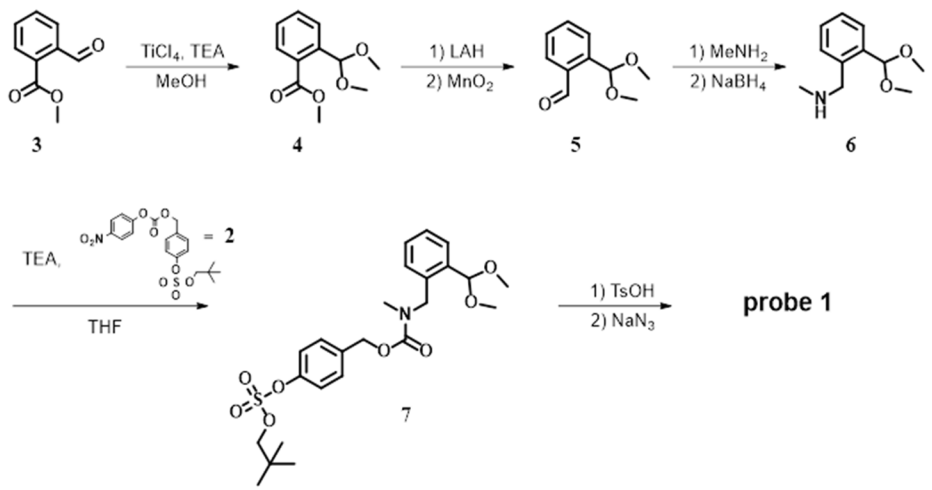

Scheme S 2. Synthesis of probe **1**

Compound 4: To a solution of methyl 2-formylbenzoate (**3**) (1.62 g, 9.87 mmol) in methanol (20 mL) at 0°Cunder N_2 was added 1 M $TiCl_4$ (1 mL, 0.1 equiv.) solution in CH_2Cl_2 in a single step. After stirring for 30 min, the resulting mixture was treated with triethylamine (3 mL, 10 equiv.), and the mixture was stirred for an additional 3 h at room temperature. After removal of all volatile compounds under reduced pressure, the residue was dissolved in ethyl acetate and washed with brine 3 times, dried over Na_2SO_4 and concentrated. The crude residue was purified by silica gel column chromatography (hexane:ethyl acetate = 5:1) to yield compound **4** (1.8 g, 8.56 mmol, 87% yield). ^{1}H NMR (300 MHz, $CDCl_3$) δ 3.39 (6H, s), 3.93 (3H, s), 6.08 (1H, m), 7.40 (1H, t, *J* = 7.5 Hz), 7.53 (1H, t, *J* = 7.6 Hz), 7.76 (1H, d, *J* = 7.7 Hz), 7.82 (1H, d, *J* = 7.6 Hz).

Compound 5: To a suspension of lithium aluminum hydride (250 mg, 2 equiv.) in anhydrous THF compound **4** (900 mg, 4.3 mmol) dissolved in anhydrous THF was slowly added at 0°C under N_2. The reaction mixture was stirred at room temperature for 5 h, and was then cooled to 0°C and quenched

with a 1 M aqueous NaOH solution. The mixture was dried over Na_2SO_4 and filtered through a Celite pad. The filtrate was concentrated *in vacuo*. The resulting product was used for the next synthetic step without further purification.

To a solution of the reduction product (653 mg, 3.59 mmol) dissolved in CH_2Cl_2 was added MnO_2 (3.7 g, 10 equiv.). After being stirred at room temperature overnight, the mixture was filtered with Celite and a silica pad. The filtrate was concentrated *in vacuo* and the residue was purified by silica column chromatography (hexane:ethyl acetate = 3:1) to yield compound **5** (540 mg, 2.98 mmol, 69% yield). ^{1}H NMR (300 MHz, $CDCl_3$) δ 3.42 (6H, s), 5.90 (1H, s), 7.52 (1H, t, J = 7.3 Hz), 7.62 (1H, t, J = 7.4 Hz), 7.70 (1H, d, J = 7.5 Hz), 7.95 (1H, d, J = 7.5 Hz), 10.46 (1H, s).

Compound 6: To a solution of compound **5** (540 mg, 2.98 mmol) in methanol was added a 2 M solution of methylamine in THF (4 mL, 2 equiv.). The resulting mixture was stirred at room temperature overnight, cooled to 0°C and treated with sodium borohydride (570 mg, 5 equiv). The mixture was stirred for 1 h and then quenched with water. After removal of all volatile compounds under reduced pressure, the residue was dissolved in ethyl acetate and washed with saturated aqueous $NaHCO_3$ solution and brine, dried over Na_2SO_4 and concentrated *in vacuo*. Product **6** was used for the next synthetic step without further purification (219 mg).

To a solution of compound **6** (89 mg, 0.46 mmol) in THF were added triethylamine (192 μL, 3 equiv.) and compound **2** (200 mg, 1 equiv.). The mixture was stirred at room temperature overnight and concentrated *in vacuo*, and the residue was dissolved in ethyl acetate and washed with aqueous

$NaHCO_3$ solution and saturated aqueous NH_4Cl solution, dried over Na_2SO_4 and concentrated. The residue was purified by silica column chromatography (chloroform:acetone = 50:1) to yield compound **7** (107 mg, 0.22 mmol, 47% yield). ^{1}H NMR (300 MHz, CDCl3) δ 1.02 (9H, s), 2.92 (3H, d, J = 24 Hz), 3.31(6H, d, J = 10 Hz), 4.10 (2H, s), 4.69 (2H, s), 5.19 (2H, d, J = 15.6 Hz) 5.41 (1H, d, J = 23Hz), 7.16-7.23 (2H, br), 7.31 (3H, m), 7.46 (1H, m), 7.55 (1H, s).

Probe 1: To a solution of compound **6** (57 mg, 0.12 mmol) in acetone was added *p*-toluenesulfonic acid monohydrate (6.5 mg, 0.3 equiv.) and the resulting solution was stirred at room temperature for 2 h. Acetone was removed *in vacuo* and the residue was purified by silica column chromatography (chloroform:acetone = 30:1). The resulting product (50 mg, 0.11 mmol) and sodium azide (10 mg, 1.2 equiv.) were then dissolved in DMF. The resulting solution was heated with stirring at 70°C overnight and concentrated *in vacuo*. The crude product was purified by silica gel column chromatography (CH_2Cl_2:methanol = 10:1) and yielded probe **1** as the sodium salt (37 mg, 0.098 mmol, 88% yield). ^{1}H NMR (300 MHz, CD_3OD) δ 2.95 (3H, s), 4.96 (2H, s), 5.12 (2H, d, J = 21 Hz) 7.21-7.39 (5H, m), 7.52 (1H, t, J = 7.3 Hz), 7.60 (1H, s), 7.92 (1H, d, J = 7.1 Hz), 10.15 (1H, d, J = 19 Hz); ^{13}C NMR (75 MHz, CD_3OD) δ 29.38, 49.67, 66.68, 121.11, 125.85, 127.45, 128.74, 133.58, 133.58, 133.91, 152.35, 193.72; HRMS (FAB): m/z calcd. for $[C_{17}H_{16}NNaO_7S + H^+]$ 402.0623, found 402.0621.

1.4.3. Optical responses of probe 1 with treatment of sulfatases

Fluorescence changes in probe **1** were measured by treating 20 μM probe **1**

with 0.25 mg/mL sulfatase at 37°C in 50 mM Tris-buffer (100 mM NaCl, $MgCl_2$, $CaCl_2$, pH 7.4) in the presence and absence of 1 mM GSH or 1 mM TCEP over a period of 0-70 min as follows;

A stock solution of 10 mM probe **1** was prepared in DMSO. A second stock solution of 500 μM probe **1** was prepared by dissolving 50 μL of the 10 mM probe stock solution in 1 mL of 50 mM Tris buffer. Thereafter, 10 μL of the second probe stock solution (500 μM) was diluted with 200 μL of 50 mM Tris-buffer to give a 20 μM solution of probe **1**. A stock solution of 0.625 mg/mL *Helix pomatia* arylsulfatase (S9626, Sigma-Aldrich) as prepared in 50 mM Tris buffer, and 100 μL of this 0.625 mg/mL sulfatase stock solution and 150 μL of 50 mM Tris-buffer were mixed in a 96-well plate to give a 0.25 mg/mL sulfatase solution.

A stock solution of 0.625 mg/mL sulfatase was prepared in 50 mM Tris buffer containing 1.25 mM GSH or in 50 mM Tris buffer containing 1.25 mM TCEP, and 100 μL of each sulfatase stock solution and 100 μL of 50 mM Tris-buffer containing 1.25 mM GSH or TCEP were mixed with 40 μL of 50 mM Tris buffer without GSH or TCEP and 10 μL of a 500 μM probe stock solution in a 96-well plate to give final concentrations of 0.25 mg/mL sulfatase, 20 μM probe **1**, and 1 mM reducing agents, respectively.

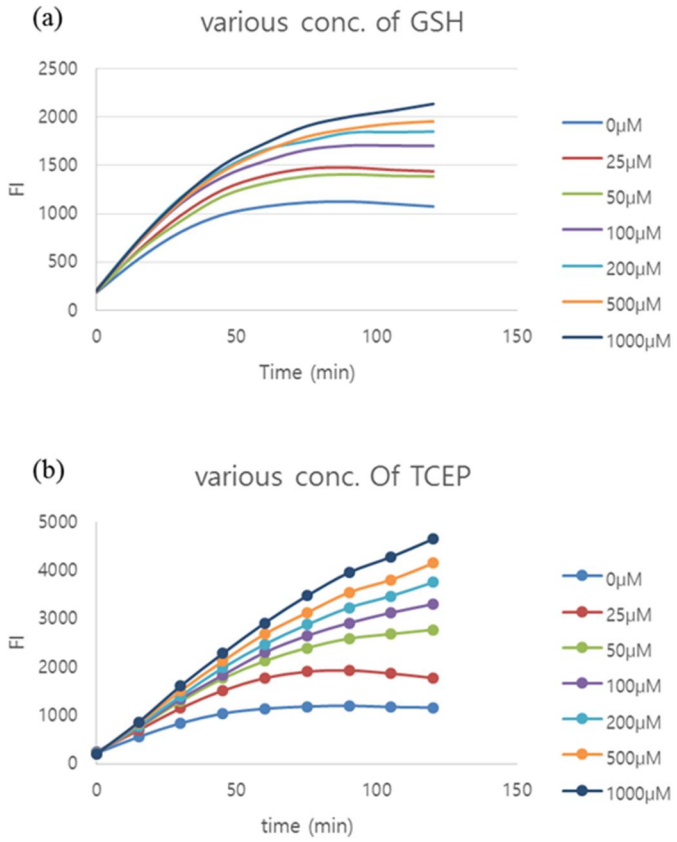

Figure S 1. time-course fluorescence intensity changes under the conditions of various concentration of (a) GSH and (b) TCEP for120min.

1.4.4. Diels-Alder reactions

A mixture of 40 μL of 500 μM probe stock solution and 400 μL of 0.625 mg/mL sulfatase stock solution in 560 μL of 50 mM Tris buffer was incubated for 45 min to generate *N*-methylisoindole. The final concentrations of probe **1** and sulfatase were 20 μM and 0.25 mg/mL, respectively. To generate *N*-methylisoindole under reducing conditions, 40 μL of 500 μM probe stock solution and 160 μL of 50 mM Tris buffer without reducing agents were

added to a microtube containing 400 μL of 0.625 mg/mL sulfatase stock solution dissolved in 1.25 mM GSH- or TCEP-containing buffer and 400 μL of 50 mM Tris buffer with 1.25 mM GSH or TCEP, and the resulting solution was incubated for 45 min. The final concentrations of probe **1**, sulfatase, and reducing agents were 20 μM, 0.25 mg/mL, and 1 mM, respectively. The resulting solution was then poured into a *N*-phenylmaleimide solution in THF and stirred at 70°C overnight. The reaction mixture was extracted with CH_2Cl_2, dried over Na_2SO_4, filtered, and concentrated *in vacuo*. The residue was dissolved in 1 mL of methanol and subjected to liquid chromatography-mass spectrometry (LC/MS) analysis with 1260 infinity (Agilent technologies) (Fig. S2) to monitor for the formation of Diels-Alder adducts.

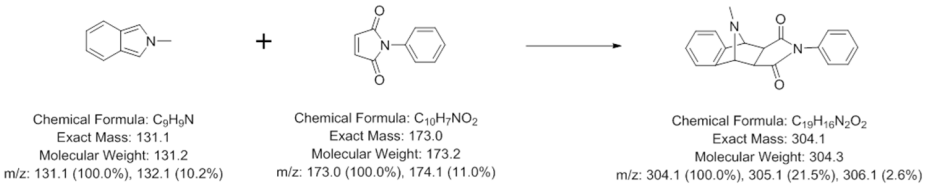

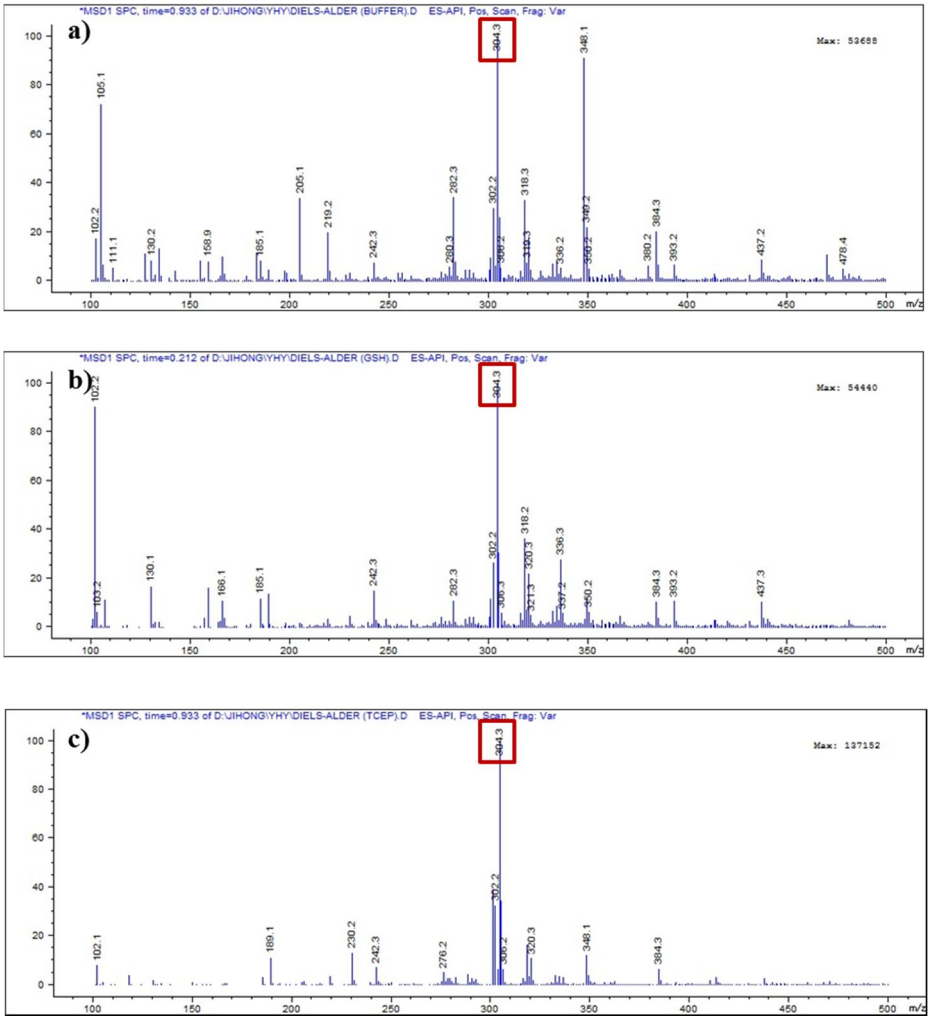

Figure S 2. MS analysis after diels alder reactions of products of probe 1 with sulfatase in 50mM Tris buffer containing a) no additive, b) 1mM GSH, and c) 1mM TCEP.

1.4.5. Fluorescence changes upon sulfatase treatment in acidic conditions

Fluorescence changes of probe **1** with the treatment of sulfatase were measured by treating 20 μM probe **1** with 0.25 mg/mL sulfatase at 37°C in 50 mM Tris-buffer (100 mM NaCl, 1 mM $MgCl_2$, 1 mM $CaCl_2$, pH 7.4) and 100

mM potassium acetate buffer (100 mM NaCl, 0.25 mM $MgCl_2$, 0.25 mM $CaCl_2$, 0.25 mM $MnCl_2$ pH 5.0) in the presence and absence of 1 mM GSH or 1 mM TCEP over a period of 0-70 min. Sulfatase from Helix pomatia (S9626) was reported to show activity at pH 5.0 and 37˚C

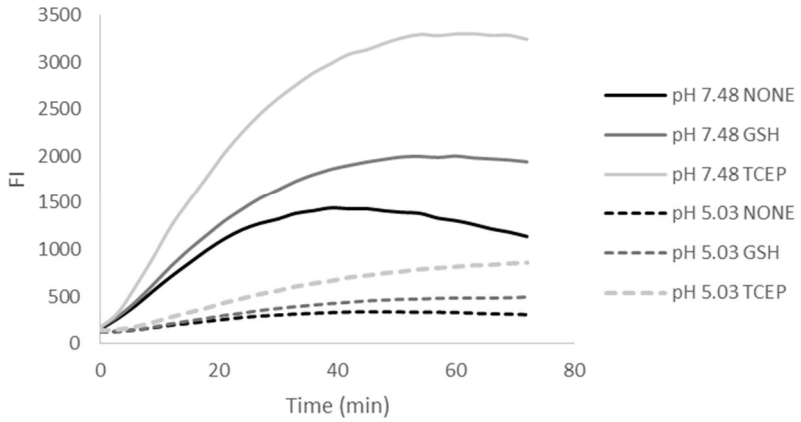

Figure S 3. Fluorescence enhancement of probe 1 upon the treatment of sulfatase in neutral and acidic conditions with and without reducing agents in time-dependent manner.

1.4.6. Enzyme kinetics

Kinetic experiments were carried out using 0.25 mg/mL sulfatase and various concentrations of probe **1** (50, 20, 10, 5, 2.4, 1.2 μM) at 37°C in 50 mM Tris buffers with and without 1 mM reducing agents (pH 7.4). Fluorescence measurements were performed using a SpectraMax M2 multi-detection reader (Molecular Device). The rate of increase in fluorescence intensity at 415 nm when excited at 325 nm was measured to determine the kinetic parameters of enzyme hydrolysis. The values of the kinetic parameters (K_m and V_{max}) were obtained by fitting the data to the Michaelis-Menten equation. K_m and V_{max}

values were calculated by nonlinear fitting of the Michaelis–Menten equation using SigmaPlot 8.0 (Systat Software Inc.) (Fig. S3).

a)

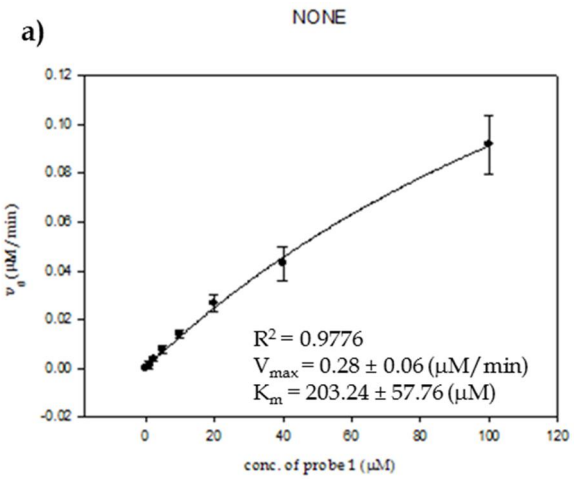
NONE
v_0 (μM/min)
conc. of probe 1 (μM)
R^2 = 0.9776
V_{max} = 0.28 ± 0.06 (μM/min)
K_m = 203.24 ± 57.76 (μM)

b)

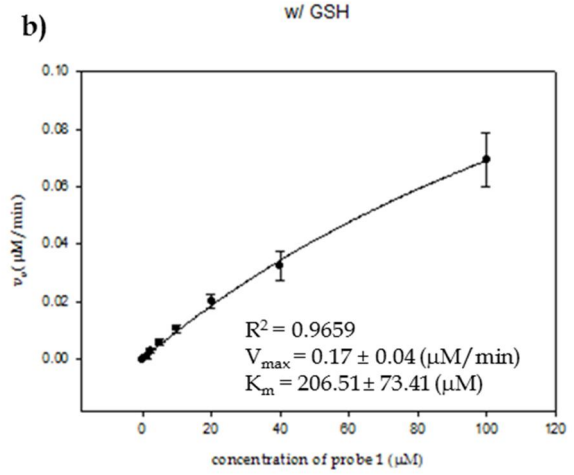
w/ GSH
v_0 (μM/min)
concentration of probe 1 (μM)
R^2 = 0.9659
V_{max} = 0.17 ± 0.04 (μM/min)
K_m = 206.51 ± 73.41 (μM)

c)

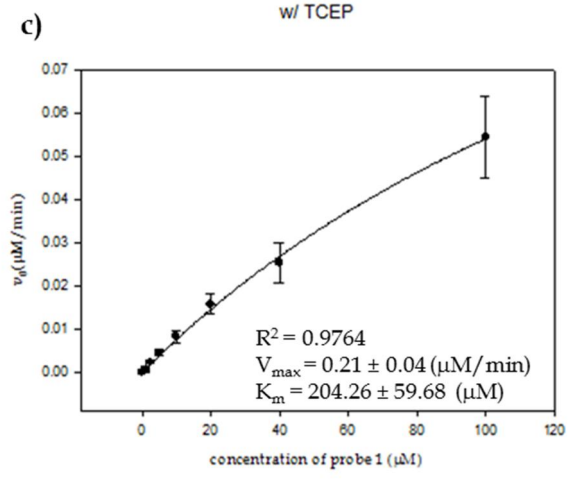
w/ TCEP
v_0(μM/min)
concentration of probe 1 (μM)
R^2 = 0.9764
V_{max} = 0.21 ± 0.04 (μM/min)
K_m = 204.26 ± 59.68 (μM)

Figure S 4. Calculated Km and Vmax values when probe 1 reated with sulfatase in 50mM Tris buffer containing a) no additive, b) 1mM GSH, and c) 1mM TCEP.

1.4.7. Inhibitory potency measurements

Measurements of inhibitory potency were carried out with 0.25 mg/mL sulfatase, 20 μM probe **1**, and various concentrations of estrone 3-O-sulfamate (EMATE, 0, 12, 25, 50, 100, 200 and 500 nM) at 37°C in 50 mM Tris buffers with and without 1 mM reducing agents (pH 7.4) as follows:

A mixture of 100 μL of sulfatase stock solution (0.625 mg/mL) and 40 μL of various concentrations of EMATE in 100 μL of 50 mM Tris buffer was incubated in a 96-well plate for 1 h at 37°C. Following this, 10 μL of the second probe stock solution (0.5 mM) was added to make the final volume 250 μL and fluorescence intensities were measured. The final concentrations of EMATE were 0, 12, 25, 50, 100, 200 and 500 nM. For the measurements of inhibitory potency under reducing conditions, sulfatase stock solutions dissolved in 50 mM Tris buffer containing 1.25 mM GSH or TCEP were used. The rate of decrease in fluorescence intensity at 415 nm was measured to determine the IC_{50} of EMATE. The IC_{50} values were calculated by fitting with the Hill equation using Sigmaplot 8.0 (Fig. S4).

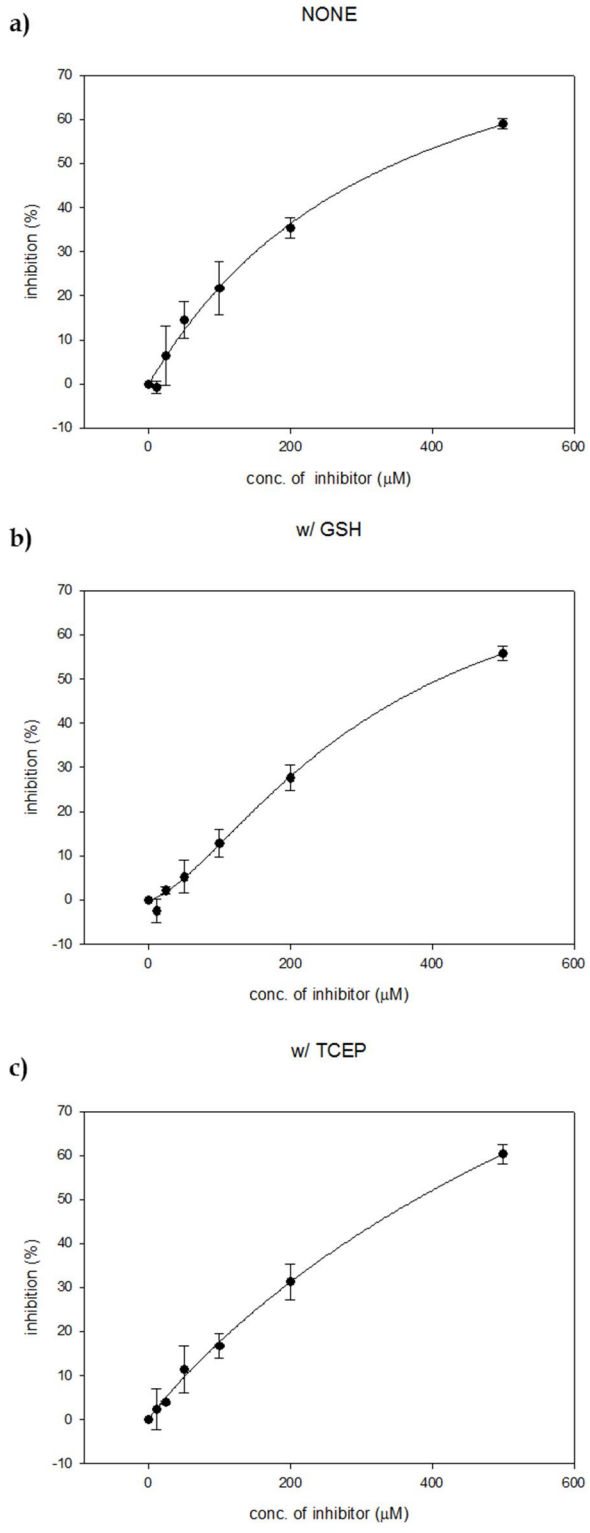

Figure S 5. Inhibitory potency when the reaction carried out in 50mM Tris buffer

containing a) no additive, b) 1mM GSH, and c) 1mM TCEP.

Section 2.
Detection of bacterial sulfatase activity and discrimination of periplasmic sulfatase activity through liquid- and solid-phase colony-based assays

2.1. Introduction

Sulfur is a chemical element essential to all organisms, as it is required for the biosynthesis of cysteine and methionine; it is also involved in many redox reactions that take place in biological systems [78]. Microorganisms are capable of acquiring sulfur for biosynthesis by assimilating inorganic sulfates or organosulfur compounds, such as sulfonates and sulfate esters [78, 79]. Bacterial arylsulfatases catalyze the hydrolysis of aromatic sulfate esters and participate in the metabolic pathways through which sulfur is procured by organosulfur compounds. Considering the ability to degrade organosulfur compounds, bacterial arylsulfatases would be useful for many areas such as industry and agriculture.[80] In practice, bacterial arylsulfatases are applied in

the desulfation of agar [81-83]. Their activity is strongly influenced by the bacterial growth environment conditions and thus their measurements can be used for soil quality assessment [84, 85]. In addition, it was suggested that sulfatase activity is related with the degradation of endosulfan, an extensively used insecticide [86, 87]. Recently, it was reported that sulfatases are potentially implicated in bacterial pathogenesis [88]. In some reports, bacterial sulfatases might be involved in decomposition of sulfated mucins [89] and reconstruction of extracellular structures by desulfation of glycosaminoglycans [90] for bacterial infection. However, despite of the various usages and the importance of sulfatase activity, only a few bacterial sulfatases were characterized.

Sulfatases contain the conserved Cys/Ser-X-Pro-X-Arg motif in their active sites. The first residue of the motif, which can be either cysteine or serine, is post-translationally modified to form C_{α}-formylglycine (FGly), a unique amino acid that is the key catalytic residue for sulfate ester cleavage.[53, 91] In eukaryotes, the first residue of the motif is cysteine; inability to post-translationally modify this residue to form FGly in humans results in a rare lysosomal storage disease called multiple sulfatase deficiency (MSD) [52, 53, 92]. In prokaryotes, the first residue of the active site motif, i.e., the FGly progenitor, can be either cysteine or serine [93-95]. Accordingly, bacterial arylsulfatases are classified into Ser- and Cys-type enzymes. All known Ser-type arylsulfatases are periplasmic, whereas Cys-type arylsulfatases are located in the cytosol of bacteria. The two types of arylsulfatases are believed to either have different FGly formation pathways or have a common pathway but different modulating cofactors, with these cofactors localized in the periplasm or the cytosol in the cases of Ser- and Cys-type enzymes,

respectively [78]. Elucidation of the FGly formation pathways has been the focus of intense research efforts [95-99]. These reports meant that bacterial arylsulfatase activity depends on post-translational regulation; moreover, the location or stability of arylsulfatases relates to FGly progenitors and FGly formation pathways and all expressed sulfatases may not be capable to hydrolyze sulfate ester [53, 100]. Thus, it is necessary to develop diverse assay methods to detect the activity of sulfatases.

Determination of microorganisms expressing arylsulfatase requires a simple and easy assay method. Investigation into the FGly formation pathways also requires a simple and easy assay method for distinguishing each type of sulfatases. Many methods for detection of arylsulfatase activity used bacteria cell lysates which were prepared through time–consuming and complicated processes and they are unable to determine the type and location of arylsulfatases in one step. Colony-based assays are simple methods and enable to reduce sample preparation time. In addition, they also allow functional information to be acquired in an organism's physiological environment [7]. Solid-phase assays are proper ways to screen and isolate the potential bacterial strains that express arylsulfatases. Solid-phase assays that exhibit sharp and clear image changes according to sulfatase activity are particularly useful in directly detecting individual colonies of interest [101-103] and they could offer easy methods for industrial applications [104, 105]. Therefore, a colony-based solid-phase assay method would be most appropriate one to study bacterial arylsulfatases.

Activity-based probes, based on detecting specific enzymatic activity in a cellular context, are powerful tools for enzyme activity assays [106]. Previously reported activity-based probes for sulfatase activity assays

contained luminophores and sulfate esters, with sulfatase activity inducing an optical response [59-61, 63]. One of the probes was able to distinguish sulfatases of different mycobacterial strains. Although those probes were characterized by fast response times and low detection limits, they were deployed in purified enzyme solutions or bacterial lysates.

We previously reported an activity-based probe **1** (Scheme 1), which enables detection of sulfatase activity in purified enzyme solutions through fluorescence enhancement [107]. Probe **1** consists of sulfate ester as a substrate and benzaldehyde as a responsive unit, which are linked with a self-immolative moiety. The cleavage of the sulfate ester in probe **1** by sulfatase is followed by intramolecular cyclization, resulting in the formation of *N*-methyl isoindole which emits fluorescence at 415 nm. However, *N*-methyl isoindole is unstable and easily undergoes autooxidation and polymerization [67, 68, 70]. The polymerization of *N*-methyl isoindole would trigger the formation of colored precipitates when a higher concentration of probe **1** was incubated with sulfatase for a longer period of time (Scheme 2). These properties of probe 1 enabled us to detect sulfatase activity and discriminate two types of arylsulfatases through liquid- and solid-phase colony-based assays. It has been reported that solid-phase assays are particularly useful in directly detecting individual colonies of interest [101-103].

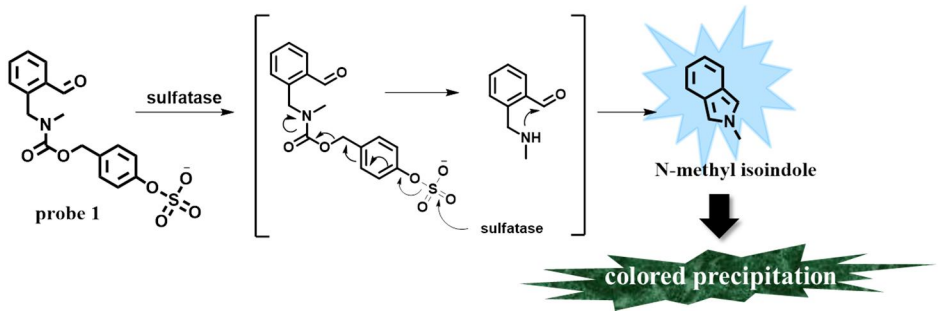

Scheme 2. Structures of probe 1 and the product created upon treatment with sulfatases.

2.2. Results and Discussion

To evaluate the ability of probe **1** to detect sulfatase activity, we compared the fluorescence intensities and color changes of probe **1** in the presence or absence of a commercially available arylsulfatase from *Helix pomatia* and *Aerobacter aerogenes*. We used 1 mM probe **1** and 0.1 mg/ml of sulfata se from *H. pomatia*, dissolved in 50 mM Tris buffer at pH 7.4. For abo ut one hour after the initiation of the reaction with the sulfatase, the fl uorescence intensity increased in a time-dependent manner. Then, the int ensity decreased and colored precipitates formed spontaneously (Fig. 12, Fig. S6, and S7). The fluorescence enhancement was elicited by the gene ration of *N*-methyl isoindole upon treatment with the sulfatase [107], wh ile precipitation might be caused by post-polymerization of *N*-methyl iso indole molecules [102]. These results indicated that probe **1** could be uti lized for sulfatase activity assays based on the enhancement of fluoresce nce and the formation of colored precipitates.

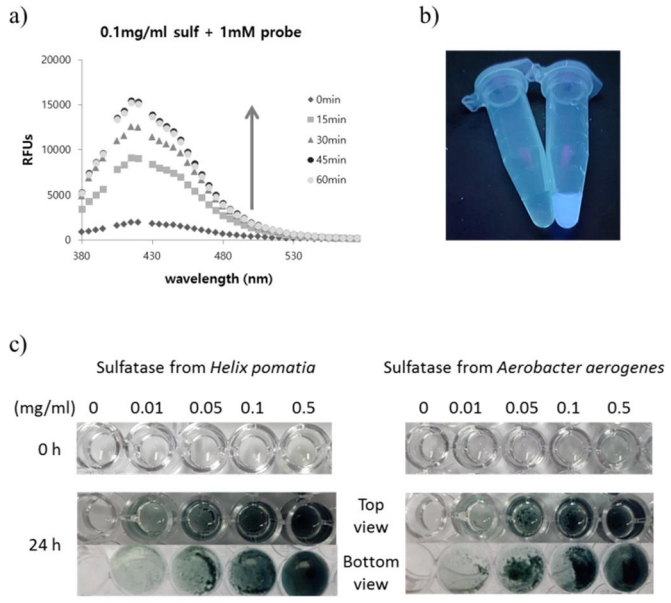

Figure 12. a) Fluorescence intensity enhancement of probe **1** upon treatment with sulfatase, b) fluorescent emission of probe **1** under UV lamp incubated with sulfatase for 30min and c) generation of colored precipitates after 24-hour incubation; 1 mM probe 1 with sulfatase from *Helix pomatia* (left) and from *Aerobacter aerogenes* (right).

We also measured kinetic parameters and detection limits of probe **1**. For the calculation of the kinetic values, we used 0.02 mg/ml sulfatase from *A. Aerogenes* in 50 mM Tris buffer (pH 7.48) at 37℃. As shown in Table 3 and Figure S8, the K_m and V_{max} values of sulfatase from *A. Aerogenes* were determined using probe **1** to be 187 ± 13 μM and 10.9 ± 0.2 μM/min, respectively. The K_m value obtained using probe **1** was comparable to those obtained using previously reported fluorogenic sulfatase activity probes, 3-O-methylfluorescein-sulfate (MFS) and resorufine-sulfate (RS) [61]. In addition, comparing to the V_{max} values of MFS and RS which were determined to be 1.25 ± 0.08 pmol/s and 10.1 ± 0.2 pmol/s [61], probe **1** reacted with sulfatase

from *A. Aerogenes* more rapidly. These values indicated that probe **1** could be a good substrate for bacterial sulfatases. To determine the detection limit (LOD) values, 1 mM probe **1** was used in 50 mM Tris buffer at 37℃ (pH 7.48). LOD values of probe **1** calculated through fluorescence enhancement were 61 ng/ml for *H. Pomatia* sulfatase and 35 ng/ml for *A. Aerogenes* sulfatase (Table 3 and Table S1). On the other hand, the LODs for *H. Pomatia* sulfatase and *A. Aerogenes* sulfatase determined by UV absorbance changes at 630 nm after 2 hour incubation were 2.5 μg/ml and 1.99 μg/ml, respectively. The reported LODs of a fluorogenic probe MFS and a chromogenic probe *p*-NPS were 158 ng and 15.8 ng after 10 min incubation [61]. Considering the incubation time, the LOD values measured by fluorescence changes of probe **1** would be similar to the reported values of MFS and RS, but the LOD value measured by UV absorbance of probe **1** was larger than that of *p*-NPS. This is presumably due to the post-polymerizaion of *N*-methyl isoindole, which was generated and accumulated through the hydrolysis of probe **1** by sulfatases. In spite of the less sensitivity and longer incubation time for the observation of color changes, probe **1** could also provide an easy and simple detection method through naked eye. Thus, these results showed that probe **1** could detect sulfatase activity by fluorometric and colorimetric assays.

Table 3. Kinetic parameters of *A. Aerogenes* sulfatase and detection limits

	K_m (μM)	V_{max} (μM/min)	LOD (FI) (ng/ml)	LOD (UV) (μg/ml)
Probe **1**	187±13	10.9±0.2	35.3±2.6 [b]	1.99±0.09 [c]

MFS [a]	598±67	(75±4.8)×10^{-6}	158[d]	
RS [a]	162±10	(606±12)×10^{-6}	15.8[d]	
p-NPS [a]	1,800±120			0.0158[d]

[a] The values were reported in reference, Smith et al. 2014.

[b] The values were calculated by fluorescence intensity changes at 415 nm after 30 min incubation.

[c] The values were calculated by UV absorption changes at 630 nm after 2 hour incubation.

[d] The values were obtained after 10 min incubation.

Our next step was to apply probe **1** to microorganisms in order to determine the feasibility to detect arylsulfatase activity and discriminate two types of arylsulfatases in colony-based liquid-phase assays. *Klebsiella aerogenes*, *Pseudomonas aeruginosa*, *Mycobacterium avium*, *Mycobacterium smegmatis*, and *Staphylococcus aureus* were used for the tests. *Klebsiella aerogenes* and Pseudomonas aeruginosa are both gram-negative bacterium, but *K. aerogenes* expresses a Ser-type sulfatase localized in the periplasm, whereas *P. aeruginosa* produces a Cys-type sulfatase localized in the cytosol [93, 95, 97]. *Mycobacterium avium* and *Mycobacterium smegmatis* possessing arylsulfatase activity which might be related with infection and their sulfatase activity was reported to exhibit in membrane fractions [108] and *Staphylococcus aureus* lacking sulfatase genes was used as a control [109]. Colony-based liquid-phase assays were performed by incubating 1 mM probe **1** with bacterial cultures (OD_{600}= 3.0) or with 5.0 × 10^{10} cfu/ml of *K. aerogenes* colony in 50 mM Tris buffer (see supplementary

section) [110-114]. The fluorescence intensities of probe **1** incubated with *K. aerogenes*, *M. avium* and *M. smegmatis* colonies and lysates for about an hour increased by 2~6-fold (Fig. 13a, S9 and S11), while there were no fluorescence changes of probe **1** incubated with *S. aureus* colonies and lysates that lack sulfatase genes and activity. These results indicated that three bacterial colonies and lysates having sulfatase activity hydrolyzed the sulfate ester of probe **1** to generate fluorescent *N*-methyl isoindole. Moreover, coloured precipitates were observed in the lysates of *K. aerogenes*, *M. avium*, and *M. smegmatis* after overnight incubation with probe **1**, while probe **1** incubated with *K. aerogenes* and *M. avium* colonies generated coloured precipitates after 3 days (Fig. 13). In case of *M. smegmatis* colonies, the fluorescence intensity was slowly increased but coloured precipitates were rarely observed (Fig. 13b and S11): The sulfate ester moiety of probe **1** was slowly hydrolysed by *M. smegmatis* colonies to generate *N*-methyl isoindole which was not effectively polymerized. It was presumed that slow hydrolysis rate of *M. smegmatis* colonies generated insufficient amounts of *N*-methyl isoindole, thus precluding the consequent polymerization (Fig. S11). Incubation of probe **1** with *S. aureus* colonies and lysates generated no coloured precipitates (Fig. 13). To confirm that the changes in the fluorescence signal was solely due to sulfatases, the specific activity of sulfatases which was measured by fluorescence changes of probe **1** incubated with different concentrations of protein of *M. avium* lysate for 30 min were compared. The values of specific activities between different concentrations of the proteins were almost identical, which indicated that the fluorescence enhancement of probe **1** was induced by

sulfatase in *M. avium* (Fig. S11). As a result, it was implied that the sulfate ester of probe **1** was cleaved to generate a fluorescent *N*-methyl isoindole by colonies and lysates of *K. aerogenes*, *M. avium* and *M. smegmatis* having sulfatase activity, and a sufficient amount of *N*-methyl isoindole accelerated the formation of coloured precipitates. In contrast, probe **1** did not react with *S. aureus* which lacks sulfatase genes. Therefore, probe **1** can be used to detect sulfatase activity of bacteria through fluorescence enhancement and naked eye in liquid-phase colony-based assays.

In addition, to demonstrate the capability of probe 1 to distinguish periplasmic from cytosolic sulfatase, the results from *K. aerogenes* and *P. aeruginosa* was compared. In this study, 1 mM of probe **1** was incubated with 5.0×10^{10} cfu/ml of each bacterial colony at the corresponding optimal conditions (see supplementary section) [110-114]. The fluorescence intensity of the probe incubated with *K. aerogenes* increased during the first hour of treatment, while colored precipitates were observed after overnight incubation (Fig. 13 and Fig. S9). In contrast, the fluorescence of the probe incubated with *P. aeruginosa* remained unchanged and no precipitates were generated (Fig. 13 and Fig. S10). These results implied that the sulfate ester of the probe was cleaved when incubated with *K. aerogenes* colonies, but not with *P. aeruginosa* colonies. This phenomenon could be attributed to the different location of each sulfatase. Specifically, the presence of a sulfate anion in probe **1** might preclude it from entering the cytosol, thus preventing it from reacting with the cytosolic Cys-type sulfatase of *P. aeruginosa*. In order to test this hypothesis, we incubated overnight 1 mM of probe **1** with lysates from each of the two bacteria. In *K. aerogenes*, the lysates gave results similar

to the ones obtained from the colonies, i.e., a fluorescence enhancement and the formation of coloured precipitates (Fig. 13). Moreover, the rate of fluorescence enhancement was dependent upon *K. aerogenes* colony and lysate, respectively (Fig S11). In the case of *P. aeruginosa*, there were clear differences between colonies and lysates. Unlike colonies, where no reaction with probe **1** was observed, *P. aeruginosa* lysates incubated with probe **1** exhibited an increase in the fluorescence intensity that reached a plateau after 100 minutes, while coloured precipitates were observed after overnight incubation (Fig. 13 and S10). The rate of fluorescence enhancement of probe **1** was also increased with increasing of the protein amount in *P. aeruginosa* lysate (Fig. S10). The relatively weaker responses of probe **1** in the presence of the *P. aeruginosa* lysate compared to the *K. aerogenes* lysate might be caused by the arylsulfatase of *P. aeruginosa* being less specific for probe **1** or expressed at a low level under the experimental conditions. Nevertheless, probe **1** exhibited distinct changes when incubated with the *P. aeruginosa* lysate (Fig. 13), indicating that probe **1** was hydrolyzed by the *P. aeruginosa* sulfatase. These results clearly suggested that location of the target enzymes was responsible for the lack of changes when the probe was incubated with *P. aeruginosa* colonies. Since probe **1** only reacts with periplasmic sulfatases due to its inability to enter the cytosol, the *N*-methylisoindole and their precipitates might be localized in the periplasmic space of the bacteria. To observe the location of the *N*-methylisoindole precipitates, transmission electron image (TEM) analysis was performed. *K. aerogenes* colony incubated with probe **1** overnight was prepared as a sample and *K. aerogenes* colony withour probe **1** was used as control. Compared to *K. aerogenes* colony without probe **1**, *K. aerogenes* incubated with probe **1** showed that the

periplasmic space was filled with electron-dense material (Fig. S12). However, the electron-dense material could not be confirmed to be identical to *N*-methylisoindole precipitates and probe **1** was improper to image of periplasmic sulfatase in bacteria cells. Despite of the incapability of probe **1** to image the location of sulfatase in *K. aerogenes*, the colony-based assays with probe **1** may be able to discriminate Ser-type periplasmic arylsulfatases from Cys-type cytosolic arylsulfatases in a single step.

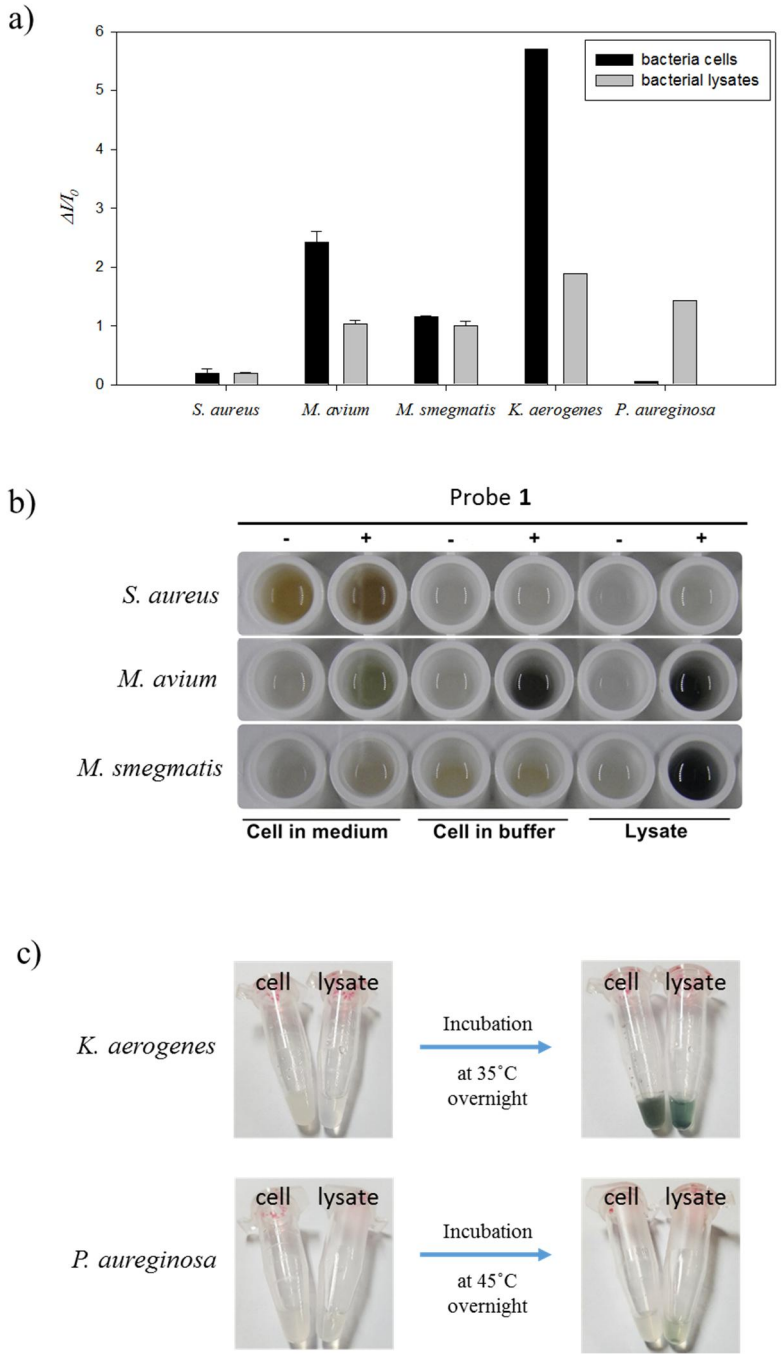

Figure 13. a) Fluorescence intensity changes of 1 mM probe **1** incubated with *K. aerogenes* colonies (5.0×10^{10} cfu/ml) and lysates (0.37 mg of protein/ml) at 35 °C for 80 min. b) Fluorescence intensity changes of 1 mM probe **1** incubated with *P.*

aeruginosa colonies (5.0×10^{10} cfu/ml) and lysates (0.43 mg of protein/ml) at 45 °C for 100 min. c) Formation of coloured precipitates after incubation of 1 mM probe **1** with *K. aerogenes* colonies (left) and lysates (right) at 35 °C overnight. d) Coloured precipitates were not formed after incubation with *P. aeruginosa* colonies (left) but were formed after incubation with lysates (right) at 45 °C overnight.

Finally, we assessed the applicability of probe **1** to colony-based solid-phase assays. Solid-phase assays enjoy the advantage of accurate staining, allowing the identification of target location and the selection of target colonies under heterogeneous conditions. Colonies of *K. aerogenes* and *P. aeruginosa* on cellulose acetate membrane filters (0.2 μm pore size) were placed on the top of filter papers soaked in 5 mM probe solution and incubated at 37 °C overnight. As shown in Figure 14, dark coloured colonies were observed on the membrane filter of *K. aerogenes* which was placed on the filter papers soaked in probe solution, whereas only faint colonies were visible on the membrane filter of *K. aerogenes* without probe **1**. Compared to dark coloured K. aerogenes colonies incubated with probe **1,** only faint colonies were visible on the membrane filter of *P. aeruginosa* (Fig. S13). These results indicated that probe **1** is suitable for colony-based solid-phase assays as its treatment with sulfatase leads to the formation of an insoluble coloured product. Therefore, probe **1** can also be deployed in solid-phase assays for distinguishing periplasmic sulfatase from cytosolic sulfatase and identifying colonies that express Ser-type periplasmic sulfatases.

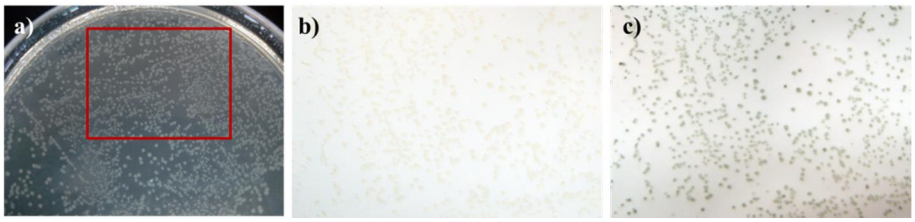

Figure 14. *K. aerogenes* a) on agar plate, b) on membrane filters without and c) with probe **1**.

2.3. Conclusion

In summary, an activity-based probe 1 was successfully used for detection of bacterial arylsulfatase activity in liquid- and solid-phase assays. Probe 1 was hydrolyzed by bacterial sulfatase, generating *N*-methyl isoindole that leads to fluorescence enhancement and colored precipitates. Although longer incubation time and enough accumulation of *N*-methyl isoindole were required to generate colored precipitates, probe 1 is applicable to bacterial sulfatase activity assays in liquid- and solid-phase through the observation of color changes as well as fluorescence enhancements. Moreover, because of the impermeability of bacterial cytosol to probe 1, the probe was able to discriminate between Ser-type *K. aerogenes* periplasmic sulfatases and Cys-type *P. aeruginosa* cytosolic sulfatases in both liquid- and solid-phase bacterial colony-based assays. Consequently, our probe may offer a simple method for screening and sorting of the potential bacterial colonies expressing arylsulfatases, especially, containing Ser-type periplasmic sulfatases.

2.4. Experiments

2.4.1. General

^{1}H and ^{13}C NMR spectra were taken on a Bruker Advance DPX-300 or a Bruker Advance 500 spectrometer. Chemical shifts are given in parts per million using as internal reference the residual resonances of deuterated solvents (^{1}H NMR chemical shifts: δ = 7.27 ppm for $CDCl_3$, δ = 2.05 ppm for acetone-d_6 and δ = 2.50 ppm for $(CD_3)_2SO$) (^{13}C NMR chemical shifts: δ = 77.23 ppm for $CDCl_3$, δ = 205.87, 30.60 ppm for acetone-d_6 and δ = 39.51 ppm for $(CD_3)_2SO$). Fast atom bombardment mass spectrometry (FAB-MS) data were obtained using a JEOL JMS-AX505WA mass spectrometer with m-nitrobenzyl alcohol (NBA) as a matrix and were reported in units of mass to charge (m/z). Analytical thin layer chromatography was performed using Kieselgel 60F-254 plates from Merck. Column chromatography was carried out on Merck silica gel 60 (70-230 mesh). UV/vis spectra were collected on a Beckman DU-800 and fluorescent spectra were collected on a Jasco FP-6500 and SpectraMax M2 spectrophotometer at 37℃ unless noted otherwise. Ultrasonications were carried out on Fisher 550 Sonic Dismembrator and centrifugation was carried out on Combi-514 of Hanil Sciences Industrial Cooperation.

All chemical reagents and sulfatases from *Helix pomatia,* (**S9626 Sigma**) were purchased from either Sigma-Aldrich or TCI and used without any further purification.

2.4.2. Preparation

2.4.2.1. Cultures and growth conditions

Klebsiella aerogenes (Hideko Urushihara, University of Tsukuba) and *Pseudomonas aeruginosa* KACC10186 (ATCC 9027) supplied by Prof. Kyeong-Ryang Park (Hannam Univ., Deajeon, Korea) were cultured in nutrient medium or nutrient agar plates at 30℃ for *K. aerogenes* and 35℃ for *P. aeruginosa* [110-114]. Growth was monitored by the optical density at 600 nm. Amounts of colonies were determined by standard plate count method.

2.4.2.2. Lysis

Each cultured colony was washed 3 times with 1 x PBS. *K. aerogenes* colonies were collected in 50 mM Tris buffer (pH 7.4) and *P. aeruginosa* colonies were collected in 50 mM Tris buffer (pH 8.9) and they were ultrasonicated in ice bath. Debris was removed by centrifugation (3500 rpm for 30 min at 4℃). Protein concentrations were quantified using the Bradford assay (BioRad) with bovine serum albumin (BSA) as the calibrating standard.

The fully-grown bacterial culture was centrifuged at 3300 rpm for 10 minutes. The collected pellets were washed three time with distilled water and then re-suspended in 50 mM Tris-buffer (pH 7.4) with a final OD_{600} of 3.0. To obtain lysate of the bacteria, 300 µl of the re-suspension was added to a 1.5 ml sonication tube and then sonicated for 5 minutes. After the sonication, centrifuge was applied and the supernatant was transferred to a new tube. The Bradford method was used to determine the protein concentration of the lysate.

2.4.3. Experiments

2.4.3.1. Optical response of probe 1 dependent on purified sulfatase activity

Biochemical activity assays with purchased *H. Pomatia* sulfatase (Sigma, S9226) were carried out in 96 well-plate with total volume of 250 μl at 37℃ and pH 7.4. Stock solution of sulfatases was prepared to be 0.625 mg/ml in 50 mM Tris buffer (500 mM NaCl, 1 mM $MgCl_2$, 1 mM $CaCl_2$, pH 7.4) and stock solution of probe **1** was prepared to be 100 mM in DMSO. Then, 1 mM probe and various amounts of sulfatase in 50 mM Tris buffer were used. Fluorescent intensity (λ_{ex}=327 nm, λ_{em}=415 nm) was measured time-dependently (0– 165 min.).

For the observation of colored precipitates, 1 μl of probe stock solution, 16 μl of 0.625 mg/ml sulfatase solution and 83 μl of 50mM Tris buffer were added in a microtube. The final concentration of probe **1** and sulfatase was 1 mM and 0.1 mg/ml sulfatase, respectively. The solution was incubated at 37℃. The precipitates were observed after 2 h, 4 h and overnight (Fig. S6c).

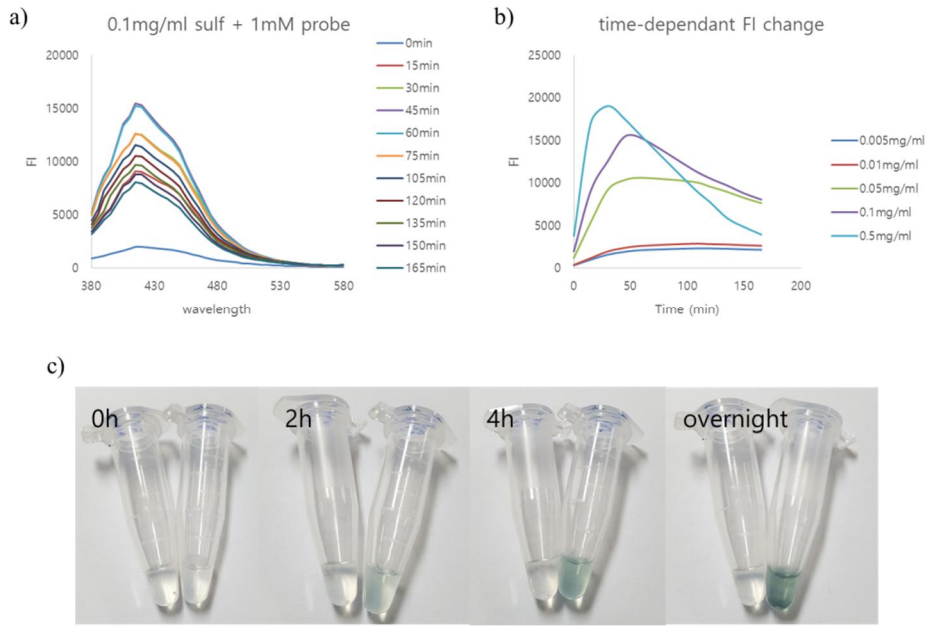

Figure S 6. (a) fluorescence changes of 1 mM probe **1** with 0.1 mg/ml of sulfatase, (b) time-dependent fluorescence changes of 1 mM probe **1** with various amounts of sulfatase, (c) time-course generation of colored precipitates; probe **1** with (right) and without (left) sulfatase

For the UV absorbance studies, 1 mM probe 1 with various amounts of sulfatase were incubated at 37℃. Stock solution of *A. aerogenes* sulfatase was prepared to be 0.05 mg/ml in 50 mM Tris buffer (500 mM NaCl, 1 mM $MgCl_2$, 1 mM $CaCl_2$, pH 7.4).

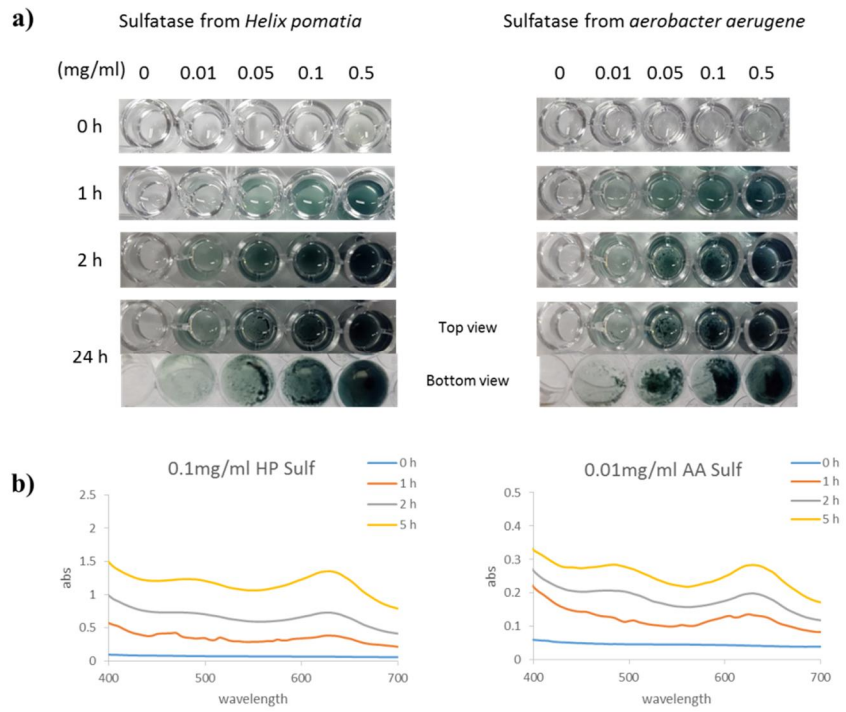

Figure S 7. (a) Formation of colored precipitates upon incubation of 1 mM probe 1 with various concentrations of sulfatase from H. pomatia (left) and A. aerogenes (right) at 37℃ for 1 h, 2 h and 24 h, b) time-course UV absorption changes upon treatment of probe 1 with sulfatase from H. pomatia (left) and A. aerogenes (right).

2.4.3.2. Enzyme kinetics and limit of detection

Kinetic experiments of probe **1** with *A. aerogenes* (AA) sulfatase were carried out at 37 °C in 50 mM Tris buffer (pH 7.48). The fluorescence intensities of a series of different concentrations of probe **1** (0, 10, 20, 50, 100, 200, 500, 1000 and 2000 μM) with AA sulfatase (0.02 mg/mL) in a 96-well black bottom plate were measured in a time-dependent manner. The rate of increase in fluorescence intensity at 415 nm was used to determine the kinetic parameters of enzyme hydrolysis. The kinetic parameters (K_M and V_{max}) were determined from triple-reciprocal plots of hydrolysis rates versus substrate

concentration (Michaelis-Menten plot).

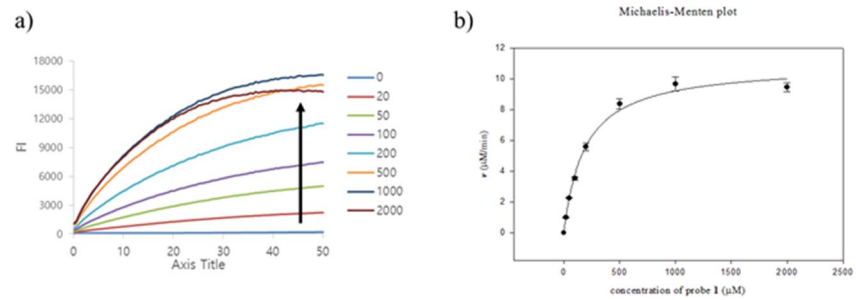

Figure S 8. a) Fluorescence intensity enhancement of probe 1 in various concentrations incubated with AA sulfatase in a time-dependent manner, b) Michaelis-Menten plot.

Table S1. Kinetic parameters of *H. pomatia* sulfatase and LOD of probe **1**

	K_m (μM)	V_{max} (μM/min)	LOD [b] (ng/ml)	LOD [c] (μg/ml)
H. pomatia	203± 57[a]	0.27 ± 0.06 [a]	61.4 ± 0.2	2.50 ± 0.02

[a] The values were reported in reference 107

2.4.3.3. *Pseudomonas aeruginosa* and *Klebsiella aerogenes* – colony-based liquid-phase assays

The numbers of colonies in the culture media were 0.60×10^{11} cfu/ml for *K. aerogenes* and 0.16×10^{12} cfu/ml for *P. aeruginosa* 0.834 ml of *K. aerogenes* colonies and 0.312 ml of *P.aeruginosa* colonies were harvested by centrifugation and washed twice with 50 mM Tris buffer. Then, *K. aerogenes* colonies were resuspended in 1 mL of 50 mM Tris buffer at pH 7.4 and *P. aeruginosa* colonies in 1 ml of 50 mM Tris buffer at pH 8.9. For fluorescent response study, 2.5 μl of 100 mM probe solution was added to 250 μl of the

colonies in a 96-well plate. For the observation of colored precipitates, 1 μl of 100 mM probe solution and 100 μl of colonies were added into a microtube. The final concentration of probe was 1 mM and the final amount of colonies was 5.0×10^{10} cfu/ml.

For lysate studies, 2.5 μl of 100 mM probe solution was dissolved in the lysates to a final concentration of 1 mM.

The tests with *K. aerogenes* were carried out at pH 7.5 and 35℃ [110, 111, 114] and the tests with *P. aeruginosa* were carried out at pH 8.9 and 45℃ [112, 113]. The fluorescence intensity was measured for 2 h and colored precipitates were observed after overnight.

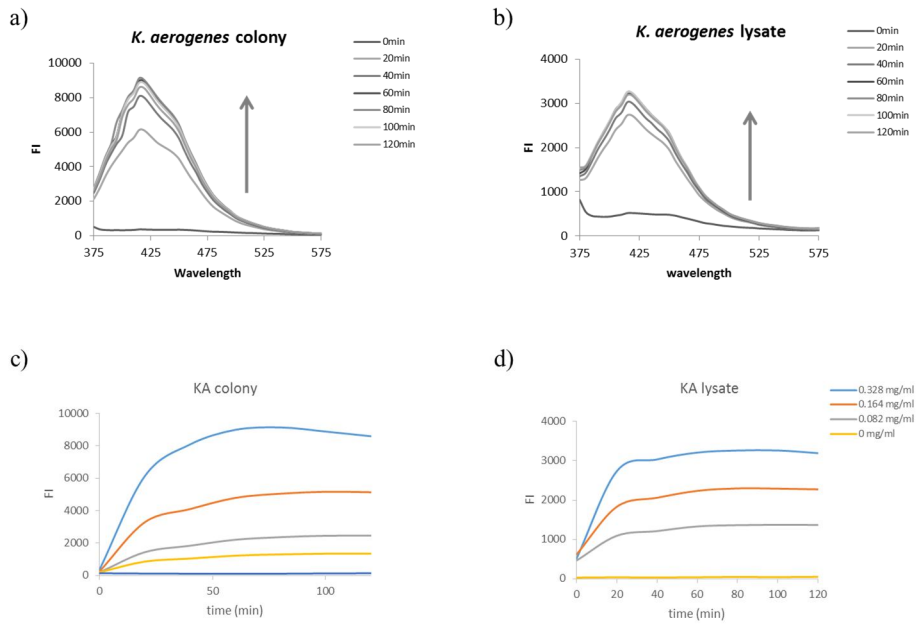

Figure S 9. Fluorescence enhancements of 1 mM probe **1** with 5.0×10^{10} cfu/ml of *K. aerogenes* colonies (a) and with *K. aerogenes* lysate (0.37 mg of protein/ml) (b).

Time-dependent fluorescence changes of 1 mM probe **1** with various amounts of *K. aerogenes* colony (1×10^{10}, 0.5×10^{10}, 0.2×10^{10} and 0.1×10^{10} cfu/ml) (c) and with various amounts of protein in *K. aerogenes* lysates (d).

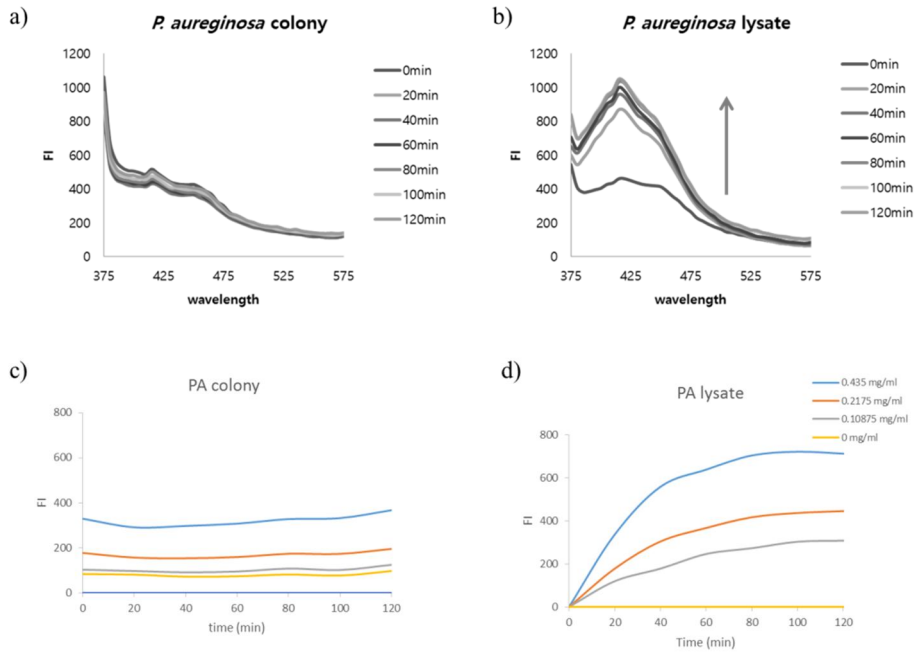

Figure S 10 (a) fluorescence changes of 1 mM probe **1** with 5.0×10^{10} cfu/ml of *P. aeruginosa* colonies, (b) fluorescence changes of 1 mM probe **1** with *P. aeruginosa* lysate (0.43 mg of protein/ml), Time-dependent fluorescence changes of 1 mM probe **1** with various amounts of *P. aeruginosa* colony (1×10^{10}, 0.5×10^{10}, 0.2×10^{10} and 0.1×10^{10} cfu/ml) (c) and with various amounts of protein in *P. aeruginosa* lysates (d).

2.4.3.4. *Klebsiella aerogenes, Mycobacterium avium, Mycobacterium smegmatis* and *S. aureus*– colony-based liquid-phase assays

For fluorescence reading, 250 µl of bacteria and the isolated bacterial lysate in Tris buffer (50 mM, pH 7.4) were prepared in the 96-well black plate with

clear bottom (Greiner). 2.5 µl of probe **1** (1 mM) was added to test wells, and the same volume of DMSO (1 mM) was added to control wells. Immediately after the addition, fluorescence (ex 327 nm/em 415 nm) was measured by a multi-label plate reader, Victor 3 (Perkin-Elmer) with 37°C plate incubation. For precipitation observation, duplicate plates were prepared in the 96-well white plate (Falcon) and incubated in 37°C for 24 hours.

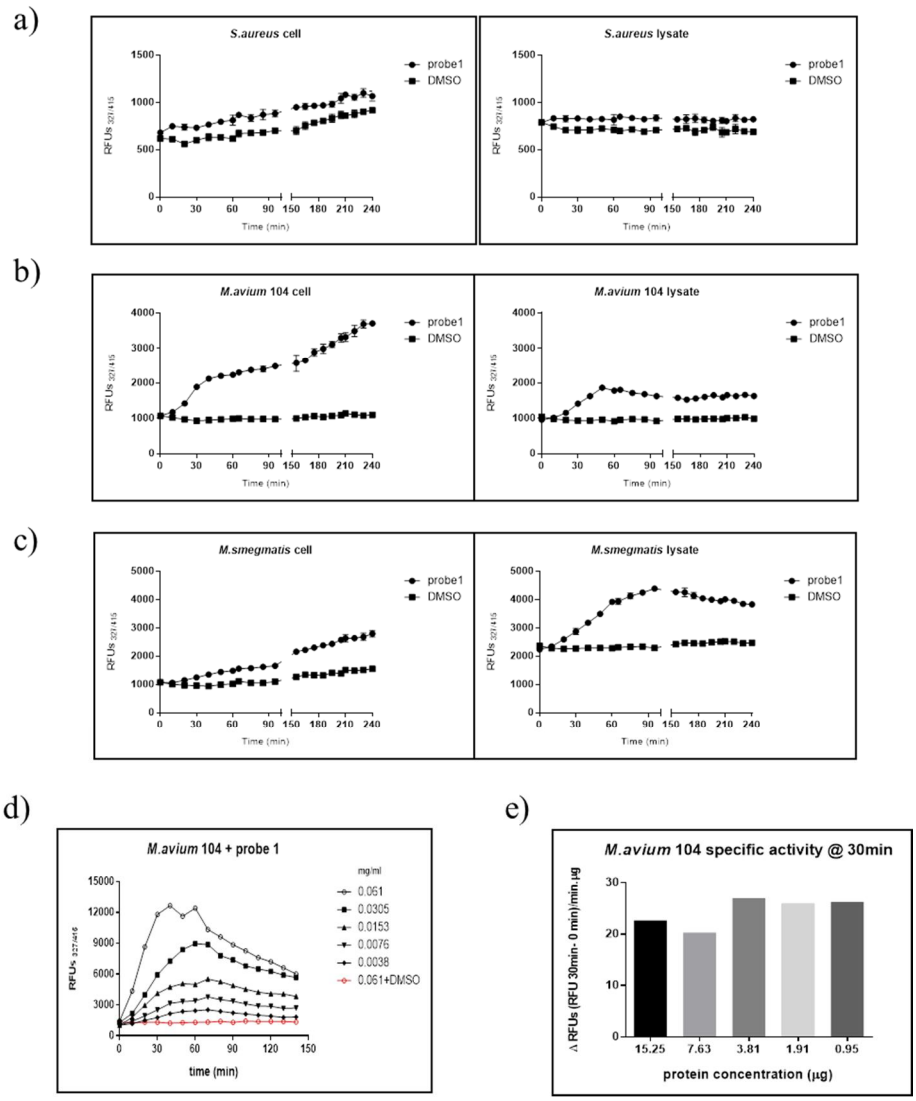

Figure S 11. Fluorescence intensity enhancement of probe 1 incubated with a) *S.*

aureus colony (left) and lysate (right, 4.2 μg of protein/ml), b) *M. avium* colony (left) and lysate (right, 4.5 μg of protein/ml), c) *M. smegmatis* colony (left) and lysate (right, 19.5 μg of protein/ml), d) fluorescence enhancement of probe 1 upon treatment of different protein concentrations of *M. avium* lysate, and e) specific activity of sulfatase in *M. avium* measured by probe **1**.

2.4.3.5. TEM images

For the TEM imaging analysis, K. aerogenes colony and 1 mM of probe 1 were incubated at 37 ℃ overnight and the cells were collected by centrifuge. The collected cells were fixed for 4 h with 2% glutaraldehyde and 2% paraformaldehyde, washed, and postfixed with 1% OsO_4. The samples were dehydrated with graded ethanol series, including en bloc staining with 3% uranyl acetate in 30% ethanol, and then embedded in Spurr's resin. Ultrathin sections were prepared by untramicrotome (EM UC7, Leica, Germany) and microscopy was performed with Transmission electrone microscopy (JEM1010, JEOL, Japan) at 80kV.

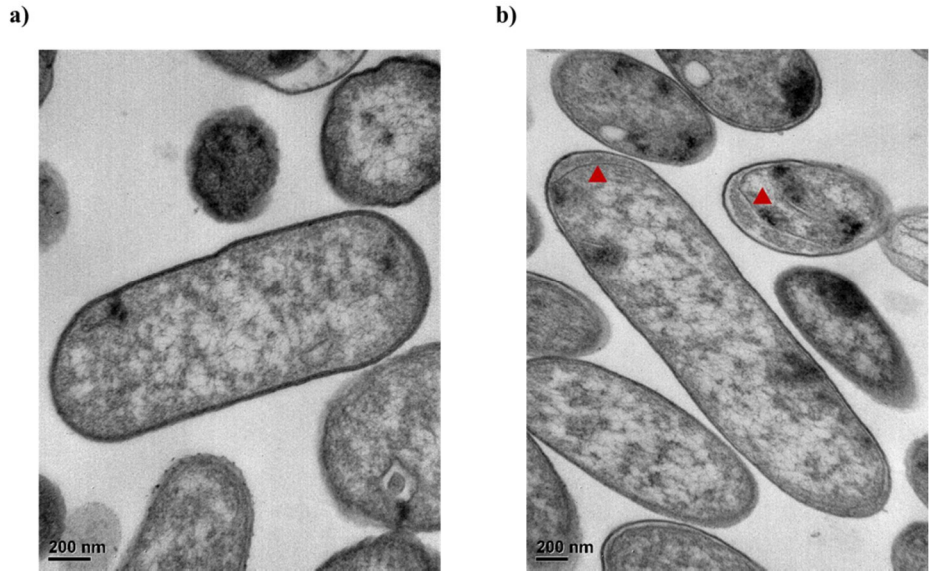

Figure S 12 TEM images of *K. aerogenes* without probe **1** (a) and with probe **1** (b); red arrow: inner membrane.

2.4.3.6. Colony-based solid-phase assays

We carried out the solid-phase assay with probe **1** following the published procedures [101-103].

Cultured colonies were diluted when OD_{600} was 1.0. Serial dilutions of colonies in sterile H_2O were plated onto cellulose acetate membrane filters (Advantec MFS Inc. 0.2 μm of pore size) on the surface of NB-agar. Plates were incubated at 30 ºC for *K. aerogenes* and at 35 ºC for *P. aeruginosa* overnight. Filter papers (Whatman) were soaked in a solution of 5 mM of probe **1** in 50 mM Tris buffer (pH 7.4 for *K. aerogenes* and pH 8.9 for *P. aeruginosa*). The membranes were placed on top of the soaked paper with probe solution and incubated overnight at 37 ºC.

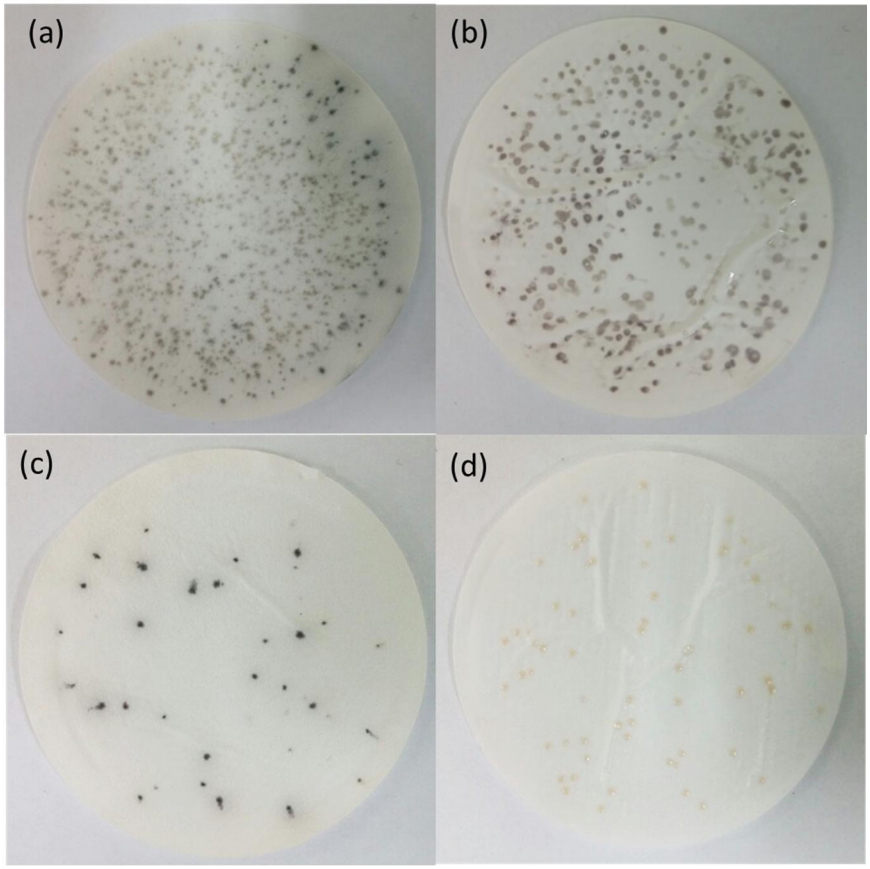

Figure S 13 colony-based solid-phase assays with $1/10^{9}$ dilution (a), $1/10^{10}$ dilution (b), $1/10^{11}$ dilution (c) of *K. aerogenes* and $1/10^{11}$ dilution of *P. aeruginosa* (d).

Section 3.
Efforts of improvement of probe 1 using diverse signal generation strategies

3.1. Introduction

Cells contain endogenous fluorescent chromophores, including porphyrin, tryptophan, collagen, and reduced nicotinamide adenine dinucleotide (NADH), which exhibit cell autofluorescence. Because fluorescent images of cells are influenced by many factors, such as endogenous fluorescent compounds, imaging agents should be target-selective and have a high signal-to-noise ratio. The previously reported probe 1 was demonstrated to be able to detect sulfatase activity through fluorescence enhancement. Probe 1 was excited at 327 nm and emitted at 415 nm, which are similar to the excitation and emission wavelengths of tryptophan (indole unit), causing a false signal, so probe 1 is not suitable for imaging the sulfatase activity in a living system. Moreover, the precipitation process of probe 1 was successfully applicable for

detecting bacterial sulfatase activity through solid-phase assay, but the images of bacterial sulfatase activity were not clear. To overcome the short emission wavelength, three types of probes (5 or 6-NI-Sulf, TPE-Sulf, and Pyr-Sulf), which are able to exhibit longer emissions, are proposed (Scheme 3). The first probe consisted of naphthalimide as a reporter, a core unit to generate isoindole through sulfatase activity, and sulfatase substrate. Upon sulfatase activity, the sulfate ester of 5 or 6-NI-Sulf was cleaved to form N-methylisoindole, which can be a donor of FRET to induce energy transfer to naphthalimide, an acceptor, exhibiting the emission of naphthalimide. TPE-Sulf is based on an aggregation-induced emission process. Tetraphenylethylene (TPE), a well-known AIE dye, was linked to the core unit incorporating sulfate ester to generate N-methyl isoindole through the reaction of sulfatase. Polymerization of the formed N-methylisoindole by sulfatase induced precipitates to intensify the TPE fluorescence. Pyr-probe was designed on the basis of excimer formation by the polymerization of the product by enzymatic reaction. It was comprised of pyrene and a core unit conjugated with phenyl sulfate ester. Sulfatase catalyzed the cleavage of the sulfatase ester of the pyr-probe, generating N-methyl isoindole. The hydrophobic and planar N-methyl isoindole was expected to aggregate with another product to generate pyrene excimer. With each different strategy, the probes were tested to improve the capabilities for bioimaging in a living system.

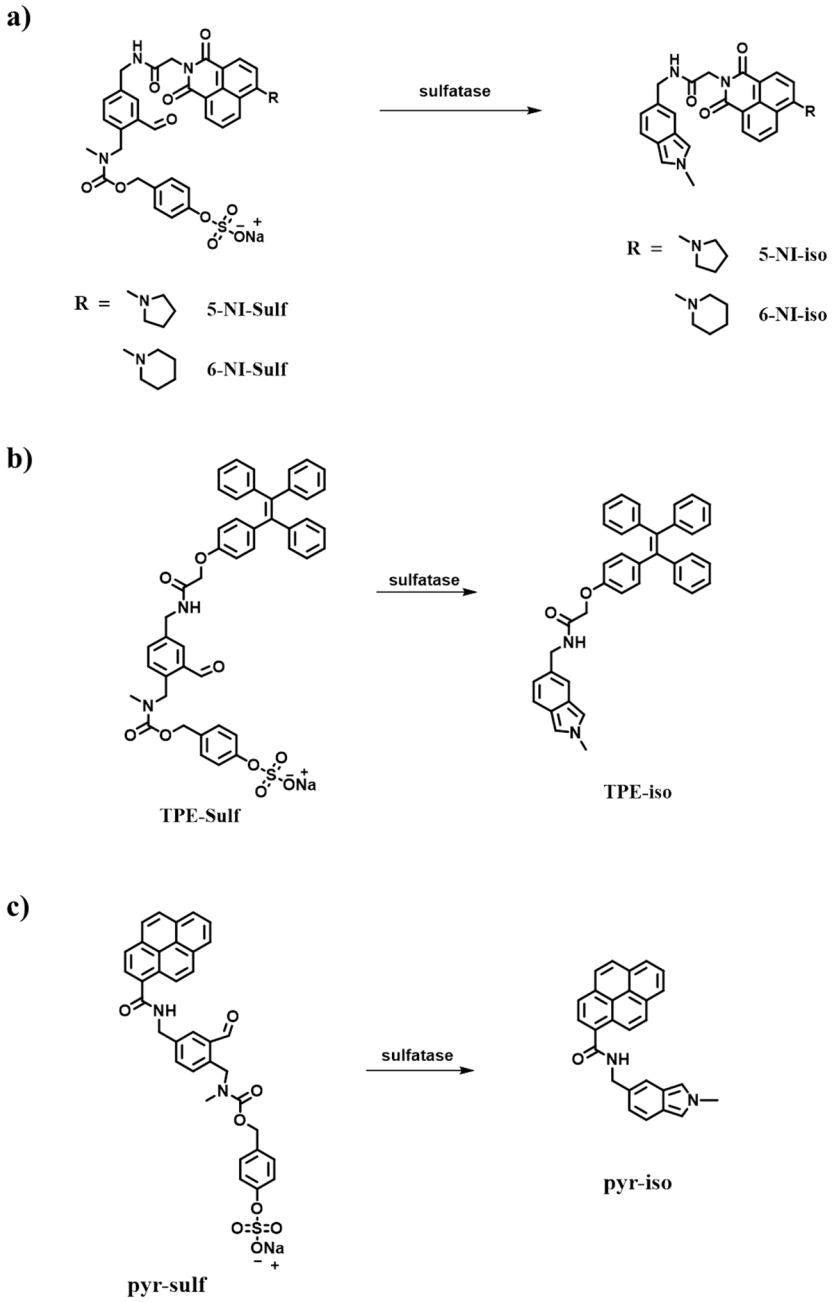

scheme 3 Strategies of a) FRET-based probe, 5-NI-Sulf or 6-NI-Sulf, b) AIE-based probe, TPE-Sulf, and c) excimer formation-based probe, pyr-sulf.

3.2. Results and Discussion

To test whether the FRET process would occur from the generation of N-methylisoindole upon sulfatase activity, the emission spectrum of N-methyl isoindole, a donor, and the absorption spectrum of 5 or 6-NI-sulf were measured. Because the isolation of N-methylisoindole is impossible, the spectrum was measured after the incubation of probe 1 with sulfatase for 40 min in 1 mM of GSH-containing buffer. As shown in Fig. 16, the absorption spectrum of 6-NI-sulf was almost identical to the emission of N-methylisoindole, which is not suitable for the FRET process. In contrast, 5-NI-sulf seemed to have been used for the FRET process, because the absorption spectrum of 5-NI-sulf overlapped with the emission spectrum of N-methylisoindole. Then, the fluorescence changes of 5-NI-sulf by enzymatic cleavage were measured. A total of 5 μM of 5-NI-sulf and 0.5 mg/ml of sulfatase in 1mM of GSH-containing Tris buffer were used for the monitoring. GSH was used as a reducing agent to increase the fluorescence intensity of N-methylisoindole. When it excited at 327 nm, the excitation wavelength of N-methylisoindole, or 450 nm, the excitation wavelength of naphthalimide, the emission spectrum was almost unchanged (Fig. 16b). Moreover, the fluorescence intensity disappeared overnight. To confirm the reason why the FRET process did not occur, DFT calculation was carried out. According to the DFT calculation, the distance between the donor, N-methylisoindole, and the acceptor, naphthalimide, was approximately 6.63 Å, which is outside of the range of 10–100 Å, a Förster distance. Thus, in the probe, Dexter energy transfer might have occurred instead of Förster energy transfer. As a result, the FRET process did not occur in this probe.

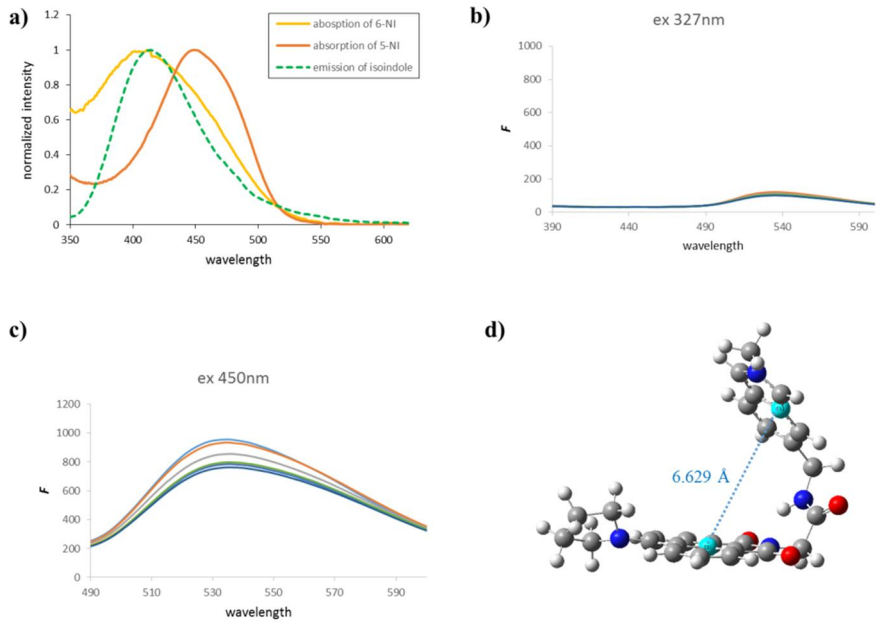

Figure 15 A) spectral overlap between the emission spectrum of N-methylisoindole (green dash) and the absorption of 5-NI (red solid) or 6-NI (yellow solid). The fluorescence changes of 5-NI-Sulf upon the treatment of sulfatase with 327 nm excitation (b), and 450 nm (c). d) DFT optimized structure of 5-NI-iso.

To test the availability of TPE-sulf, an AIE-based probe, to detect sulfatase activity, the fluorescence intensity and color changes of TPE-sulf with the treatment of sulfatase were observed. Because of the solubility of TPE-sulf, 10 mM of TPE-sulf stock solution in DMSO was dissolved in 50 mM of Tris buffer to be contained in 1% DMSO for the tests. The fluorescence of 500 μM or 1 mM of TPE-sulf incubated with various amounts of sulfatase (0–0.5 mg/ml) in 50mM of Tris buffer containing 1% DMSO was measured in a time-dependent manner. The concentration of TPE-probe was high enough to induce aggregation-induced emission at 465 nm, the intensity was decreased, and the decrease rates were dependent on the amount of sulfatase. The

emission at 415 nm, which is the fluorescence of N-methylisoindole, was almost unchanged (Fig. 17 and S15). After the incubation of TPE-sulf with sulfatase overnight, color changes of the solution were observed and remarkable precipitation did not occur. To confirm the generation of N-methylisoindole upon the treatment of sulfatase, Diels–Alder reaction with N-phenylmaleimide and mass spectrometric analysis of the product were performed. The peak of the Diels–Alder adduct was observed at m/z 721, which was identical to the calculated molecular weight of the adduct (Figure S16). As a result, it was shown that sulfatase catalyzed the hydrolysis of TPE-sulf to form N-methylisoindole, but the AIE process of TPE was not influenced by the generation or polymerization of N-methylisoindole, rather than the intensity was decreased. Therefore, these results mean that TPE-probe did not show improved properties for probe 1 or that it was capable of bioimaging.

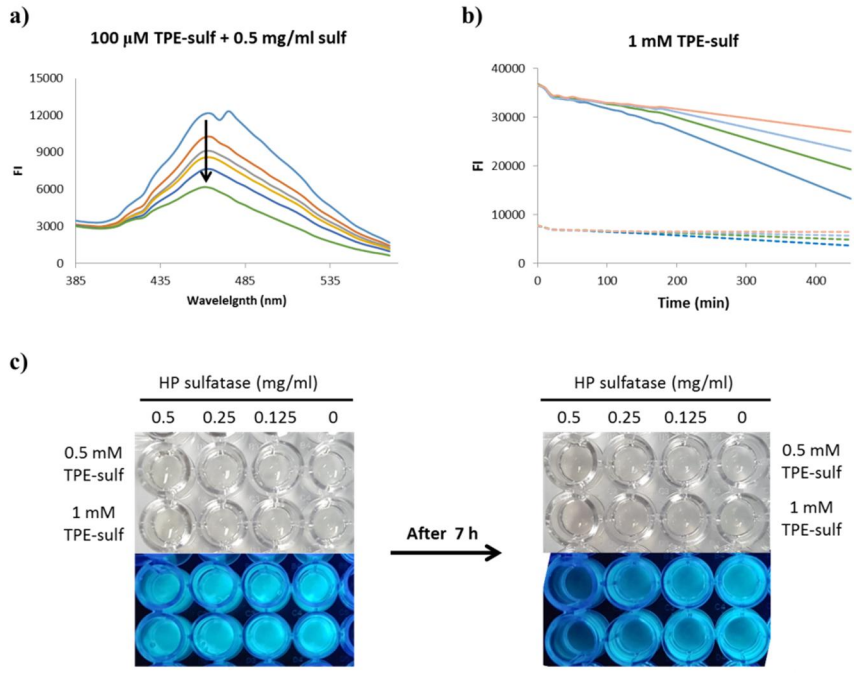

Figure 16. The emission spectrum of aggregate induced emission of TPE-sulf (100 μM) upon the treatment of sulfatase (0.5 mg/ml) in tim-dependent manner (a), The fluorescence changes at 465 nm (solid line) and at 415 nm (dash line) in a time-dependent manner; 1 mM of TPE-sulf was incubated with 0.5 mg/ ml (blue), 0.25 mg/ml (green), 0.125 mg/ml (skyblue) of sulfatase and without sulfatase (orange). Color changes and fluorescence decreas under UV light after 7h-incubation (c).

To confirm the availability of pyr-probe to detect sulfatase activity, we monitored the fluorescence changes of pyr-probe upon the treatment of sulfatase. A total of 5 μM of pyr-sulf or 1mM of pyr-sulf and 0.1 mg/ml of sulfatase in 50mM of Tris buffer (pH7.47, 37˚C) were used for the monitoring. As shown in Fig. 18, 5 μM of pyr-sulf and HP sulfatase was excited either at 327nm or 345nm, and the monomer and isoindole peaks, which were unable to be separated, were increased in a time-dependent manner. In contrast, 1

mM of pyr-probe in buffer exhibited the excimer emission at 485 nm and the addition of sulfatase induced a decrease of excimer emission and relatively small increase of monomer emission (420 nm). Moreover, after 1 hour of incubation of 1 mM of pyr-sulf with HP sulfatase, colored precipitates started to be observed, which darkened overnight (Fig. 18). To confirm the generation of *N*-methylisoindole by enzymatic reaction, a Diels–Alder reaction using *N*-phenylmaleimide was performed to trap isoindoles [67] and mass spectrometric analysis was implemented. The peak of the Diels–Alder adduct was observed at m/z 563, which corresponds to the calculated molecular weight of the adduct (Figure S17). The results confirmed that pyr-sulf was cleaved by sulfatase to generate N-methylisoindole. Thus, the fluorescence enhancement at 415 nm and colored precipitates could be considered to have been formed by N-methylisoindole. However, the fact that the excimer fluorescence at 485 nm was not increased in a low concentration of pyr-sulf or intensified in a high concentration of pyr-sulf meant that the hydrophobic and planar N-methylisoindole was not affected by aggregates or excimer formation. Nevertheless, pyr-sulf generated colored precipitates upon sulfatase activity and the probe could also be applied to bacterial sulfatase activity through solid-phase assay.

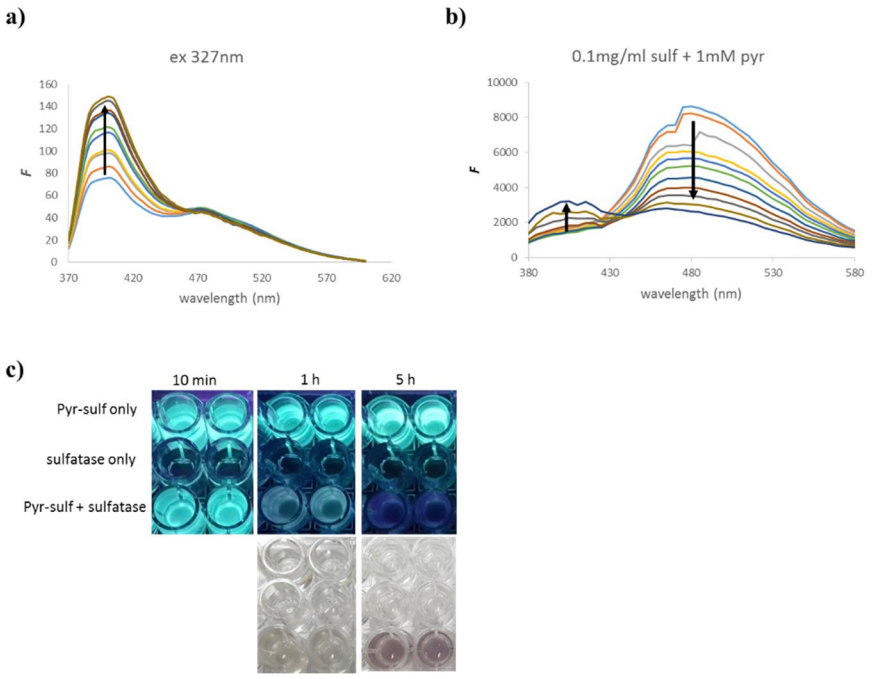

Figure 17. The fluorescnce changes of 5 uM of pyr-sulf incubated with 0.25 mg/ml sulfatase (a) and 1 mM pyr-sulf incubated with 0.1 mg/ml sulfatase (b) in time-course response, and fluorescence changes under UV light and color changes of 1 mM pyr-sulf incubated with sulfatase (c).

To demonstrate the feasibility of pyr-sulf for bacterial sulfatase activity assay, 1mM of pyr-sulf was incubated with the *K. aerogenes* and *P. aeruginosa* colony and lysate. As explained in the previous section, *K. aerogenes* sulfatase is periplasmic sulfatase and *P. aeruginosa* sulfatase is cytosolic sulfatase. In the case of pyr-sulf incubated with the *K. aerogenes* colony, the fluorescence increase rate at 415 was proportional to the amount of the colony (Fig. 19). The excimer fluorescence was increased with 1×10^{10} cfu /ml and 0.5×10^{10} cfu /ml of the colony, but the other two samples were unchanged, which was different from the result of pyr-sulf with purified HP sulfatase. In the tests with the *P. aeruginosa* colony, the fluorescences at 415 nm and 485 nm were almost unchanged. The fluorescence of pyr-sulf incubated with

lysates of *K. aerogenes* and *P. aeruginosa* was slightly increased at 415 nm and decreased at 485 nm in a time-dependent manner. In spite of the results of the lysate tests showing a similar tendency to the purified HP sulfatase test, in the colony tests, the excimer fluorescence could have been influenced by environmental factors, such as interaction with many components on the colony surface, which would impede the observation of the sulfatase activity selectively and deliberately with fluorescence changes. However, pyr-sulf generated colored precipitates only with the *K. aerogenes* colony to be applied to the colony-based solid-phase assay. In Figure 19, a color change was observed and the fluorescence decreased in the sample of pyr-sulf with the *K. aerogenes* colony compared with the sample of pyr-sulf with the *P. aeruginosa* colony. In addition, the precipitates of the probe from the periplasmic sulfatase of *K. aerogenes* stained the *K. aerogene* colony on the membrane (Fig. 19b). As a result, pyr-probe was cleaved by sulfatase activity to generate colored precipitates staining the bacterial colony, but it was unsuitable for detecting sulfatase through the fluorescence changes.

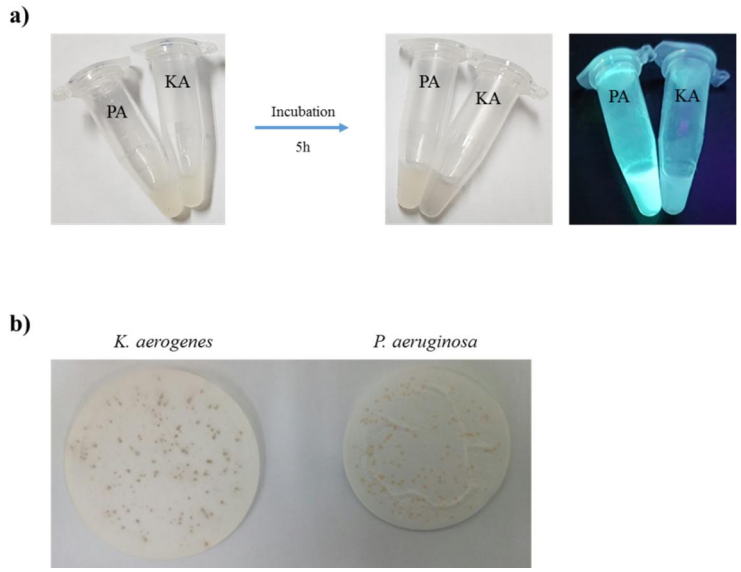

Figure 18. The fluorescence changes under UV light and color changes of pyr-sulf with p. aeruginosa and K. aerogenes colony (a), and *K. aerogenes* (left) and *P. aureginosa* (right) colony stained with pyr-iso at solid-phase (b).

3.3. Conclusion

In conclusion, three types of probes were synthesized and applied to detect sulfatase activity. 5-NI-sulf, a FRET-based probe, did not induce the FRET process because of the overly short distance between N-methylisoindole and naphthalimide. TPE-sulf, an AIE-based probe, did not increase fluorescence intensity, but a color change was observed. Pyr-probe, which was expected to form an excimer, showed that the fluorescence decreased and colored precipitates were generated by the sulfatase activity. The excimer formation was not implicated by the generation of N-methylisoindole and its precipitates. Finally, all three probes failed to improve the optical properties for bioimaging.

3.4. Experiments

3.4.1. General

^{1}H and ^{13}C NMR spectra were taken on a Bruker Advance DPX-300 spectrometer. Fast atom bombardment mass spectrometry (FAB-MS) data were obtained using a JEOL JMS-AX505WA mass spectrometer with m-nitrobenzyl alcohol (NBA) as a matrix and were reported in units of mass to charge (m/z). Analytical thin layer chromatography was performed using Kieselgel 60F-254 plates from Merck. Column chromatography was carried out on Merck silica gel 60 (70-230 mesh). UV/vis spectra were collected on a Beckman DU-800 and fluorescent spectra were collected on a Jasco FP-6500 and SpectraMax M2 spectrophotometer at 25℃ unless noted otherwise. K_m and V_{max} were calculated by nonlinear fitting of the Michaelis–Menten equation using SigmaPlot 8.0. For inhibition experiments, the IC_{50} curves were generated using SigmaPlot 8.0.

All chemical reagents and helix pomatia aryl sulfatase were purchased from either Sigma-Aldrich or TCI and used without any further purification. Deuterated solvents were acquired from Cambridge Isotopic Laboratories. CH_2Cl_2, pyridine and triethyl amine (TEA) were purified by distillation from CaH_2. THF were distilled from sodium benzophenone. Acetone was dried with anhydrous $MgSO_4$ before use. $CHCl_3$ were distilled from $CaCl_2$. All anion salts were purchased from Aldrich or TOKYO KASEI KOGYO chemical company.

3.4.2. Chemical Synthesis

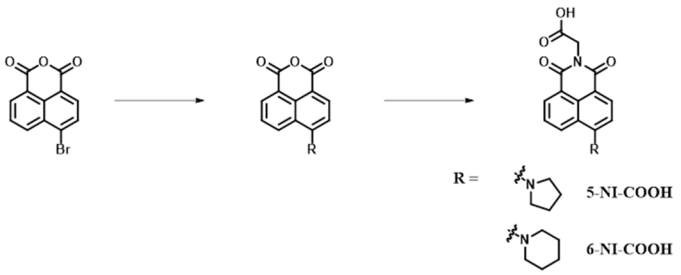

5(6)–NI-COOH was prepared following the published procedures [115, 116].

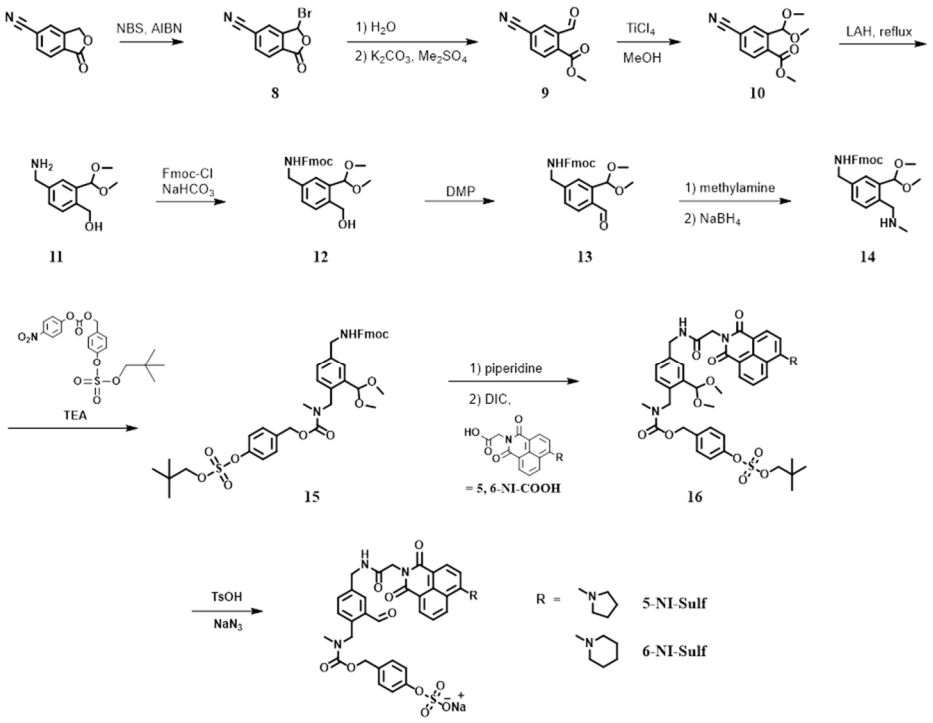

Scheme S 3 Synthesis of FRET-based probe, 5-NI-sulf and 6-NI-Sulf.

Compound 9: compound 9 was synthesized following the reported procedures [117, 118]. To a solution of 5-Cynanophthalide (2 g, 12.57 mmol) in chloroform was added NBS (6.7 g, 3 equiv.) and benzoyl peroxide (304 mg,

0.1 equiv.) and the mixture was refluxed overnight. After the completion of reaction, the reaction mixture was cooled down to room temperature and filtered off. The combined filtrates were concentrated under reduced pressure to afford the crude compound 8. Without purification, the crude compound 8 was suspended in 25 mL of H_2O and refluxed for 1h. Then, the mixture was cooled to room temperature and extracted with EtOAc. The combined extracts were dried over Na_2SO_4, filtered and concentrated under reduced pressure to give a white solid product. To a solution of the product in acetone was added Me_2SO_4 (1.2 ml, 1 equiv.) and K_2CO_3 (1.74 g, 1 equiv.). After stirring overnight at room temperature, the mixture was refluxed for 1 h and cooled to ambient temperature, filtered and washed with acetone. The combined filtrates were concentrated in vacuo and the residue was purified by silica gel chromatography (Hexane:EA= 4:1) to give compound 9 (1.54 g, 8.14 mmol, 65% yield). ^{1}H NMR (300 MHz, $CDCl_3$) δ 4.05 (3H, s), 7.94 (1H, d, J = 6.3 Hz), 8.12 (1H, d, J = 8.1 Hz) 8.24 (1H, s), 10.62 (1H, s).

Compound 10: To a solution of compound **9** (1.5 g, 7.93 mmol) in MeOH (50 ml) was added 1M $TiCl_4$ in methylene chloride (793 μl, 0.1 equiv.) in one portion at 0℃. After stirring for 1h at 0℃., the mixture was allowed to warm up to room temperature and sitirred overnight. TEA (1.12 ml, 1 equiv.) was added to the reaction mixture and stirring was continued for 30min. After concentration in vacuo, the residue was dissolved in ethyl acetate and washed with brine several times and concentrated in vacuo. The crude product was purified by silica gel column chromatography (Hexane:EA=7:1) to give compound **10** (1.4 g, 5.9 mmol, 74% yield). ^{1}H NMR (300 MHz, $CDCl_3$) δ 3.38 (6H, s), 3.96 (3H, s), 6.02(1H, s), 7.70 (2H, d, J= 6.6 Hz), 7.85 (2H, d, J = 7.8 Hz), 8.01 (1H, s).

Compound 11: To a suspension of lithium aluminum hydride (165 mg, 2.5 equiv.) in anhydrous THF was added compound **10** (440 mg, 1.87 mmol) dissolved in anhydrous THF at 0℃ slowly under N_2. The reaction mixture was refluxed overnight. Then, the solution was cooled down to 0℃ and quenched by 1 M aqueous NaOH solution. The mixture was dried with Na_2SO_4 and filtered through a pad of Celite. The filtrate was concentrated in vacuo. The reduction product was used for the next synthetic step without further purification.

Compound 12: To a solution of compound **11** (190 mg, 0.899 mmol) and $NaHCO_3$ (83 mg, 1.1 equiv.) in dioxane:H_2O (1:1) was added Fmoc-Cl (233mg, 1 equiv.) at 0℃. The suspension was stirred overnight at room temperature. After removal of solvent in vacuo, the residue were dissolved in ethyl acetate and washed with saturated NH_4Cl aqueous solution several times and concentrated in vacuo. The crude product was purified by silica gel column chromatography (Hexane:EA = 3:1) to give compound **12** (230 mg, 0.53 mmol, 59% yield). ^{1}H NMR (300 MHz, $CDCl_3$) δ 3.02 (1H, br), 3.38 (6H, s), 4.25 (1H, t, J = 6.6 Hz), 4.43 (2H, d, J = 5.7 Hz), 4.47 (2H, d, J = 6.9 Hz), 4.72 (2H, d, J = 5.1 Hz), 5.10 (1H, br), 5.51 (1H, s), 7.39 (7H, m), 7.61 (2H, d, J = 7.2 Hz), 7.78 (2H, d, J = 7.2 Hz).

Compound 13: To a solution of compound **12** (280 mg, 0.64 mmol) in anhydrous methylene chloride was added Dess martin periodinane (225 mg, 1 equiv.) and the mixture was stirred at room temperature overnight. To the reaction mixture was added saturated aquous sodium thiosulfate and stirred for 30min. The diluted reaction mixture in ethyl acetate was washed with saturated sodium bicarbonate, and dried over anhydrous sodium sulfate and

concentrated in vacuo. The product was used for a next step without further purification. ^{1}H NMR (300 MHz, $CDCl_3$) δ 3.41 (6H, s), 4.26 (1H, br), 4.51 (4H, m), 5.16 (1H, br), 5.89 (1H, s), 7.39 (6H, m), 7.62 (2H, m), 7.79 (2H, d, J = 7.4 Hz), 7.91 (1H, d, J = 7.7 Hz), 10.41 (1H, s).

Compound 14: To a solution of compound **13** (0.64 mmol) in methanol (35ml) was added 2.0 M CH_3NH_2 in THF (240 μl, 0.8 equiv.) at 0℃ and stirring continued overnight at room temperature. After completion of the reaction, the reaction mixture was cooled down to 0℃ and 10ml methanol was added. Then, sodium borohydride (26mg, 1.1 equiv.) was added to the reaction mixture. After stirring for 1h at 0℃, the mixture was concentrated in vacuo to afford the crude compound **14**. The product (compound 14) was used for a next step without further purification.

Compound 15: Compound **14** and compound **2** (225 mg, 1 equiv.) was dissolved in THF (45ml) and stirring continued overnight at room temperature. After removal of THF, the residue was dissolved in EA and washed with saturated aquous NH_4Cl several times. The crude product was purified by silica gel chromatography (chloroform:acetone= 50:1) to give compound **15** (298mg, 0.399mmol, 62% yield). ^{1}H NMR (300 MHz, $CDCl_3$) δ 3.41 (6H, s), 4.26 (1H, br), 4.51 (4H, m), 5.16 (1H, br), 5.89 (1H, s), 7.39 (6H, m), 7.62 (2H, m), 7.79 (2H, d, J = 7.4 Hz), 7.91 (1H, d, J = 7.7 Hz), 10.41 (1H, s).

Compound 16: compound **15** (50 mg, 0.067 mmol) was dissolved in methylene chloride containing 20% piperidine and stirring continued for 1h at room temperature. The reaction mixture was concentrated in vacuo, and the residue was dissolved in EA and washed with saturated aquous $NaHCO_3$ and brine. The organic layer was dried over anhydrous sodium sulfate and

concentrated in vacuo. To a solution of the residue and 5(6)-NI-COOH (1equiv.) in THF was added *N, N'*-Diisopropylcarbodiimide (DIC, 11.4 μl, 1.1 equiv.). The reaction mixture was stirred overnight at room temperature. After removal of THF, the residue dissolved in EA was washed with brine, dried over sodium sulfate and concentrated. The crude product was purified by silica gel chromatography (Chloroform:Acetone=10:1) to give compound 16.

Compound 16 (6-NI): (30 mg, 0.0355mmol, 53% yield).). ^{1}H NMR (300 MHz, $CDCl_3$) δ 1.02 (9H, s), 1.75 (2H, m), 1.90 (4H, m), 2.90 (3H, d, *J* = 21 Hz), 3.27 (10H, m), 4.11 (2H, s), 4.51 (2H, d, *J* = 5.6 Hz), 4.65 (2H, s), 4.91 (2H, s), 5.17 (2H, d, *J* = 14 Hz), 5.26 (1H, d, *J* = 17 Hz), 7.20 (2H, d, *J* = 8.1 Hz), 7.31-7.45 (7H, m), 7.68 (1H, d, *J* = 8.3 Hz), 7.74 (1H, d, *J* = 11 Hz), 8.43 (1H, d, *J* = 7.6 Hz), 8.52 (1H, d, *J* = 8.1 Hz), 8.60 (1H, d, *J* = 6.6 Hz).

Compound 16 (5-NI): (8.7mg, 0.01mmol, 18% yield) ^{1}H NMR (300 MHz, $CDCl_3$) δ 1.02 (9H, s), 2.13 (4H, s), 2.87 (3H, d, *J* = 21 Hz), 3.29 (6H, m), 3.82 (4H, br), 4.12 (2H, m), 4.51 (2H, d, *J* = 5.6 Hz), 4.65 (2H, s), 4.92 (2H, s), 5.17 (2H, d, *J* = 15 Hz), 5.34 (1H, d, *J* = 22 Hz), 6.83 (1H, d, *J* = 8.7 Hz), 7.44-7.58 (7H, m), 8.44 (1H, d, *J* = 8.6 Hz), 8.62 (3H, m).

6-NI-Sulf : To solution of compound 16 (30 mg, 0.0355 mmol) in acetone was added *p*-toluenesulfonic acid monohydrate (1.5 mg, 0.2 equiv.) and stirred at room temperature for 2 h. Acetone was removed in vacuo and the residue was purified through silica column chromatography (chloroform:acetone = 10:1). Then, the resulting product (12 mg, 0.015 mmol) and sodium azide (1 mg, 1 equiv.) were dissolved in DMF. The solution was stirred and heated at 70℃ overnight. Solvent was removed in vacuo and the crude product was purified by silica gel column chromatography

(CH_2Cl_2:methanol = 10:1) gave 6-NI-Sulf as the sodium salt (10 mg, 0.013 mmol, 37% yield).). ^{1}H NMR (300 MHz, CD_3OD) δ 1.75 (2H, m), 1.90 (4H, m), 2.95 (3H, s), 3.25 (4H, m), 4.50 (2H, s), 4.65 (2H, s), 4.90 (4H, s), 5.10 (2H, d, *J* = 25 Hz), 5.26 (1H, d, *J* = 17 Hz), 7.12-7.54 (7H, m), 7.71 (1H, t, *J* = 8.2 Hz), 7.87 (1H, s), 8.42 (2H, t, *J* = 7.9 Hz), 8.49 (1H, d, *J* = 7.1 Hz), 10.13 (1H, d, *J* = 21 Hz).

5-NI-Sulf : To solution of compound 16 (8.7 mg, 0.01 mmol) in acetone was added *p*-toluenesulfonic acid monohydrate (1 mg, 0.5 equiv.) and stirred at room temperature for 2 h. Acetone was removed in vacuo and the residue was purified through silica column chromatography (chloroform:acetone = 10:1). Then, the resulting product (6.3 mg, 0.008 mmol) and sodium azide (0.5 mg, 1 equiv.) were dissolved in DMF. The solution was stirred and heated at 70℃ overnight. Solvent was removed in vacuo and the crude product was purified by silica gel column chromatography (CH_2Cl_2:methanol = 10:1) gave 5-NI-Sulf as the sodium salt (6 mg, 0.814 μmol, 8% yield). ^{1}H NMR (300 MHz, CD_3OD) δ 2.12 (4H, s), 2.96 (3H, s), 3.84 (4H, s), 4.52 (2H, s), 4.93 (2H, s), 5.13 (2H, d, *J* = 25 Hz), 6.90 (1H, d, *J* = 8.8 Hz), 7.20-7.40 (5H, m), 7.60 (2H, t, *J* = 8.4 Hz), 7.74 (1H, s), 8.33 (1H, d, *J* = 8.7 Hz), 8.51 (1H, d, *J* = 7.2 Hz), 8.77 (1H, d, *J* = 8.6 Hz), 10.15 (1H, d, *J* = 21 Hz).

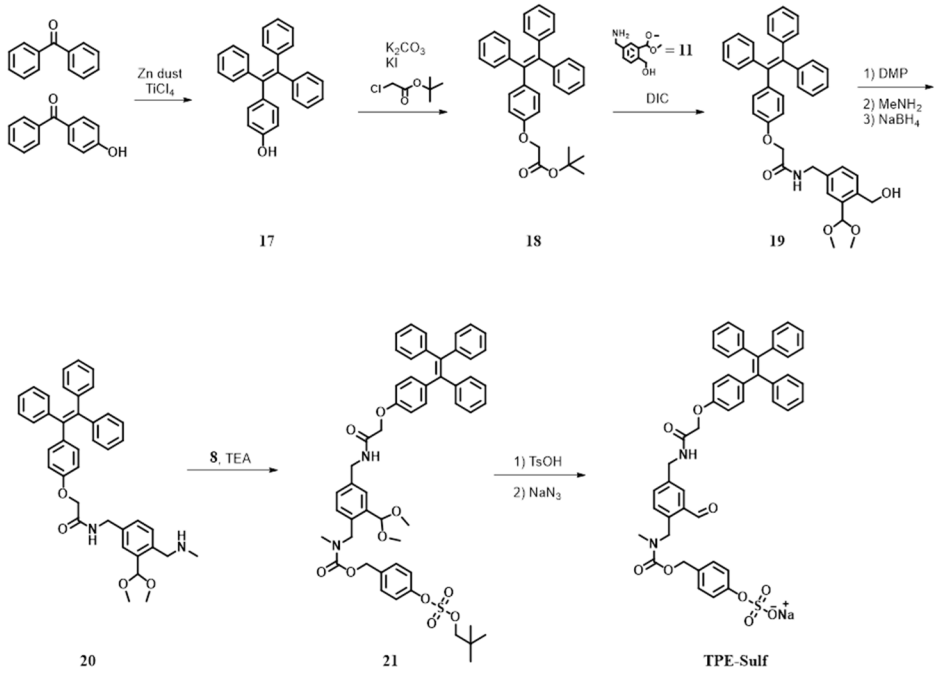

Scheme S 4 Synthesis of AIE-based probe, TPE-Sulf

Compound 17: Benzophenone (1.82 g, 10 mmol), 4-hydrobenzophenone (1.98 g, 10 mmol), zinc dust (1.63 g, 2.5 equiv.) and 100 ml of THF were added into two-necked flask under stirring at -78 ℃. 1.5 ml of TiCl4 was slowly added into the flask and refluxed overnight. After the reaction mixture was cooled down to room temperature, 2 M K_2CO_3 solution was added to the mixture. The crude product was extracted with methylene chloride and purified by a silica gel column chromatography and compound 17 was obstained (1 g, 2.87 mmol, 28 % yield). ^{1}H NMR (300 MHz, $CDCl_3$) δ 3.45 (6H, s), 4.94 (2H, d, J = 5.7 Hz), 5.95 (1H, s), 6.53 (1H, br), 7.64 (1H, , d, J = 9.3 Hz), 7.82 (1H, s), 7.98-8.28 (9H, m), 8.65 (1H, d, J = 9.3 Hz), 10.45 (1H, s).

Compound 18: To a solution of compound 17 (350 mg, 1 mmol) in acetonitrile were added tert-buthyl chloroacetate (170 µl, 1.2 equiv.),

potassium carbonate (210 mg, 1.5 equiv.) and potassium iodide (250 mg, 1.5 equiv.) and refluxed under nitrogen overnight. The reaction mixture was concentrated in vacuo, and the residue dissolved in EA was washed with ammonium chloride solution. The crude product was purified by silica gel chromatography (Hex:MC=2:1) to give compound 18 (183 mg, 0.395 mmol, 39.5% yield). ^{1}H NMR (300 MHz, $CDCl_3$) δ 1.47 (9H, s), 4.46 (2H, s), 6.64 (2H, d, *J* = 8.6 Hz), 6.95 (2H, d, *J* = 8.5 Hz), 7.03-7.10 (15H, m).

Compound 19: compound **18** (93 mg, 0.2 mmol) was dissolved in methylene chloride containing TFA and stirring continued for 2 h at 0 ℃. The reaction mixture was concentrated in vacuo, and the residue dissolved in THF was added to a solution of compound **2** (1equiv.) and *N, N′*-Diisopropylcarbodiimide (DIC, 31 μl, 1.1 equiv.) in THF. The reaction mixture was stirred overnight at room temperature. After removal of THF, the residue dissolved in EA was washed with brine, dried over sodium sulfate and concentrated. The crude product was purified by silica gel chromatography (Hexane:Acetone=2:1) to give compound **19** (40 mg, 0.067 mmol, 33 % yield). ^{1}H NMR (300 MHz, $CDCl_3$) δ 2.19 (6H, s), 3.97 (2H, m), 4.30 (2H, m), 4.69 (2H, s), 4.78 (1H, s), 6.65 (2H, d, *J* = 8.7 Hz), 6.96 (2H, d, *J* = 8.7 Hz), 7.01-7.17 (11H, m), 7.25 (1H, m), 7.32 (2H, m).

Compound 20: To a solution of compound **19** (40mg, 0.067 mmol) in methylene chloride was added Dess martin periodinane (28.5 mg, 1 equiv.) and stirring continued overnight at room temperature. To the reaction mixture was added saturated aquous sodium thiosulfate and the mixture was stirred for 30 min. The diluted reaction mixture in ethyl acetate was washed with saturated sodium bicarbonate, and dried over anhydrous sodium sulfate and

concentrated in vacuo. The product was used for a next step without further purification.

The product and 2M CH_3NH_2 in THF (50 µl, 2 equiv.) were dissolved in methanol and stirred overnight at room temperature. To the reaction mixture was added sodium borohydride (13 mg, 10 equiv.) and stirring continued for 3h. After removal of methanol, the residue was dissolved in EA and washed with saturated aquous $NaHCO_3$ and brine. The organic layer was dried over sodium sulfate and concentrated to afford compound **20** and the crude product was used without further purification.

Compound 21: To a solution of compound **20** (0.067 mmol) and TEA (30 µl, 2 equiv.) in THF was added compound **2** (29 mg, 1equiv.) and the mixture was stirred overnight at room temperature. After removal of THF, the residue dissolved in EA was washed with brine, dried over with $NaSO_4$ and concentrated in vacuo. The crude product was purified by silica gel chromatography (Hexane:acetone=2:1) to give compound **21** (26 mg, 0.0285 mmol, 42 % yield).

TPE-Sulf: To solution of compound **21** (26 mg, 0.0285 mmol) in acetone was added *p*-toluenesulfonic acid monohydrate (1 mg, 0.1 equiv.) and stirred at room temperature for 2 h. Acetone was removed in vacuo and the residue was purified through silica column chromatography (hexane:acetone = 3:1). Then, the resulting product and sodium azide (1 mg,) were dissolved in DMF. The solution was stirred and heated at 70℃ overnight. Solvent was removed in vacuo and the crude product was purified by silica gel column chromatography (CH_2Cl_2:methanol = 10:1) to give **TPE-Sulf** as the sodium salt (6.4 mg, 7.815 µmol, 27% yield). ^{1}H NMR (300 MHz, CD_3OD) δ 2.96

(3H, s), 4.51 (4H, m), 4.93 (2H, s), 5.12 (2H, d, J = 17 Hz), 6.76 (2H, d, J = 8.5 Hz), 6.92-7.07 (19H, m), 7.20-7.32 (5H, m), 7.47-7.55(2H, m), 10.10 (1H, d, J = 27 Hz).

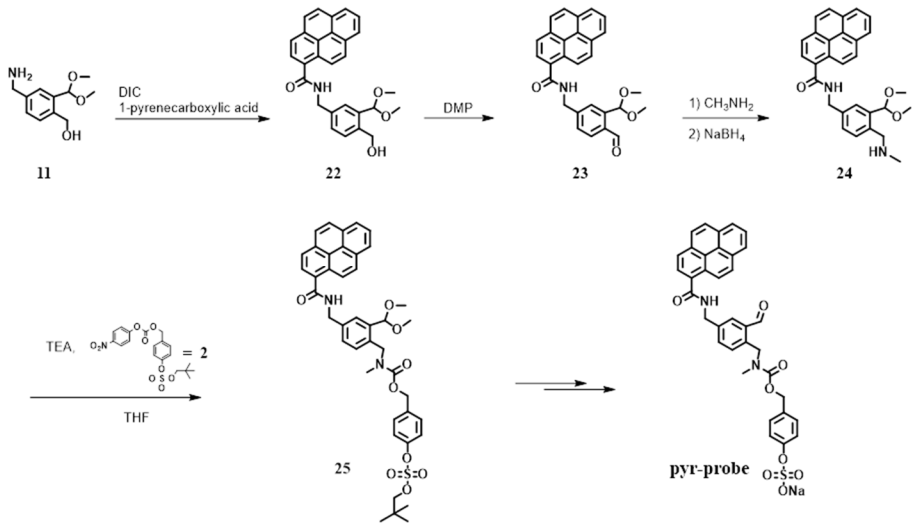

Scheme S 5 Synthesis of pyr-Sulf, an excimer formation-based probe.

Compound 22: To a solution of 1-pyrene carboxylic acid (58.3 mg, 1 equiv.), *N, N′*-Diisopropylcarbodiimide (DIC, 36.7 µl, 1 equiv.) and N-hydroxybenzotriazole (32 mg, 1 equiv.) in DMF was added compound **11** (50 mg, 0.237 mmol) and DIPEA (124 µl, 3equiv.). After stiring overnight at room temperature, DMF was removed. The residue dissolved in EA was washed saturated aquous $NaHCO_3$ and brine, dried over with $NaSO_4$ and concentrated in vacuo. The crude product was purified by silica gel chromatography (Hexane:EA=1:1) to give compound **22** (40 mg, 0.091 mmol, 38% yield). ^{1}H NMR (300 MHz, $CDCl_3$) δ 3.41 (6H, s), 4.74 (2H, s), 4.79 (1H, s), 4.85 (2H, d, J = 5.7 Hz), 5.55 (1H, s), 6.50 (1H, br), 7.46 (1H, m), 7.66 (1H, s), 8.08-8.26 (9H, m), 8.62 (1H, d, J = 9.3 Hz).

Compound 23: To a solution of compound **22** (70mg, 0.16 mmol) in methylene chloride was added Dess martin periodinane (68 mg, 1 equiv.) and stirring continued overnight at room temperature. To the reaction mixture was added saturated aquous sodium thiosulfate and the mixture was stirred for 30 min. The diluted reaction mixture in ethyl acetate was washed with saturated sodium bicarbonate, and dried over anhydrous sodium sulfate and concentrated in vacuo. The product was used for a next step without further purification. ^{1}H NMR (300 MHz, $CDCl_3$) δ 3.45 (6H, s), 4.94 (2H, d, *J* = 5.7 Hz), 5.95 (1H, s), 6.53 (1H, br), 7.64 (1H, , d, *J* = 9.3 Hz), 7.82 (1H, s), 7.98-8.28 (9H, m), 8.65 (1H, d, *J* = 9.3 Hz), 10.45 (1H, s).

Compound 24: compound **23** (0.16 mmol) and 2M CH_3NH_2 in THF (200μl, 2 equiv.) were dissolved in methanol and stirred overnight at room temperature. To the reaction mixture was added sodium borohydride (60mg, 10 equiv.) and stirring continued for 3h. After removal of methanol, the residue was dissolved in EA and washed with saturated aquous $NaHCO_3$ and brine. The organic layer was dried over sodium sulfate and concentrated to afford compound **24** and the crude product was used without further purification.

Compound 25: To a solution of compound **24** (0.124 mmol) and TEA (45 μl, 2 equiv.) in THF was added compound **2** (54 mg, 1equiv.) and the mixture was stirred overnight at room temperature. After removal of THF, the residue dissolved in EA was washed with brine, dried over with $NaSO_4$ and concentrated in vacuo. The crude product was purified by silica gel chromatography (Chloroform:Acetone=30:1) to give compound **25** (35 mg, 0.0465 mmol, 37% yield). ^{1}H NMR (300 MHz, $CDCl_3$) δ 0.98 (9H, d, *J* = 11.1 Hz), 2.92 (3H, d, *J* = 19.2 Hz), 3.31-3.37 (6H, m), 4.07 (2H, d, *J* = 14.7 Hz),

4.67 (2H, s), 4.82 (2H, m), 5.16 (2H, d, *J* = 14.1 Hz), 5.46 (1H, m), 6.50 (1H, br), 7.27-7.46 (5H, m), 7.68 (1H, d, J = 9.3 Hz), 7.97-8.21 (8H, m), 8.57 (1H, d, *J* = 9.3 Hz).

Pyr-Sulf: To solution of compound **25** (35 mg, 0.0465 mmol) in acetone was added *p*-toluenesulfonic acid monohydrate (1 mg, 0.1 equiv.) and stirred at room temperature for 2 h. Acetone was removed in vacuo and the residue was purified through silica column chromatography (chloroform:acetone = 10:1). Then, the resulting product (27 mg, 0.0382 mmol) and sodium azide (3 mg, 1.2 equiv.) were dissolved in DMF. The solution was stirred and heated at 70℃ overnight. Solvent was removed in vacuo and the crude product was purified by silica gel column chromatography (CH_2Cl_2:methanol = 10:1) to give **pyr-sulf** as the sodium salt (18 mg, 0.027 μmol, 59% yield). ^{1}H NMR (300 MHz, CD_3OD) δ 2.91 (3H, s), 4.72 (2H, d, J = 5.7 Hz), 4.93 (2H, s), 5.06 (2H, s), 7.16-7.31 (5H, m), 7.78 (1H, d, *J* = 7.4 Hz), 8.03 (1H, s), 8.13 (1H, t, J=7.5 Hz), 8.21-8.38 (5H, m), 8.53 (1H, d, *J* = 9.3 Hz), 9.36 (1H, t, 5.6 Hz), 10.15 (1H, d, *J* = 19 Hz);

3.4.3. Optical responses of 5-NI-Sulf and 6-NI-Sulf with treatment of sulfatases

For the optical response studies, stock solutions of 5-NI-Sulf and 6-NI-Sulf were prepared to be 10 mM in DMSO. The UV absorbance of 5 μM of 5-NI-COOH and 6-NI-COOH were measured in 50 mM Tris buffer with 1mM GSH at pH 7.48. The fluorescence spectrum of N-methyl isoindole, which was prepared by the reaction of probe 1 with sulfatase in 50 mM Tris buffer containg 1mM GSH at pH 7.48, was also measured.

For the optical response of 5-NI-Sulf and 6-NI-Sulf upon the treatmnet with

sulfatase, 5 uM of 5-NI-Sulf or 6-NI-Sulf was incubated with 0.125 mg/ml of sulfatase with the excitation at 327 nm, the excitation wavelength of N-methyl isoindole and at 450 nm or 425 nm, the excitation wavelength of 5-NI-COOH or 6-NI-COOH, respectively.

The optimized structure of 5-NI-Sulf was obtained using density functional theory (DFT) calculations with Gaussian 09.

3.4.4. Spectral responses of TPE-Sulf upon the treatment with sulfatase

Stock solutions of TPE-Sulf (10 mM in DMSO) was diluted to 100 μM, 500 μM and 1 mM in 50 mM Tris buffer at pH = 7.4). The fluorescence spectra of 100 μM of TPE-Sulf incubated with sulfatase was measured with excitation at 330 nm.

Time-dependent fluorescence emissions at 465 nm and 415 nm with exciatation at 330 nm were measured using 1mM TPE-Sulf or 500 μM TPE-Sulf with the treatment of various amounts of sulfatase (0~0.5 mg/ml) (Fig. S15a). To observe color changes, 0.5 mM of TPE-Sulf was incubated with 0.25 mg/ml of sulfatase in 50 mM Tris buffer (pH 7.48) for 7 h or 2 days at 37℃ (Fig. S15b).

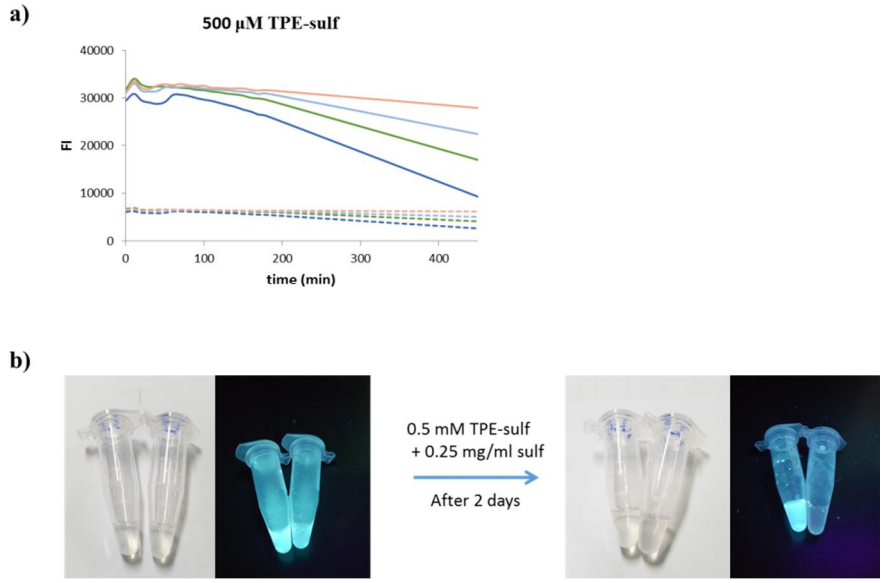

Figure S 14 a) time-dependent fluorescence decrease of 0.5 mM of TPE-Sulf at 465 nm (solid line) and 415 nm (dash line) upon the treatment of various amounts of sulfatase; 0.5 mg/ml (blue line), 0.25 mg/ml (green line), 0.125 mg/ml (sky blue line) and no sulfatase (oranges line). (b) The color changes and fluorescence changes under UV light of 0.5 mM TPE-Sulf with sulfatase.

3.4.5. Diels-alder reaction of TPE-sulf

20 μM of TPE-Sulf was incubated with 0.25 mg/ml of sulfatase in 50 mM Tris buffer (pH 7.48) for 40 min to generate *N*-methylisoindole. Then, the resulting solution was added into a *N*-phenylmaleimide solution in THF and stirred at 70°C overnight. The reaction mixture was extracted with CH_2Cl_2, dried over Na_2SO_4, filtered, and concentrated *in vacuo*. The residue was dissolved in 1 mL of methanol and subjected to liquid chromatography-mass spectrometry (LC/MS) analysis with 1260 infinity (Agilent technologies) (Fig. S16) to monitor for the formation of Diels-Alder adducts ($C_{48}H_{39}N_3O_4$+5H^+=726.33).

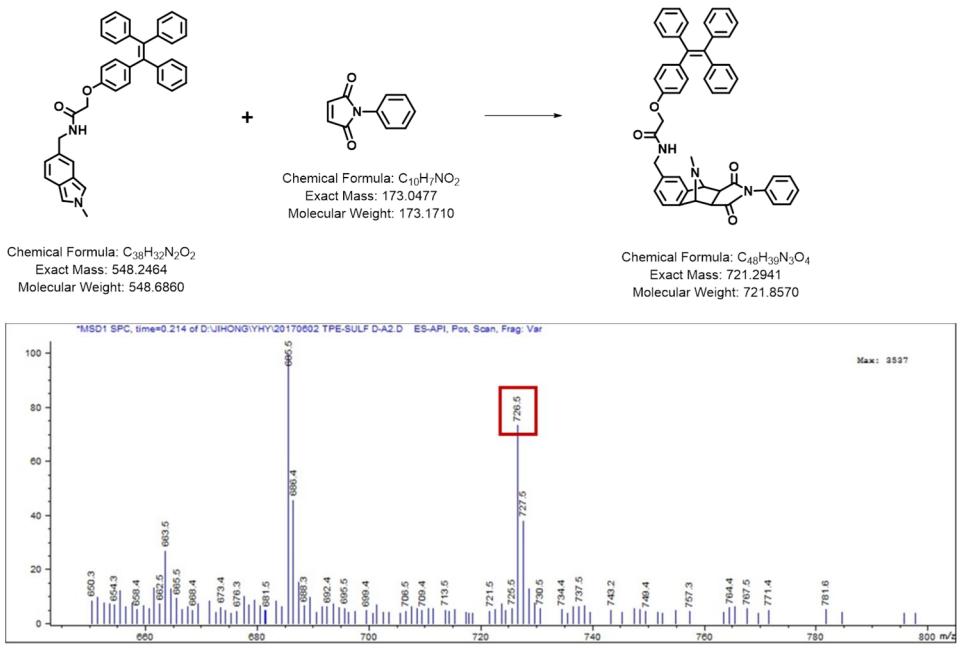

Figure S 15 liquid chromatography-mass spectrometry (LC/MS) analysis

3.4.6. Spectral response of pyr-sulf with the treatment of purified sulfatase

A stock solution of 10 mM pyr-probe and 100 mM pyr-probe were prepared in DMSO. A stock solution of 1.25 mg/mL *Helix pomatia* arylsulfatase (S9626, Sigma-Aldrich) as prepared in 50 mM Tris buffer (pH 7.48).

Fluorescence changes of pyr-probe were measured by treating 5 μM pyr-probe or 1 mM pyr-probe with 0.1 mg/mL HP sulfatase at 37°C in 50 mM Tris-buffer (100 mM NaCl, $MgCl_2$, $CaCl_2$, pH 7.4) over a period of 0-150 min.

3.4.7. Diels-Alder reaction of pyr-iso

20 μM of TPE-Sulf was incubated with 0.25 mg/ml of sulfatase in 50 mM Tris buffer (pH 7.48) for 40 min to generate *N*-methylisoindole. Then, the resulting solution was added into a *N*-phenylmaleimide solution in THF and stirred at

70°C overnight. The reaction mixture was extracted with CH_2Cl_2, dried over Na_2SO_4, filtered, and concentrated *in vacuo*. The residue was dissolved in 1 mL of methanol and subjected to liquid chromatography-mass spectrometry (LC/MS) analysis with 1260 infinity (Agilent technologies) (Fig. S17) to monitor for the formation of Diels-Alder adducts ($C_{37}H_{27}N_3O_3$+$2H^+$ = 563.22).

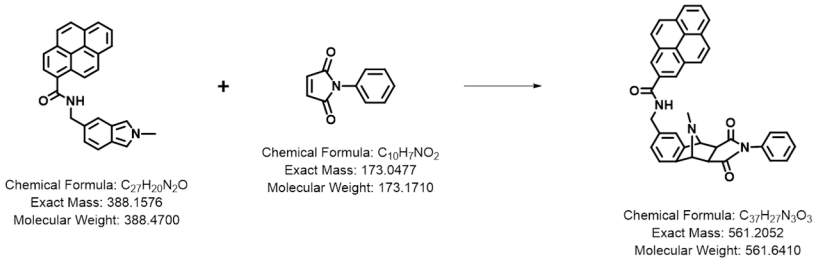

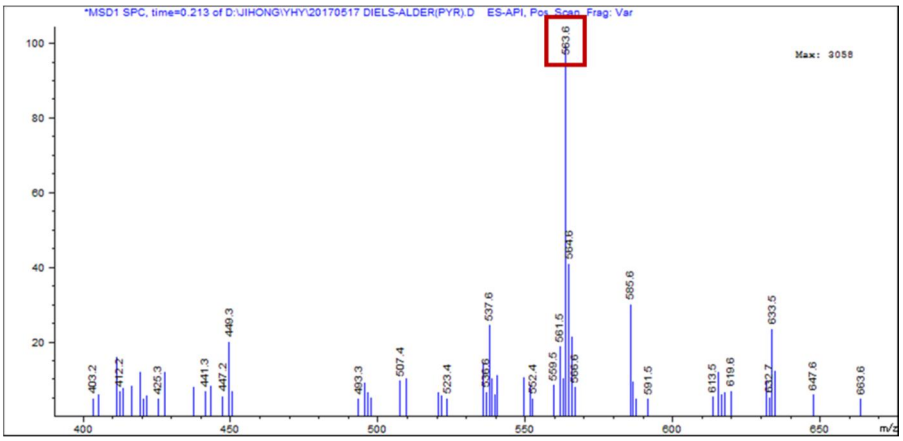

Figure S 16 to liquid chromatography-mass spectrometry (LC/MS) analysis

For the observation of time-course fluorescence changes, 1 mM pyr-sulf was incubated with various amounts of HP sulfatase (0.5mg/ml, 0.25mg/ml, 0.125mg/ml and none). Pyr-sulf also incubated with various amounts of K.aerogenes colony and lysate and P. aeruginosa colony and lysate. The Emissions at 485 nm and at 415 nm with excitation at 330 nm were observed (Fig. S18).

For the observation of colored precipitates, the final concentration of pyr-sulf and sulfatase was 1 mM and 0.1 mg/ml sulfatase, respectively. The solution was incubated at 37℃. The precipitates were observed after 2 h, 4 h and overnight.

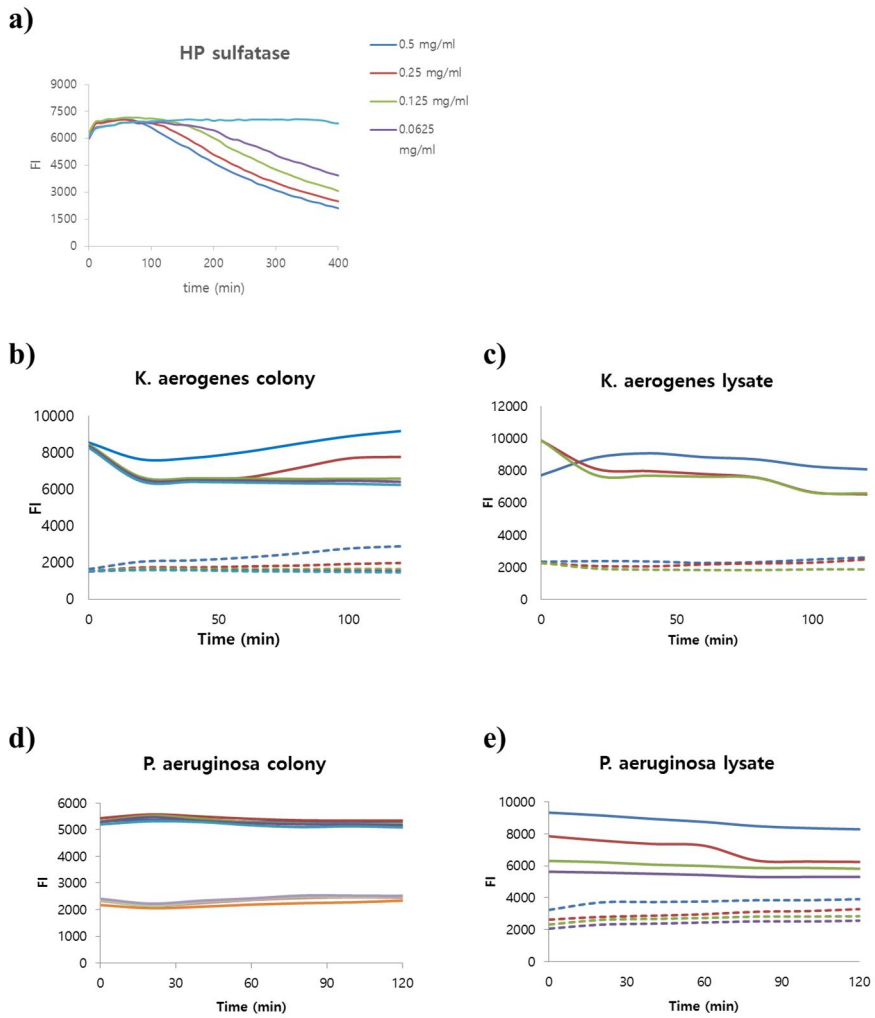

Figure S 17 The fluorescence changes of pyr-sulf (ex 327 nm, em 415nm and 485 nm) (a) with the treatment ofvarous amount of purified sulfatase (0.5 mg/ml, 0.25 mg/ml, 0.125 mg/ml, none), (b) with K. aerogenes and (d) P.aeruginosa colony (blue:

1×10^{10}, red: 0.5×10^{10}, green: 0.2×10^{10}, sky blue: 0 cfu/ml) and with (c) K. aerogenes (blue: 0.328, red: 0.164, green: 0.082 mg of protein/ml) and (e) P. aeruginosa lysate (blue: 0.435, red: 0.217, green: 0.108 mg of proteins /ml)

III.

Probes inducing signal changes by intramolecular charge transfer upon the treatment of enzyme

Section 1.
Small-molecule probe using dual signals to monitor leucine aminopeptidase activity

1.1. Introduction

Aminopeptidases play important roles as transcriptional repressors, site-specific recombination factors, and viral or toxin receptors, as well as being proteolytic enzymes for the *N*-terminus of proteins and bioactive peptides in bacteria and animals. Leucine aminopeptidases (LAPs) are one of the exopeptidases which catalyze the hydrolysis of the *N*-terminal leucine residues of proteins or peptides. Some LAPs are key enzymes and are able to affect diverse biological and physiological phenomena [119-122]. They could therefore be used as diagnostic or prognostic biomarkers, and assays for their activity are necessary. Several assays for LAP activities have been developed [119, 123-127]. Known probes for monitoring LAP activities consist of a fluorescent reporter and an amide group coupled with leucine, and they can exhibit colorimetric and fluorogenic signals on interaction with LAPs [119].

However, they have short excitation and emission wavelengths, making it hard to monitor LAP activity in living cells, and they need large amounts of LAP for high-throughput screening for potent inhibitors. To address these problems, we developed a probe, using a 2-dicyanomethylene-3-cyano-2, 5-dihydrofuran (DCDHF) unit as an electron-accepting unit, for fluorescent measurement of LAP activity and inhibitor potency at longer wavelengths.

We designed a probe which has a DCDHF unit and a leucine-linked π-conjugated system (DCDHF–Leu). This probe has good cell permeability and can be applied in bioimaging [38, 128-130]. The capped amine functionality of leucine could block fluorescence emission by reducing the donor ability of the NH moiety in DCDHF–Leu. However, DCDHF–Leu is expected to show color changes and fluorescence turn-on when the leucine is uncapped by treatment with LAP, forming DCDHF–NH_2 (Scheme 4).

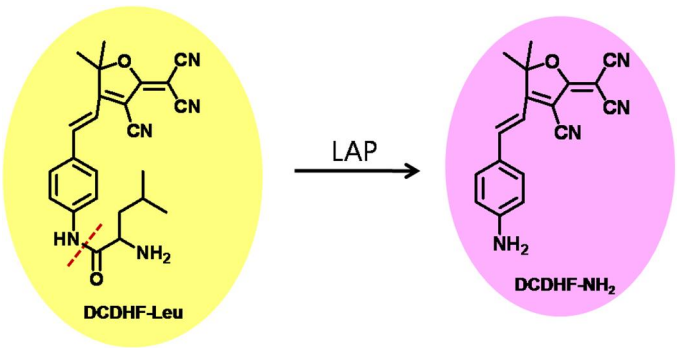

Scheme 4. Probe based on the 2-dicyanomethylene-3-cyano-2, 5-dihydrofuran (DCDHF) unit.

1.2. Result and Discussion

We evaluated the optical response to LAP activity using DCDHF–Leu *in vitro*.

When it was excited at 525 nm, DCDHF–Leu was non-fluorescent, but DCDHF–NH_2 showed significant fluorescence enhancement in HEPES buffer at pH 7.4 (Figure 19A). The emission spectrum of DCDHF–Leu after treatment with porcine kidney microsomal LAP (PKLAP) was examined with time (Figure 19B). The fluorescence intensity at 605 nm increased by up to 10-fold, and was saturated in 30 min. This indicates that PKLAP removes the leucine residue from DCDHF–Leu to form DCDHF–NH_2 within minutes, which means that DCDHF–Leu is a good fluorogenic substrate for PKLAP. Moreover, incubation of DCDHF–Leu with LAP for 30 min triggered a solution color change from yellow to red. It was demonstrated that PKLAP activity using the probe could also be observed by the naked eye (Figure 19C). DCDHF–Leu is therefore an efficient probe that can measure LAP activity by fluorescent and color changes.

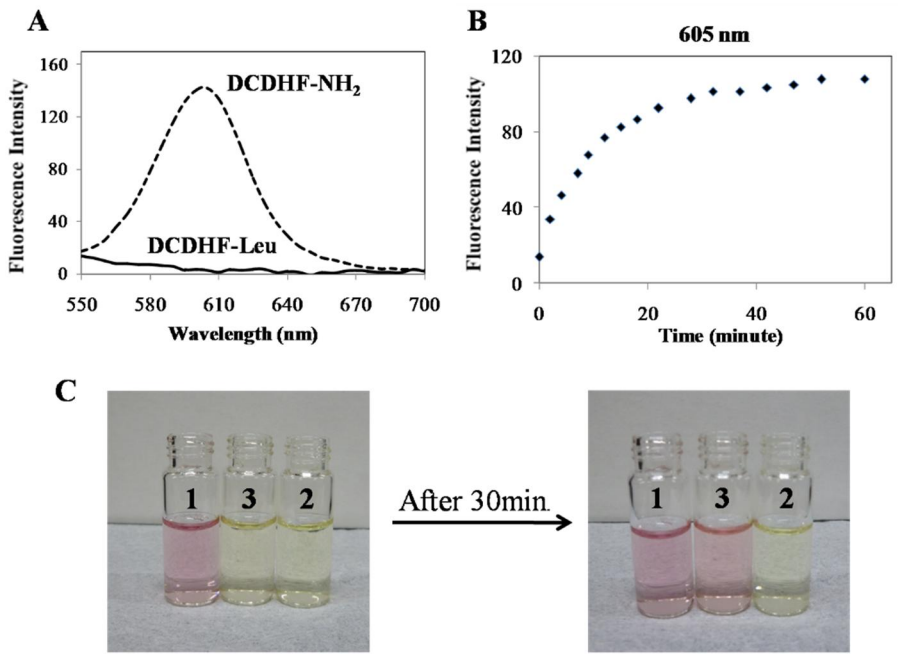

Figure 19. A) Fluorescence spectra of DCDHF–NH_2 and DCDHF–Leu. B) Time-

dependent fluorescence changes of a DCDHF–Leu probe (10 μM) with PKLAP (0.2 μg/mL) at 605 nm. C) Color change of a DCDHF–Leu probe after 30 min incubation with PKLAP: 1, 20 μM DCDHF–NH_2; 2, 20 μM DCDHF–Leu; 3, 20 μM DCDHF–Leu with 0.2 μg/mL PKLAP.

To determine the enzyme kinetics, the fluorescence intensity was examined with different concentrations of DCDHF–Leu and a constant amount of PKLAP. Concentrations of DCDHF–Leu from 1.2 μM to 50 μM, and 0.2 μg/mL PKLAP in 10 mM HEPES buffer at pH 7.4, were used (Figure S18 and S19). The maximum velocity (V_{max}) was determined to be 6.64 ± 0.46 μmol/min.mg and the Michaelis constant (K_m) was 8.87 ± 1.72 μM. Compared to previously reported data (Table 4) [119], DCDHF–Leu has a similar V_{max} and smaller K_m. These data indicate that DCDHF–Leu could bind to LAP more tightly, and that it is a better substrate for LAP than other reported or commercial substrates.

Table 4. Enzymatic parameters and inhibitory potency

Substrate	V_{max} (μmol/min.mg)	K_m (μM)	IC_{50} of bestatin[b] (μM)
l-leucine-*p*-nitroanilide[a]	3.9 ± 0.2	3000 ± 200	25 ± 4
N-(6-Methoxypyridine-3-yl), (*S*)-2-amino-4-methylpentanamide[a]	7.7 ± 0.2	65 ± 4	7 ± 1
DCDHF-Leu	6.64 ± 0.46	8.87 ± 1.72	4.41 ± 0.61

[a] ref. 119

[b] the measured value with each substrate

To explore whether the DCDHF–Leu probe can measure inhibitory potency,

we determined the inhibition potency (IC_{50}) of bestatin, which is known to be a slow-binding competitive inhibitor of LAP [131-133]. A constant amount of PKLAP (0.2 μg/mL) was incubated with various concentrations of bestatin, from 0.6 μM to 50 μM, for 10 min, prior to addition of 10 μM DCDHF–Leu. The maximum fluorescence intensity at 605 nm and the initial DCDHF–Leu velocity with PKLAP decreased dose-dependently (Figure 20). The IC_{50} obtained in this experiment is 4.41 ± 0.61 μM, which is the same order of magnitude as previously reported data (Table 4) [119]. Our experiment reveals that DCDHF–Leu is an excellent probe, which can detect compounds with high inhibition potency for LAP, and also enables high-throughput screening.

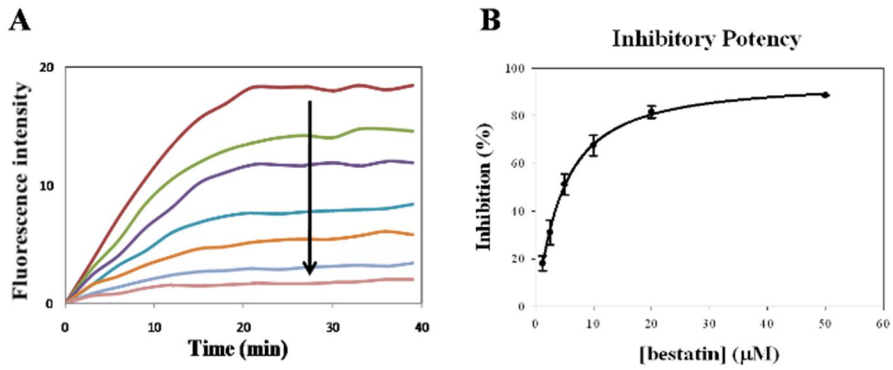

Figure 20 A) Fluorescence decrease of DCDHF–Leu with bestatin concentration (0.6, 1.2, 2.5, 5, 10, 20, and 50 μM). B). Inhibitory potency.

Finally, to demonstrate the potential practical applications of DCDHF–Leu, we applied the probe to a living cell for fluorescence imaging. DCDHF–NH_2 is a red fluorescent substrate, which has longer excitation and emission wavelengths than previously known probes [119]. Two sets of HCT 116 cells were incubated with 20 μM DCDHF–Leu, with and without bestatin, for 20 min at room temperature. The HCT 116 cells without bestatin showed red

fluorescent imaging, indicating the presence of DCDHF–NH_2 from reaction with LAP; the other set, with bestatin, which could block the LAP activity, was non-fluorescent (Figure 21).The fluorescent intensity of HCT 116 cell lysates incubated with 20 μM DCDHF–Leu and no bestatin was about six-fold higher than that of HCT 116 cell lysates incubated with the probe and bestatin (Figure S20). The same results were obtained from the cell lysate and the living cell, indicating that DCDHF–Leu has good cell permeability. All our experiments reveal that DCDHF–Leu is an efficient probe for monitoring LAP activity in living cells.

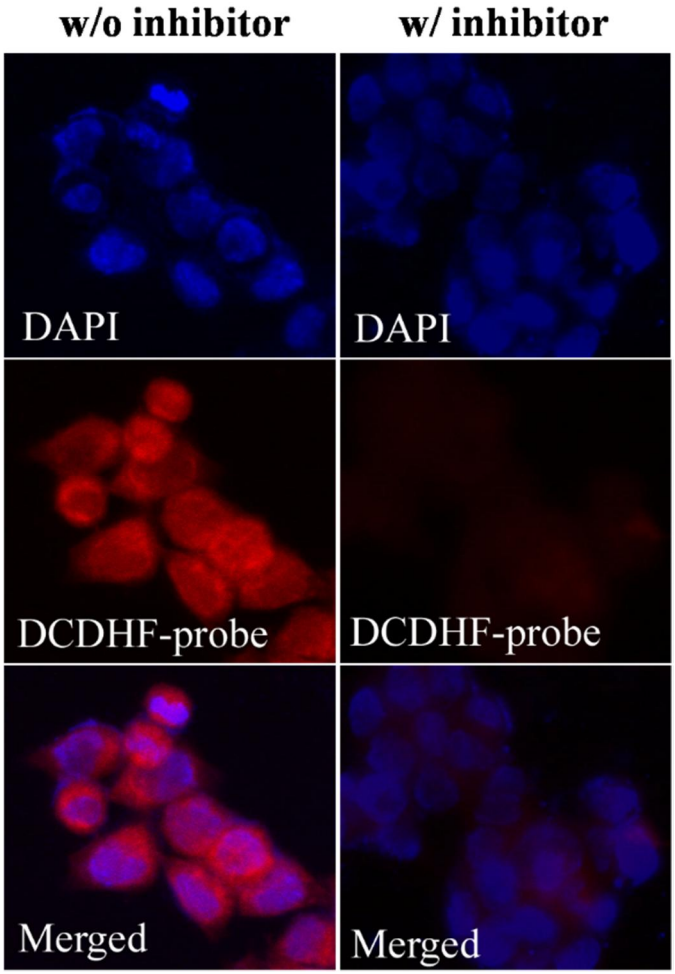

Figure 21. A) HCT 116 cells imaging with 20 μM DCDHF–Leu incubated for 20 min (left), and with 20 μM DCDHF–Leu incubated with 100 μM bestatin for 20 min (right). Cells were fixed and stained with a DCDHF probe (red) against LAPs and with DAPI stain (blue) to identify the nucleus. Original magnification, ×400.

1.3. Conclusion

In conclusion, we have developed a fluorescent probe (DCDHF–Leu) that can monitor LAP activity in living cells. It was demonstrated that DCDHF–Leu showed significant fluorescent enhancement and a color change on reaction with LAP. In addition, it was illustrated that DCDHF–Leu was an efficient

probe for measuring the inhibitory potency of LAP inhibitors.

1.4. Experiments

1.4.1. General

^{1}H and ^{13}C NMR spectra were taken on a Bruker Advance DPX-300 or a Bruker Advance 500 spectrometer. Chemical shifts are given in parts per million using as internal reference the residual resonances of deuterated solvents (δ = in chloroform-*d*, acetone-d_6 and DMSO-d_6 (^{1}H NMR chemical shifts: δ = 7.27 ppm for $CDCl_3$, δ = 2.05 ppm for acetone-d_6 and δ = 2.50 ppm for $(CD_3)_2SO$) (^{13}C NMR chemical shifts: δ = 77.23 ppm for $CDCl_3$, δ = 205.87, 30.60 ppm for acetone-d_6 and δ = 39.51 ppm for $(CD_3)_2SO$). Fast atom bombardment mass spectrometry (FAB-MS) data were obtained using a JEOL JMS-AX505WA mass spectrometer with m-nitrobenzyl alcohol (NBA) as a matrix and were reported in units of mass to charge (m/z). Analytical thin layer chromatography was performed using Kieselgel 60F-254 plates from Merck. Column chromatography was carried out on Merck silica gel 60 (70-230 mesh). UV/vis spectra were collected on a Beckman DU-800 and fluorescent spectra were collected on a Jasco FP-6500 and SpectraMax M2 spectrophotometer at 25℃ unless noted otherwise. K_m and V_{max} were calculated by nonlinear fitting of the Michaelis–Menten equation using SigmaPlot 8.0. For inhibition experiments, the IC_{50} curves were generated using SigmaPlot 8.0.

All chemical reagents and PKLAP were purchased from either Sigma-Aldrich or TCI and used without any further purification. Deuterated solvents were

acquired from Cambridge Isotopic Laboratories. CH_2Cl_2, pyridine and triethyl amine (TEA) were purified by distillation from CaH_2. THF were distilled from sodium benzophenone. Acetone was dried with anhydrous $MgSO_4$ before use. $CHCl_3$ were distilled from $CaCl_2$. All anion salts were purchased from Aldrich or TOKYO KASEI KOGYO chemical company.

1.4.2. Chemical Synthesis

We synthesized DCDHF-NH_2 following the published procedures [130, 134].

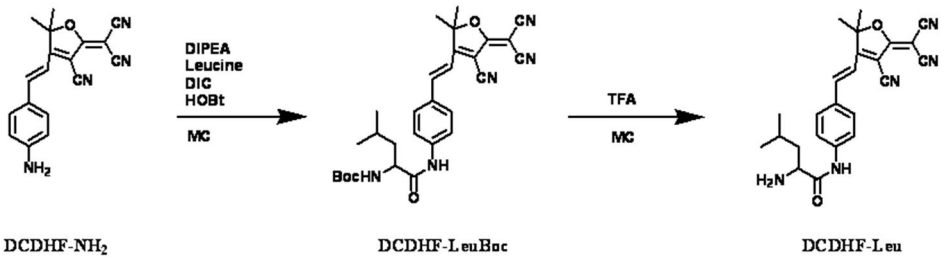

Scheme S 6 Synthtesis of DCDHF-Leu

DCDHF-LeuBoc

To a stirred solution of anhydrous CH_2Cl_2 (5 mL) containing DCDHF-NH_2(81 mg, 0.268 mmol), N-Boc-L-leucine (73.5 mg, 0.295 mmol), diisopropylethylamine (140.43 μL, 0.804 mmol), hydroxybenzotriazole (43.36 mg, 0.321 mmol) and diisopropylcarbodiimide (55.23 μL, 0.348 mmol) were added. After the mixture was stirred for 2 days, the solvent was diluted with 100 mL of water, extracted twice with 50 mL of CH_2Cl_2, washed with brine. The organic layer was dried over anhydrous Na_2SO_4, filtered, and evaporated. The crude product was purified by column chromatography on silica gel using 1:1 hexane and ethyl acetate (R_f = 0.4) as the mobile phase to give product (21 mg, 14.5%). ^{1}H NMR (300 MHz, $(CD_3)_2CO$): δ = 9.67 (s,

1H), 8.01 (d, 1H, *J* =16.5 Hz), 7.88 (q, 4H, *J* = 9.0 Hz, *J* = 18.0 Hz), 7.25 (d, 1H, *J* = 16.5 Hz), 6.30 (d, 1H, *J* = 5.7 Hz), 4.30 (d, 1H, *J* = 7.8 Hz), 1.91 (s, 6H), 1.68 (m, 3H), 1.41 (s, 9H), 0.95 (m, 6H).

FAB-MS calcd. for $C_{29}H_{33}N_5O_4$ [M]+ 515, found 515

DCDHF-Leu

To a stirred solution of anhydrous CH_2Cl_2 (1 mL) containing DCDHF-LeuBoc (10 mg, 0.019 mmol), TFA (0.5 mL) was added and stirred for 3 hr. The solution was evaporated and extracted with CH_2Cl_2, washed with 1% K_2CO_3 and then, brine. The organic layer was dried over anhydrous Na_2SO_4, filtered, and the solvent was removed under reduced pressure and dried on high vacuum to give rise to the product (64% yield). ^{1}H NMR (300 MHz, $(CD_3)_2CO$): δ = 8.03 (m, 4H), 7.47 (m, 2H), 4.90 (m, 1H), 2.64 (m, 1H), 1.93 (m, 6H), 1.42 (m, 3H), 0.98 (m, 6H).

HRMS : calcd. for $C_{24}H_{25}N_5O_2$ $[M+H]^+$ 415.2087, found 415.2089.

1.4.3. Enzymatic activity assay

1.4.3.1. The optical response of DCDHF-Leu dependent on LAP activity

Optical response experiments were carried out at 25℃ in HEPES buffer (10 mM, pH 7.4). 0.2 μg/mL of LAP was added to 10 μM of DCDHF-Leu solution in fluorescence cell. Stock solution was prepared to be 10 mM of DCDHF-Leu in DMSO. It was diluted to 10 mM with HEPES buffer and the final volume was 2 mL. Fluorescent intensity was measured time-dependently (0–40 min.).

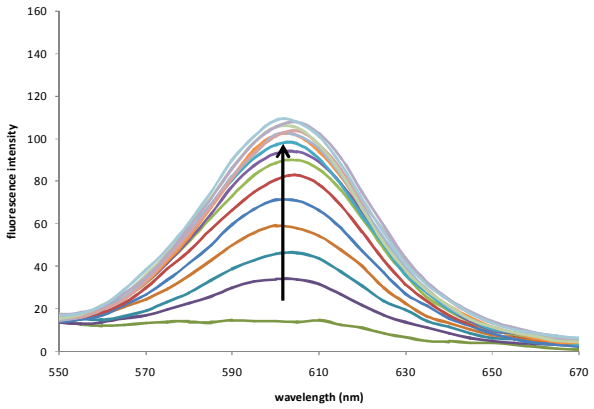

Figure S 18 Time-dependent fluorescence response

1.4.3.2. Enzyme kinetics

Kinetic experiments were carried out at 25 °C in HEPES buffer (pH 7.4). PKLAP (0.2 mg/mL) was added to a series of different concentrations of DCDHF-Leu (50, 20, 10, 5, 2.4, 1.2 μM) in a 96-well black bottom plate. The final volume in each well was 250 μL. Then, the plate was immediately transferred to a SpectraMax M2 multi-detection reader for fluorescence measurement. The rate of increase in fluorescence intensity at 605 nm was used to determine the kinetic parameters of enzyme hydrolysis. The values of the kinetic parameters (K_M and V_{max}) were determined from the double-reciprocal plot of the hydrolysis rate versus substrate concentration (Michaelis-Menten plot).

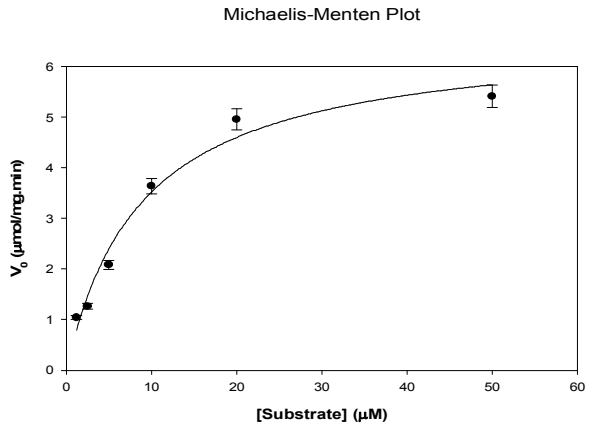

Figure S 19 Micaelis-Menten plot

1.4.3.3. Inhibitory potency measurement

To confirm the ability of our probe to measure inhibitory potency, we carried out fluorescence measurements after the addition of DCDHF-Leu prior to the incubation of different concentrations of bestatin (0.6, 1.2, 2.5, 5, 10, 20, 50 mM) with PKLAP for 10 min in a 96-well black bottom plate. Fluorescence measurements were implemented in the same way as kinetic experiments. The rate of decrease in fluorescence intensity at 605 nm was used to determine the IC_{50} of bestatin.

1.4.4. Living cell imaging with DCDHF-Leu and a cell lysate test

1.4.4.1. Cell culture and fluorescence measurements

HCT 116 (human colorectal carcinoma cell, ATCC CCL-247) cells were maintained in McCoy's 5A medium (Lonza) supplemented with 5% FBS, 10 mM HEPES buffer, 2 mM L-glutamine, and 50 ng/mL gentamicin. For fluorescence imaging experiments, cells were seeded on 24-well plate with coverslips in the same medium described above. 20 μM DCDHF-Leu was added in HCT 116 cells for 20 min. Subsequence cells were fixed with 4%

paraformaldehyde for 20 min, permeabilized in 1 x PBS with 0.4% Triton X-100 for 15 min and washed 3 times with 1 x PBS. Coverslips were affixed to glass slides using mounting media containing DAPI (Vector). For negative control, 100 μM bestatin was pretreated for 20 min and then, the same protocol was followed. The fluorescence of DCDHF-Leu complex was examined with Zeiss fluorescence microscope (Axio observer D1, Carl Zeiss).

1.4.4.2. Cell lysate test

For protein extracts, HCT 116 cells were seeded on 6-well plates. Cell monolayer washed 3 times with 1 x PBS on ice. Cells collected 500 μl of cell lysis buffer (20 mM Tris-HCl, pH 7.5) and sonication. Cell debris was removed by centrifugation (12,000 rpm for 15 min at 4 ℃). Protein concentrations were quantified using the DC assay (BioRad) with bovine serum albumin (BSA) as the calibrating standard. 20 μM of DCDHF-Leu was added in two sets of 2 mg/mL HCT 116 cell lysate solutions. One contained 100 μM of bestatin and the other contained no inhibitor. Fluorescence data were collected on SpectraMax M2 multi-detection reader (Molecular Devices)

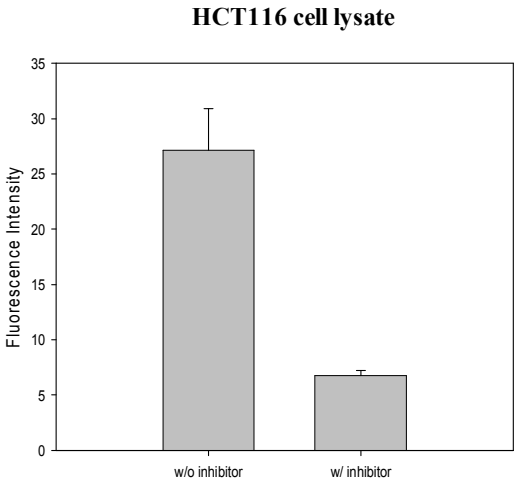

Figure S 20 Cell lysate test

Section 2.
Selectvie detection of Steroide sulfatase (STS) and ratiometric detection of sulfatase activity in living cells

2.1. Introduction

Human sulfatase hydrolyzes sulfate ester bonds from various substrates, such as glycosaminoglycans, sulfolipids, and steroid sulfates. Human sulfatases are reported to have a relation with processes such as the synthesis of hormones in the ER [135], the degradation of glycosaminoglycans and glycolipids in the lysosome [136], and the modulation of developmental-cell signaling in the extracellular membrane [137].

The pH-dependent activities of human sulfatases are criteria for classifying lysosomal sulfatases active in acidic conditions and non-lysosomal sulfatase activated under neutral conditions. The lysosomal sulfatases are involved in a catabolic function, and each sulfatase has been related to a specific lysosomal storage disorder [52]. Non-lysosomal sulfatases are localized in other

subcellular compartments, such as the ER and the Golgi apparatus. Steroid sulfatase (STS, arylsulfatase C) is the only one whose natural substrates and metabolic role have been thoroughly characterized and is involved in the metabolic pathway of several steroid molecules [138]. STS hydrolyzes estrone sulfate (E1S) to form estrone (E1) to regulate the formation of biologically active steroids. Estrone sulfate, a water-soluble inactive steroid, does not bind to the ER, and the concentrations in living systems are much higher than those of estrogen [139]. STS activity could be an important factor in the development and growth of tumors in hormone-dependent tissues, because EIS is cleaved by STS to generate an unconjugated estrogen that can bind to the ER, for which the expression level is a substantial issue in tumors [140]. Thus, sensitive and selective cell-imaging probes for the detection of STS would be of great value in developing diagnostic tools or inhibitor evaluations.

Most arylsulfatases, including STS, could catalyze the hydrolysis of artificial arylsulfate substrates, and this feature has been adopted for the probe design. Commercially available p-nitrophenol sulfate (pNPS) and 4-methylumbeliferone sulfate (4MUS) are widely used to detect sulfatase activity in color changes or fluorescence enhancements. Several activity-based probes for monitoring STS activities were developed, which released sulfate by STS to form quinone methide to be attacked by the nucleophile of STS. This reaction occurred more efficiently in neutral conditions than in acidic conditions, which could detect STS activity selectively. However, except for the strategy, most sulfatase probes could not discriminate STS activity from lysosomal sulfatases.

The fluorescence enhancement without wavelength changes can be caused by

many factors, including the localization of the probe, changes of the environment around the probe, and changes in the excitation intensity. Generally, ratiometric detection shows insusceptibility to these factors and the signal allows quantitative determination in the imaging of living cells and tissues.

Here, we developed two types of fluorescent probes based on a DCDHF unit; one is a pH-dependent fluorescence-emitting probe, and the other is a ratiometric probe (Scheme 5). The pH-dependent fluorescence-emitting probe was based on a 2-dicyanomethylene-3-cyano-2, 5-dihydrofuran (DCDHF) unit as an electron-accepting unit and sulfate ester-linked π-conjugated system (DCDHF–O-Sulf). Sulfatase hydrolyzes DCDHF-O-Sulf to DCDHF-OH, which emits at a shorter wavelength (570 nm) under acidic conditions and at a longer wavelength (605 nm) under neutral conditions. The optimal condition of STS activity is pH 7, and the observation of the emission at 605 nm allows selective detection of STS activity. The ratiometric probe was designed using a DCDHF-NH_2 unit that conjugates phenyl sulfate ester by carbamate moiety. Upon the cleavage of sulfate ester by sulfatase, the emission of DCDHF-NCOO-Sulf was decreased and the emission of DCDHF-NH_2 was increased. With the properties of the DCDHF probes, the selective detection of STS activity and an accurate quantitative assay could be achieved.

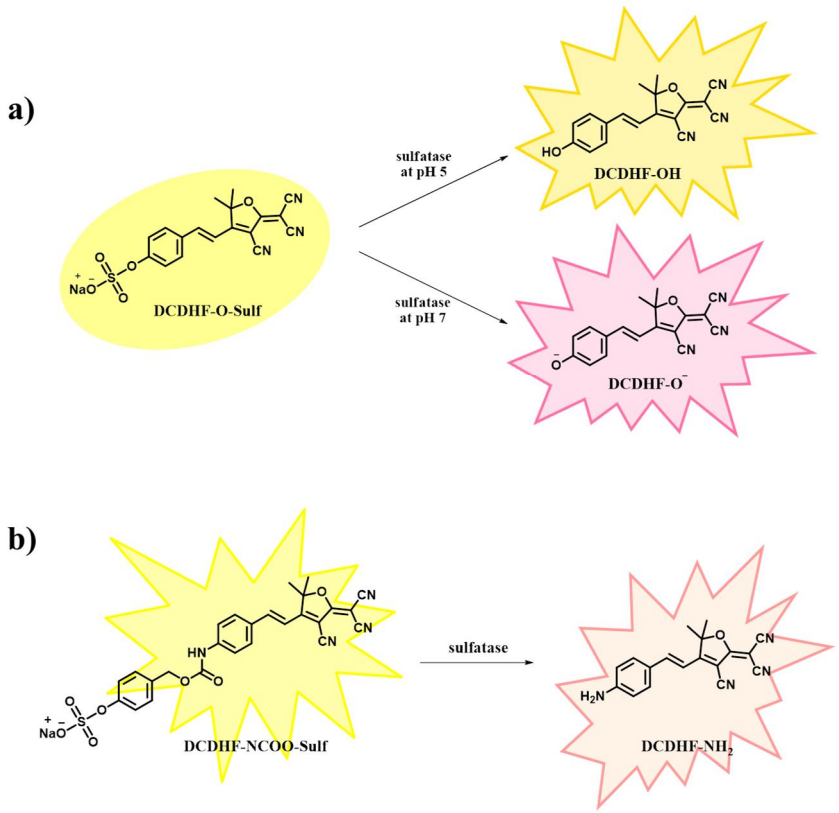

Scheme 5. (a) DCDHF-O-Sulf and (b) DCDHF-NCOO-Sulf.

2.2. Results and Discussion

To evaluate the feasibility of DCDHF probes for sulfatase activity assay, the optical responses of DCDHF-NCOO-Sulf and DCDHF-O-Sulf with the treatment of sulfatases were measured *in vitro*. To be specific, 10-μM probes and 0.5 mg/ml of *Helix pomatia* arylsulfatase in 50mM of Tris buffer (pH 7.48) or in 100 mM of potassium acetate buffer (pH 5.03) were used. The fluorescence of DCDHF-O-Sulf was quenched due to the capping of the

hydroxyl functionality with sulfate ester interfering with the ICT effect in the whole molecule [128]. However, when DCDHF-O-Sulf was converted to DCDHF-OH by the enzymatic reaction of sulfatase in 50mM of Tris buffer at pH 7.48, the emission band at 610 nm was increased with 520 nm of excitation in a time-dependent manner (Fig. 22a). In addition, color changes of the solution of DCDHF-O-Sulf and sulfatase were induced. The solution of DCDHF-O-Sulf was yellow, and that of DCDHF-OH was pink in 50mM of Tris buffer (pH 7.48). After DCDHF-O-Sulf was incubated with sulfatase at pH 7.48 for 1h, the color of the solution containing DCDHF-O-Sulf and sulfatase was changed from yellow to pink, and sulfatase activity could be observed by the naked eye (Fig. 23). This meant that the sulfate ester of DCDHF-O-Sulf was hydrolyzed by sulfatase to generate DCDHF-OH. In the case of DCDHF-NCOO-Sulf, the fluorescence response upon the treatment with sulfatase showed ratiometric changes. With 430nm of excitation, DCDHF-NCOO-Sulf showed strong emission at 575nm compared with the very weak fluorescence of DCDHF-NH_2, which was a product of the enzymatic reaction with sulfatase. On the other hand, with 545 nm of excitation, DCDHF-NCOO-Sulf was almost quenched and DCDHF-NH_2 was emitted at 605 nm (Fig. 22b). To observe the ratiometric fluorescence changes of DCDHF-N probes upon the treatment with sulfatase, the mixture of DCDHF-NCOO-Sulf and sulfatase was excited at 510 nm. With 510 nm of excitation, the emission band at 605 nm of DCDHF-NH2 was increased in a time-dependent manner (Fig. 22b). The solution color of DCDHF-NCOO-Sulf and sulfatase incubated for 1.5 hours was changed from yellow to pink as well (Fig. 24). This also meant that the sulfate ester of DCDHF-NCOO-Sulf was cleaved by sulfatase to form DCDHF-NH_2. The cleavage of sulfate ester in

DCDHF-O-Sulf or DCDHF-NCOO-Sulf by sulfatase to generate DCDHF-OH or DCDHF-NH_2 was able to trigger significant optical changes. Therefore, DCDHF-O-Sulf and DCDHF-NCOO-Sulf could be applicable as an off-on probe and a ratiometric probe for the detection of sulfatase activity, respectively.

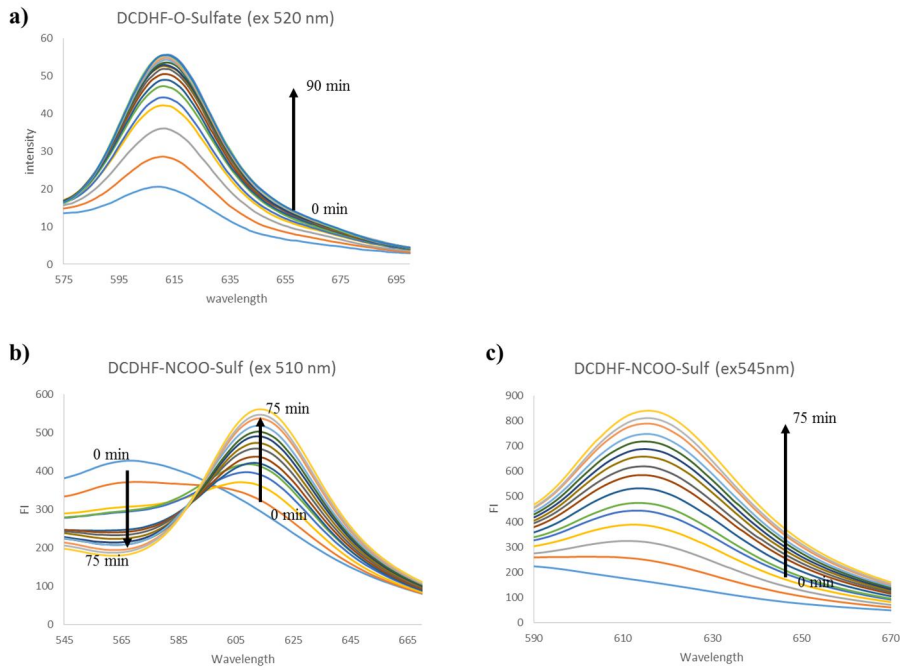

Figure 22 Fluorescence spectra of (a) 10μM DCDHF-O-Sulf (ex 520 nm), (b) 10μM DCDHF-NCOO-Sulf (ex 510 nm), (c) 10uM DCDHF-NCOO-Sulf (ex 545 nm) with the treatment of 0.5mg/ml sulfatase in 50mM Tris buffer (pH 7.48, room temperature) in time-dependant manner.

Human arylsulfatases are classified as lysosomal sulfatases, such as arylsulfatases A (ARSA) and B (ARSB) and non-lysosomal sulfatase, including arylsulfatases C (ARSC; steroid sulfatase, STS), D, E, F, and G, which are usually located at the endoplasmic reticulum or Golgi apparatus

[51-53, 141]. Among these sulfatases, ARSA, ARSB, and STS (ARSC) are the most studied. Arylsulfatase A, B, and C were named based on their ability to cleave the aromatic sulfate ester of chromogenic and fluorogenic artificial compounds in spite of their natural substrates being sulfatide, chondroitin sulfate, and steroid sulfate, respectively. The newly discovered arylsulfatases D, E, F, and G were named based on their sequence homology, but their activity has not been reported. Although all three sulfatases ARSA, ARSB, and STS could cleave aromatic sulfate ester, ARSA and ARSB are located in the lysosome and their optimal pH is 4–6, but STS is mostly located in the endoplasmic reticulum and exhibits maximal activity in neutral conditions [53].

To discriminate STS from ARSA and ARSB, the pH dependency of DCDHF probes should be observed. The absorption spectra and fluorescence emission of 10μM of DCDHF-O-Sulf and 10μM of DCDHF-OH were observed at pH 7.48 and pH 5.03, respectively. As shown in Figure 23, DCDHF-OH exhibited absorption maxima at 440 nm in acidic conditions (pH 5.03) and 570 nm in neutral conditions (pH 7.48), while the absorption bands of DCDHF-O-Sulf at pH 5.03 and pH 7.48 were identical. The solution colors of DCDHF-OH at pH 5.03 and 7.48 were yellow and pink, respectively (Fig. 23). In addition, DCDHF-OH at pH 5.03 and 7.48 exhibited different emission maxima (Fig. 23). Upon excitation at 435 nm, the fluorescence maxima of DCDHF-OH at 560 nm exhibited more strongly at pH 5.03 than at pH 7.48. On the other hand, with 520 nm of excitation, the fluorescence maxima of DCDHF-OH at pH 7.48 exhibited at 610 nm compared with the fluorescence at pH 5.03, which was almost quenched. The different spectral response of DCDHF-OH under different pH conditions was due to the increased

occupancy of the phenolate form of DCDHF-OH at pH 7.48 compared with pH 5.03 [142]. These results indicated that DCDHF-OH at different pH conditions showed different fluorescence maxima wavelengths, which was applicable to detecting pH conditions. Then, the fluorescence intensity of DCDHF-O-Sulf with 0.5 mg/ml of sulfatase at pH 5.03 and pH 7.48 was investigated (Fig. 23 and S21). The fluorescence intensity of DCDHF-O-Sulf hydrolyzed by sulfatase at pH 5.03 was quenched at 605 nm upon excitation at 520 nm, while the fluorescence at 570 nm with 435 nm of excitation was increased. At pH 7.48, the fluorescence intensity of DCDHF-O-Sulf with sulfatase was increased at 605 nm with 520 nm of excitation in a time-dependent manner, but weak intensity at 570 nm upon excitation at 435 nm was exhibited (Fig. 23 and S22). As a result, DCDHF-O-Sulf was hydrolyzed by sulfatase to generate DCDHF-OH, which exhibited different spectral responses according to the pH conditions. In neutral conditions, DCDHF-OH emitted only at 605 nm when it was excited at 520 nm, and in acidic conditions, DCDHF-OH exhibited strong fluorescence at 570 nm upon excitation at 435 nm. The fluorescence changes at 605 nm of DCDHF-OH would make it feasible to detect STS activity, for which the optimal pH is neutral, and the fluorescence changes at 570 nm would be useful for detecting lysosomal arylsulfatases. Therefore, DCDHF-OH could be suitable for pH-dependent bioimaging and discrimination of STS from other arylsulfatases that act in acidic conditions.

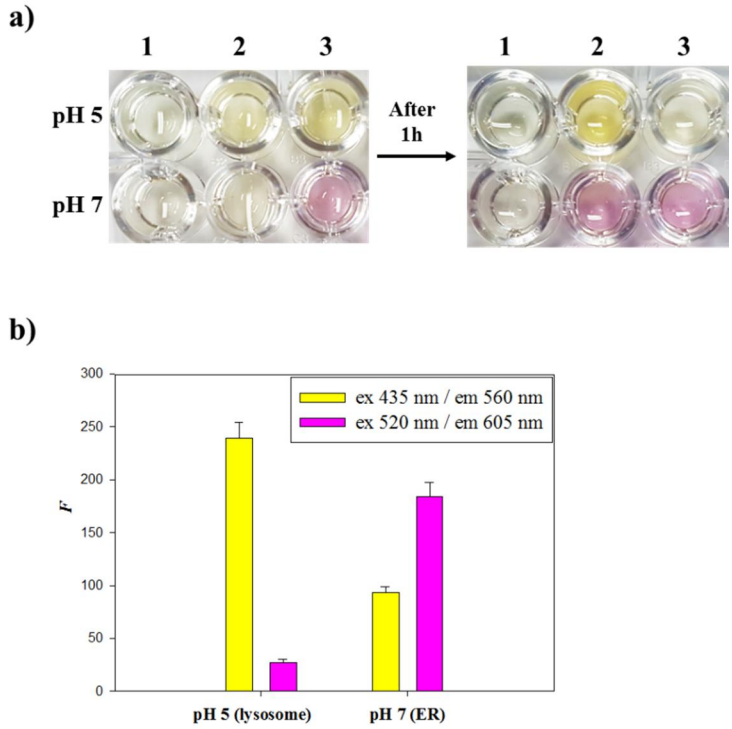

Figure 23 The color changes of DCDHF-O-Sulf with treatment of sulfatase at pH 5 and pH 7 (1: 20 μM of DCDHF-O-Sulf, 2: 20 μM DCDHF-O-Sulf and sulfatase, 3: 20 μM DCDHF-OH) (a), and the fluorescence properties of 10 μM DCDHF-OH at pH 5 and pH 7 (b).

In the cases of DCDHF-NCOO-Sulf and DCDHF-NH_2, the solutions displayed yellow and pink colors with absorption spectra at 440 nm and 500 nm, respectively, regardless of pH conditions (Fig. 24 and S23). The emission band of DCDHF-NCOO-Sulf exhibited at 570 nm, that of DCDHF-NH_2 emitted at 610 nm in both acidic and neutral conditions, and the fluorescence intensities were also similar (Fig. 24 and S23). When they were excited at 510 nm, both the fluorescence maxima wavelengths of DCDHF-NCOO-Sulf (570 nm) and DCDHF-NH2 (610 nm) were identical in both acidic and neutral conditions. This meant that the fluorescence wavelengths and the intensity of

DCDHF-NCOO-Sulf and DCDHF-NH_2 were independent of pH conditions. Then, to observe the fluorescence changes of DCDHF-NCOO-Sulf with the treatment of sulfatase at pH 5.03 and pH 7.48, 10 μM of DCDHF-NCOO-Sulf was incubated with 0.5 mg/ml of sulfatase at pH 5.03 or pH 7.48 (Fig. 24 and S21). The fluorescence intensity at 570 nm was decreased, and the fluorescence intensity at 610 nm was increased in a time-dependent manner in both acidic and neutral conditions (Fig. S21). As a result, the emission wavelengths of DCDHF-NCOO-Sulf and DCDHF-NH2 were not affected by pH conditions. Therefore, DCDHF-NCOO-Sulf would not be suitable to discriminate STS from ARSA or ARSB, but it would be useful for quantitative determination in the bioimaging of STS activity.

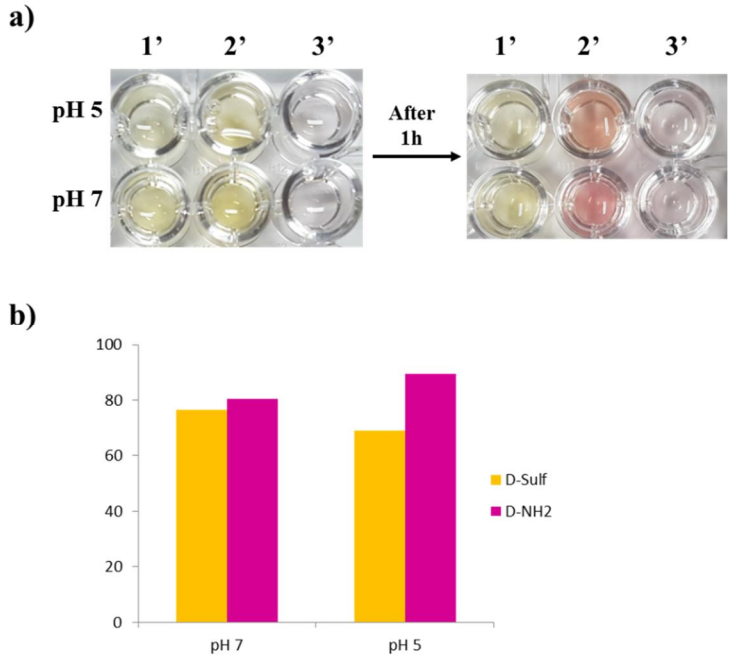

Figure 24 Color changes of DCDHF-NCOO-Sulf at pH 5 and pH 7 (1'. 20μM DCDHF-NCOO-Sulf only; 2'. 20μM DCDHF-NCOO-Sulf and 0.5 mg/ml sulfatase; 3'. 20μM DCDHF-NH_2 alone; 50mM Tris buffer at pH 7.48 and 100mM potassium acetate buffer at pH 5.03 at room temperature) (a), and the fluorescent intensities of

10μM DCDHF-NCOO-Sulf (yellow bar) and 10μM DCDHF-NH2 (pink bar) at pH 7 and pH 5 (ex 510 nm) (b).

To obtain the enzyme kinetics, the fluorescence intensity was examined with various concentrations (0, 1, 2, 5, 10, 20, and 50 μM) of probes and 0.5 mg/ml of *H. pomatia* sulfatase in 50mM of Tris buffer at pH 7.48 (Fig. S24). The maximum velocities (V_{max}) of DCDHF-O-Sulf and DCDHF-NCOO-Sulf were determined to be 2.8 ± 0.3 μmol/min and 10 ± 1 μmol/min, respectively. In addition, the Michaelis constants (K_m) of DCDHF-O-Sulf and DCDHF-NCOO-Sulf were 25 ± 6 μM and 225 ± 44 μM, respectively (Table 5). According to the values, DCDHF-O-Sulf reacted with sulfatase slower than DCDHF-NCOO-Sulf, while DCDHF-NCOO-Sulf bound to sulfatase better than DCDHF-O-Sulf. For previously reported probes, such as 4-nitrophenyl sulfate (4-NPS) and 4-methyl umbelliferon sulfate (4-MUS), the Km values with STS were determined to be 2.0 mM and 275 μM, respectively [60, 61, 141, 143]. The probes also reported the Km values with HP sulfatase that were 1.8 mM and 700 μM. Compared with the reported values for the same target, HP sulfatase, DCDHF-O-Sulf, and DCDHF-NCOO-Sulf exhibited reasonable binding affinity to HP sulfatase. However, these values do not indicate that the probes are better substrates of human STS.

To explore the feasibility of DCDHF probes to measure inhibitory potency, the inhibition potency (IC_{50}) of estrone 3-*O*-sulfamate (EMATE), which is an irreversible inhibitor of human STS [144], was determined. A constant amount of HP sulfatase (0.5 mg/mL) was incubated with various concentrations of EMATE (from 0.01 to 1 μM overnight), and then the 10-μM DCDHF–probes were added. The IC_{50} of EMATE was obtained as 252± 1 nM with DCDHF-O-Sulf and 135± 1 nM with DCDHF-NCOO-Sulf (Table 5 and Fig. 25),

which are the same order of magnitude (Table 5). This revealed that the DCDHF–probes are applicable for detecting potent inhibitors of sulfatase with HTS.

Table 5. Kinetic parameters and inhibitory potency

Substrate	V_{max} (μmol/**min.mg**)	K_m (μM)	IC_{50} of EMATE (nM)
4-MUS		**275**[a]	**56**[b]
DCDHF-O-Sulf	**2.8 ± 0.3**	25 ± 6	252 ± 1[c]
DCDHF-NCOO-Sulf	**10 ± 1**	225 ± 44	135 ± 1[c]

[a] The value was reported in ref. [143]

[b] The value was obtained by 4-MUS with purified STS [143].

[c] The values were obtained by DCDHF-probes with *Helix pomatia* sulfatase.

To demonstrate the DCDHF probes' ability to detect steroid sulfatase activity in a cell, the probes were applied to MCF-7 cells for fluorescence imaging. Two sets of MCF-7 cells were incubated with 15 μM of DCDHF–O-Sulf and DCDHF-NCOO-Sulf for 40 min at room temperature. As a control, two sets of MCF-& cells were incubated with 10 μM of EMATE overnight prior to the addition of each probe. The MCF-7 cells without EMATE exhibited the fluorescence intensity of the DCDHF probes; in comparison, the cells with EMATE showed weak fluorescence intensity (Fig. 25) For the discrimination of steroid sulfatase activity from other arylsulfatases, live cell imaging should be carried out and subcellular organelles should be observed. The fluorescence at 610 nm of DCDHF-OH would be emitted in the endoplasmic reticulum, which STS is located in under neutral conditions. These studies are

our further aims to be continued. Despite the fact that the image was not selective of steroid sulfatase activity, the results indicated that the DCDHF probes were applicable for detecting sulfatase activity and image sulfatase activity in MCF-7 cells.

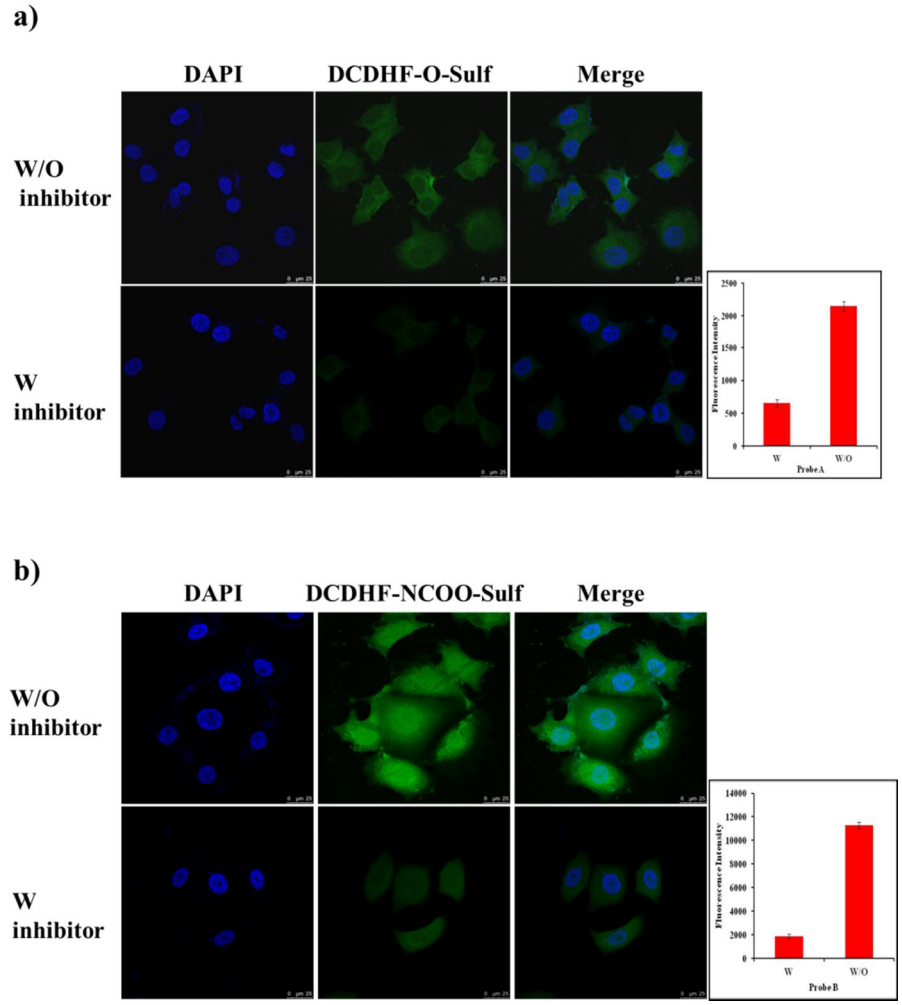

Figure 25. Application of DCDHF-probes to cell imaging. The fluorescence images of MCF-7 cells (upper row) incubated with DCDHF-O-Sulf (a, upper row, ex 520 nm) and DCDHF-NCOO-Sulf (b, upper row, ex 545 nm) for 2h. For inhibitor-treated cells, EMATE (10 mM) was pre-incubated overnight before incubation with DCDHF-O-Sulf (a, bottom row) and DCDHF-NCOO-Sulf (b, bottom row).

..

2.3. Conclusion

In summary, a pH-dependent signal-emitting probe, DCDHF-O-Sulf, and ratiometric probe, DCDHF-NCOO-Sulf, were synthesized and applied to sulfatase activity assay with fluorescence changes and color changes. DCDHF-OH, which was generated by the sulfatase activity, exhibited fluorescence at 610 nm only in neutral conditions, while it emitted at 570 nm only in acidic conditions, which could discriminate steroid sulfatase activity from lysosomal activity by observing the emission at 610 nm. The fluorescence of DCDHF-NCOO-Sulf with sulfatase decreased at 570 nm and increased at 610 nm. Both probes were shown to be applicable to the determination of image sulfatase activity on MCF-7 cells. Therefore, the DCDHF probes would be feasible for the detection and imaging of arylsulfatase activity in cells. However, for the discrimination of steroid sulfatase activity from that of others, live cell imaging should be implemented.

2.4. Experiments

2.4.1. Instrumentation

^{1}H and ^{13}C NMR spectra were recorded using an Advance 300MHz Bruker spectrometer in chloroform-d_3, CD_3OD. UV visible spectra were recorded on a Beckman DU 800 spectrophotometer. Fluorescence spectra were recorded on a Jasco FP-6500 spectrophotometer. Analytical thin-layer chromatography was performed using Kieselgel 60_F-254 plates from Merck. Column chromatography was carried out on Merck silica gel 60 (70 - 230 mesh). All

solvents and reagents were commercially available and used without further purification unless otherwise noted.

2.4.2. Materials

All reagents were purchased from either Sigma-Aldrich or TCI and used without any further purification. Deuterated solvents were acquired from Cambridge Isotopic Laboratories. All anion salts were purchased from Aldrich or TOKYO KASEI KOGYO chemical company.

2.4.3. Chemical synthesis

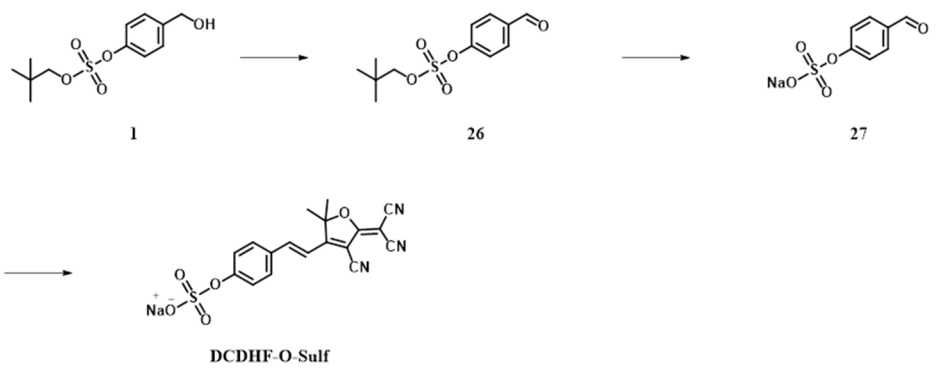

Scheme S 7 Synthesis of DCDHF-O-Sulf

Compound 26: To a solution of compound **1** (30 mg, 0.11mmol) in methylene chloride was added Dess Martin periodinane (47 mg, 1 equiv.). The reaction mixture was stirred overnight at room temperature. To the mixture was added saturated aquous sodium thiosulfate solution and stirred for 30 min. After removal of the methylene chloride, the residue was diluted in ethyl acetate, The organic layer was washed with saturated sodium bicarbonate, and dried over anhydrous sodium sulfate and concentrated in vacuo. The product was used for a next step without further purification. ^{1}H

NMR (300 MHz, $CDCl_3$) δ 1.02 (9H, s), 4.14 (2H, s), 7.50 (2H, d, *J* = 8.7 Hz), 7.99 (2H, d, *J* = 8.7 Hz), 10.04 (1H, s).

Compound 27: To a solution of compound **26** (27mg, 0.1mmol) in DMF was added sodium azide (8 mg, 1.2 equiv.) and the reaction mixture was refluxed overnight. After removal of DMF and the residue was purified by silica gel chromatography (MC:MeOH=10:1) to give compound **27** (18 mg, 0.074mmol, 74% yield). ^{1}H NMR (300 MHz, CD_3OD) δ 6.93 (2H, d, *J* = 8.4 Hz), 7.79 (2H, d, *J* = 8.4 Hz), 9.78 (1H, s).

DCDHF-O-Sulf : DCDHF (18 mg, 1.2 equiv.) and ammonium acetate (18 mg, 3 equiv.) were dissolved in anhydrous EtOH. To the solution was added compound **27** (18 mg, 0.074 mmol) and the reaction mixture was stirred overnight under nitrogene in the dark at room temperature. After the completion of the raction, EtOH was removed in vacuo, the residues was purified with silica gel chromatography (MC:MeOH=10:1) to give **DCDHF-O-Sulf** (15mg, 0.037mmol, 50% yield).^{1}H NMR (300 MHz, CD_3OD) δ 1.84 (6H, s), 7.18 (1H, d, *J* = 16.5 Hz), 7.45 (2H, d, J =6.8 Hz), 7.84 (2H, d, *J* = 8.7 Hz), 7.97 (1H, d, *J* = 16.3 Hz). ^{13}C NMR (75 MHz, CD_3OD) δ 22.64, 24.59, 27.20, 98.78, 110.31, 111.21, 111.70, 114.14, 121.20, 130.27, 130.59, 147.09, 156.23, 175.38, 176.67.

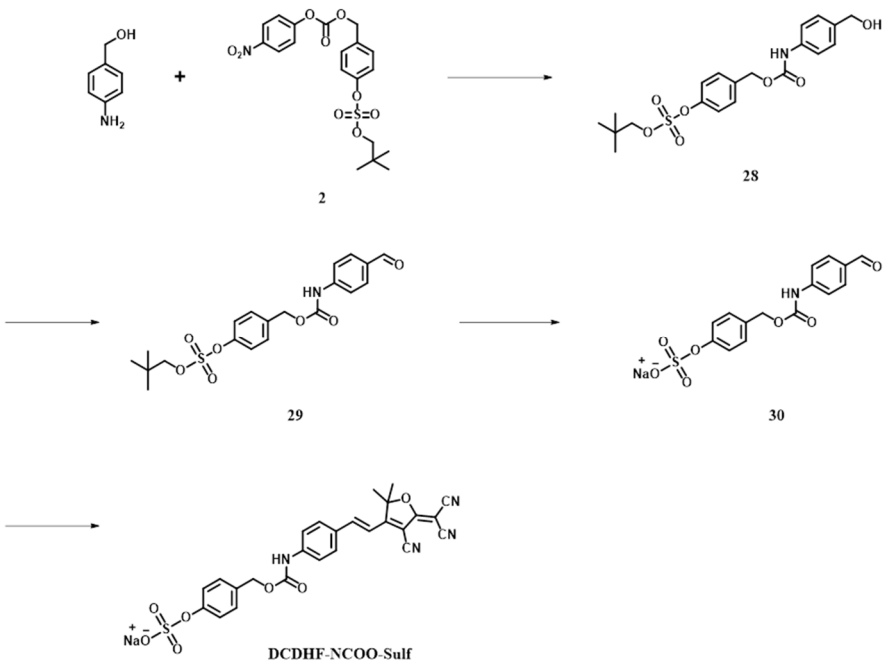

Scheme S 8 Synthesis of DCDHF-NCOO-Sulf

Compound 28: Compound **2** (440mg, 1mmol), 4-amino benzyl alcohol (185mg, 1.2equiv.) and HOBt (130mg, 1 equiv.) were dissolved in DMF. The mixture was stirred at room temperature for 16h, and then, concentrated in vacuo. The residue was dissolved in ethylacetate and washed with saturated aqous NH4Cl solution 3 times. The crude product wwas purified by silica gel chromatography (chloroform:acetone = 20:1) to give compound **28** (176mg, 0.416mmol, 41% yield).). ^{1}H NMR (300 MHz, $CDCl_3$) δ 1.02 (9H, s), 4.11 (2H, s), 4.65 (2H, s), 5.20 (2H, s), 6.84 (1H, s), 7.33 (6H, m), 7.46 (2H, d, *J* = 8.6 Hz); ^{13}C NMR (75 MHz, $CDCl_3$) δ 25.23, 31.63, 63.55, 65.07, 83.39, 118.26, 121.30, 127.31, 129.71, 136.61, 136.90, 137.90, 149.93, 153.41, 205.79.

Compound 29: To a solution of compound **28** (88 mg, 0.212 mmol) in methylene chloride was added Dess martin periodinane (90 mg, 1 equiv.) and the mixture was stirred at room temperature overnight. To the reaction

mixture was added saturated aquous sodium thiosulfate solution and stirred for 30min. The solution was diluted in ethyl acetate and washed with saturated sodium bicarbonate, and dried over anhydrous sodium sulfate and concentrated in vacuo. The product was used for a next step without further purification.

Compound 30: To a solution of compound **29** (0.22mmol) in DMF was sodium azide (16 mg, 1.1 equiv.) and the reaction mixture was refluxed overnight. After removal of DMF and the residue was purified by silica gel chromatography (MC:MeOH = 10:1) to give compound **30** (45mg, 0.12mmol, 55% yield).). ^{1}H NMR (300 MHz, CD_3OD) δ 5.20 (2H, s), 7.33 (2H, d, *J* = 8.7 Hz), 7.43 (2H, d, *J* = 8.7 Hz), 7.67 (2H, d, *J* = 8.7 Hz), 7.85 (2H, d, *J* = 8.7 Hz), 9.86 (1H, s).

DCDHF-NCOO-Sulf ; To a solution of DCDHF (36 mg, 1.5 equiv.) and ammonium acetate (35 mg, 3 equiv.) in anhydrous EtOH was added compound **30** (45 mg, 0.12 mmol) and the reaction mixture was stirred overnight under nitrogene in the dark at room temperature. After the completion of the raction, EtOH was removed in vacuo, the residues was purified with silica gel chromatography (MC:MeOH=10:1) to give **DCDHF-NCOO-Sulf** (18mg, 0.0324mmol, 27% yield). ^{1}H NMR (300 MHz, CD_3OD) δ 1.82 (6H, s), 5.19 (2H, s), 7.10 (1H, d, *J* = 16.2 Hz), 7.32 (2H, d, *J* = 8.7 Hz), 7.42 (2H, d, *J* = 8.7 Hz), 7.62 (2H, d, *J* = 8.7 Hz), 7.75 (2H, d, *J* = 8.6 Hz) 7.89 (1H, d, *J* = 16.2 Hz); ^{13}C NMR (75 MHz, CD_3OD) δ 24.69, 28.13, 30.70, 54.63, 54.73, 66.03, 97.86, 98.64, 110.51, 111.35, 111.82, 112.90, 118.31, 121.10, 128.84, 130.36, 132.82, 143.48, 147.64, 152.55, 153.76, 175.59,

176.75.

2.4.4. Enzymatic activity assay

The optical response of DCDHF-probes upon treatment with sulfatase

Fluorescence intensity experiments were carried out at room temperature in 50mM Tris buffer (pH 7.48). Stock solution was prepared to be 10 mM of DCDHF-probe in DMSO and 0.625mg/ml sulfatase in 50mM Tris buffer (pH 7.48) and in 100mM potassium acetate buffer (pH 5.03), respectively. Fluorescent intensity was measured with 0.5mg/mL of *H. pomatia* sulfatase and 10 μM of DCDHF-probe in 50mM Tris buffer (pH 7.48) in time-dependant manner (0–90 min.) and the final volume was 1 mL.

Color change was observed under the same condition.

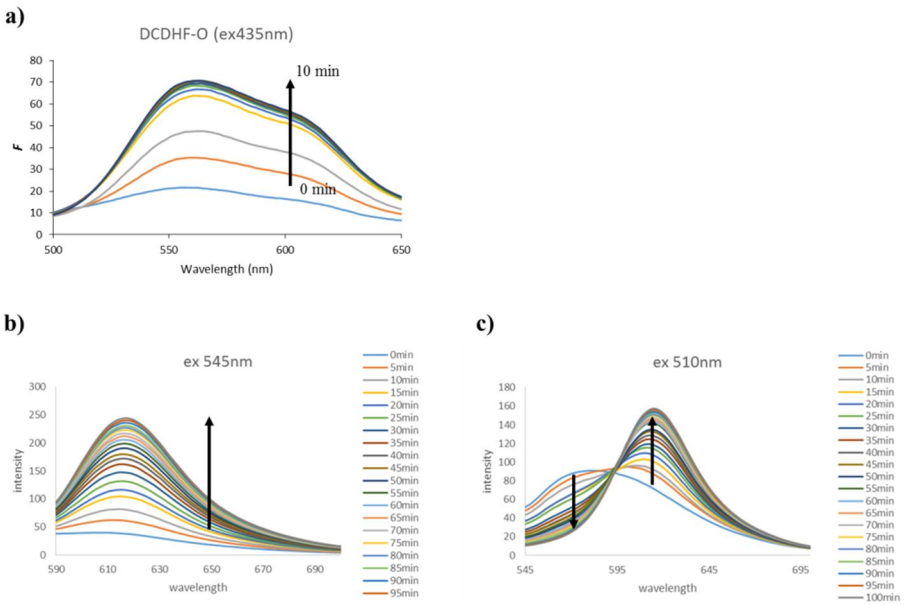

Figure S 21 Fluorescence spectra of (a) DCDHF-O-Sulf with HP sulfatase (ex 435 nm) and (b) DCDHF-NCOO-Sulf with HP sulfatase (ex 545 nm: left, ex 510nm: right)

at pH 5.03.

pH-dependence of DCDHF probes

10mM DCDHF-NCOO-Sulf in DMSO and 10mM DCDHF-O-Sulf in DMSO wereprepared as stock solution. To test the optical properties of probes upon different pH conditions, 10uM DCDHF- probes in 100mM potassium acetate buffer (pH 5.03) and 10uM DCDHF-probes in 50mM Tris buffer (pH 7.48) were used. 1ul of each 10mM DCDHF-probe stock solution was dissolved in 1ml of 100mM potassium acetate buffer (pH 5.03) and1ml of 50mM Tris buffer (pH 7.48), respectively. Fluorescence and absorption of the sample solutions were measured (Fig S22 and S23).

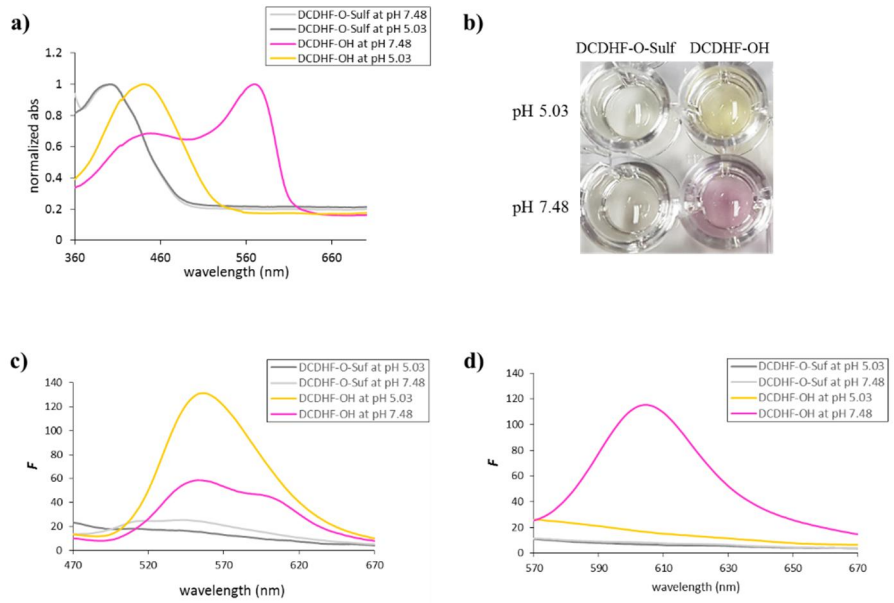

Figure S 22. Optical properties of DCDHF-O-Sulf and DCDHF-OH at pH 7.48, 50 mM Tris buffer and at pH 5.03, 100 mM potassium acetate buffer. (a) normalized absorption spectra, (b) photograph, (c) Fluorescence intensity with 435 nm excitation and (d) fluorescence intesnity with 520 nm ecxitation.

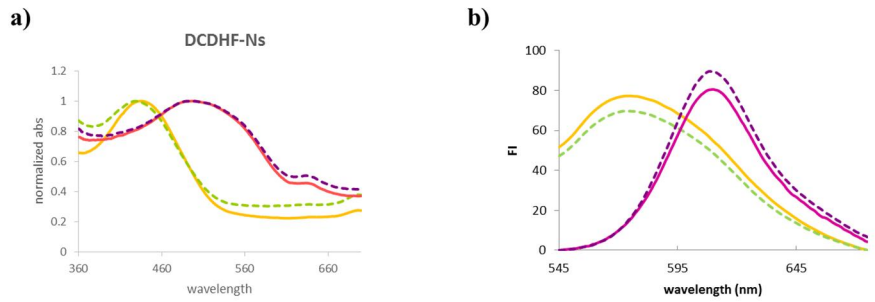

Figure S 23 Optical properties of DCDHF-NCOO-Sulf (yellow and green) and DCDHF-NH_2 (pink and purple) at pH 7.48, 50 mM Tris buffer (solid line) and at pH 5.03, 100 mM potassium acetate buffer(dashed line). (a) normalized absorption spectra, and (b) fluorescence intensity with 510 nm excitation.

Upon excitation at 430 nm, DCDHF-NCOO-Sulf emitted strong fluorescence while DCDHF-NH2 exhibited very weak fluoresceice intensity, in contrast, with 545 nm excitation, the fluorescence intensity of DCDHF-NCOO-Sulf was almost quenched but DCDHF-NH2 showed strong fluorescence intensity in acidic and neutral conditions.

Enzyme kinetics

Kinetic experiments were carried out at 37 °C in 50 mM Tris buffer (pH 7.48). A series of different concentrations of DCDHF-O-Sulf (0, 1, 2, 5, 10, 20, 50 μM) added to 0.5mg/ml H. pomatia sulfatase in a 96-well black bottom plate. The final volume in each well was 250 μL. Then, the fluorescence emission at 610 nm with 520 nm excitation was measured by a SpectraMax M2 multi-detection reader in time-course. The rate of increase in fluorescence intensity was used to determine the kinetic parameters of enzyme hydrolysis. The values of the kinetic parameters (K_M and V_{max}) were determined from the Michaelis-Menten plot of the hydrolysis rate versus substrate concentration.

The same procedure was carried out for determinations of kinetic parameters of DCDHF-NCOO-Sulf. The observed emission band was at 605 nm with 545 nm excitation.

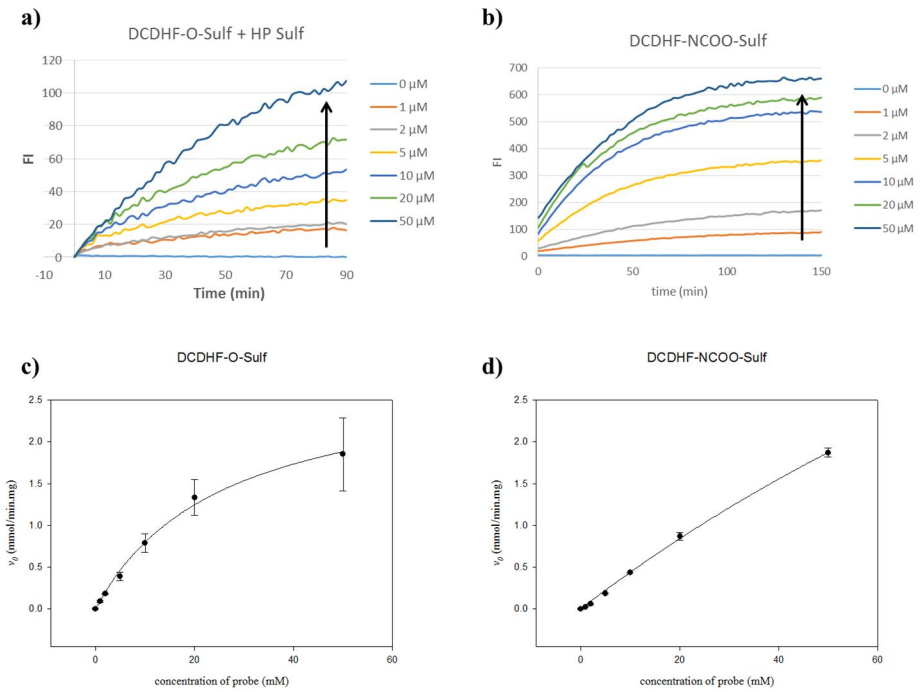

Figure S 24 Time-course fluorescence spectra of various concentration (0, 1, 2, 5, 10, 20 and 50 µM) of (a) DCDHF-O-Sulf and (b) DCDHF-NCOO-Sulf and kinetics of HP sulfatase with (c) DCDHF-O-Sulf and (d) DCDHF-NCOO-Sulf in pH 7.48, 50mM Tris buffer.

Inhibitory potency measurement

To confirm the ability of our probe to measure inhibitory potency, we carried out fluorescence measurements after the addition of 10 µM DCDHF-probes prior to the incubation of different concentrations of EMATE (0, 0.01, 0.02, 0.05, 0.1, 0.2, 0.5 and 1 µM) with 0.5 mg/ml HP sulfatase overnight. Fluorescence

measurements were implemented in the same way as kinetic experiments. The rate of decrease in fluorescence intensity at 605 nm was used to determine the IC_{50} of EMATE.

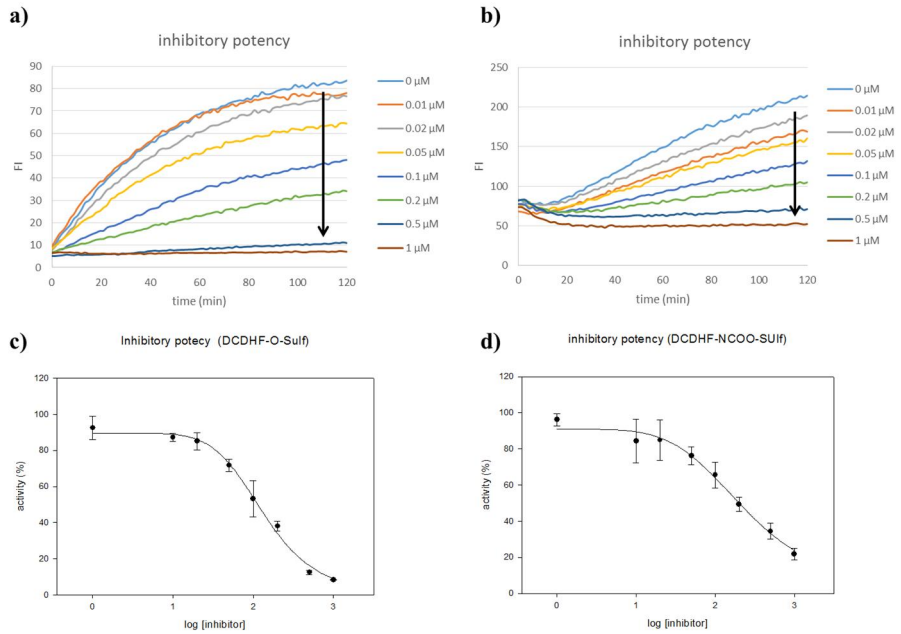

Figure S 25 Time-course fluorescence spectra of (a) DCDHF-O-Sulf and (b) DCDHF-NCOO-Sulf after incubation with various concentration (0, 0.01, 0.02, 0.05, 0.1, 0.2, 0.5 and 1 μM) of EMATE in pH 7.48, 50mM Tris buffer overnight, and inhibitory potency of EMATE measured with (c) DCDHF-O-Sulf and (d) DCDHF-NCOO-Sulf.

2.4.5. Cell imaging

Cell culture and fluorescence measurements

MCF-7 cells were fixed with 4% paraformaldehyde and 15 M of DCDHF-probes were treated for 2h. Coverslips were affixed to glass slides using mounting media containing DAPI (Vector) For negative control, 10 μM of

EMATE at 37℃ overnight and then, the same protocol was follow.

REFERENCES

[1] A.R. Mire-Sluis, The development of non-animal-based bioassays for cytokines and growth factors, Dev Biol Stand, 101 (1999) 169-175.

[2] T.K. Harris, M.M. Keshwani, Measurement of Enzyme Activity, Method Enzymol, 463 (2009) 57-71.

[3] J.M. Reymond, Enzyme assays : high-throughput screening, genetic selection, and fingerprinting Wiley-VCH, Place Published, 2006.

[4] J. Karam, J.A. Nicell, Potential applications of enzymes in waste treatment, J. Chem. Technol. Biotechnol., 69 (1997) 141-153.

[5] R.C. Kuhad, R. Gupta, A. Singh, Microbial cellulases and their industrial applications, Enzyme Res, 2011 (2011) 280696.

[6] P. Anbu, S.C.B. Gopinath, A.C. Cihan, B.P. Chaulagain, Microbial Enzymes and Their Applications in Industries and Medicine, Biomed Res Int, (2013).

[7] W.F. An, N. Tolliday, Cell-Based Assays for High-Throughput Screening, Mol. Biotechnol., 45 (2010) 180-186.

[8] W.P. Janzen, Screening Technologies for Small Molecule Discovery: The State of the Art, Chem Biol, 21 (2014) 1162-1170.

[9] J. Inglese, R.L. Johnson, A. Simeonov, M.H. Xia, W. Zheng, C.P. Austin, D.S. Auld, High-throughput screening assays for the identification of chemical probes, Nat Chem Biol, 3 (2007) 466-479.

[10] J.P. Goddard, J.L. Reymond, Enzyme assays for high-throughput screening, Curr. Opin. Biotechnol., 15 (2004) 314-322.

[11] R.L. Nicholson, M. Welch, M. Ladlow, D.R. Spring, Small-molecule

screening: Advances in microarraying and cell-imaging technologies, Acs Chem Biol, 2 (2007) 24-30.

[12] E. Terreno, D. Delli Castelli, A. Viale, S. Aime, Challenges for Molecular Magnetic Resonance Imaging, Chem. Rev., 110 (2010) 3019-3042.

[13] A. Razgulin, N. Ma, J.H. Rao, Strategies for in vivo imaging of enzyme activity: an overview and recent advances, Chem. Soc. Rev., 40 (2011) 4186-4216.

[14] M.A. Pysz, S.S. Gambhir, J.K. Willmann, Molecular imaging: current status and emerging strategies, Clin Radiol, 65 (2010) 500-516.

[15] R. Weissleder, M.J. Pittet, Imaging in the era of molecular oncology, Nature, 452 (2008) 580-589.

[16] A.M. Wu, P.D. Senter, Arming antibodies: prospects and challenges for immunoconjugates, Nat. Biotechnol., 23 (2005) 1137-1146.

[17] H. Kobayashi, P.L. Choyke, Target-Cancer-Cell-Specific Activatable Fluorescence Imaging Probes: Rational Design and in Vivo Applications, Acc. Chem. Res., 44 (2011) 83-90.

[18] H. Kobayashi, M. Ogawa, R. Alford, P.L. Choyke, Y. Urano, New Strategies for Fluorescent Probe Design in Medical Diagnostic Imaging, Chem. Rev., 110 (2010) 2620-2640.

[19] B.N.G. Giepmans, S.R. Adams, M.H. Ellisman, R.Y. Tsien, Review - The fluorescent toolbox for assessing protein location and function, Science, 312 (2006) 217-224.

[20] V. Ntziachristos, C. Bremer, R. Weissleder, Fluorescence imaging with near-infrared light: new technological advances that enable in vivo molecular imaging, Eur Radiol, 13 (2003) 195-208.

[21] J. Zhang, R.E. Campbell, A.Y. Ting, R.Y. Tsien, Creating new fluorescent

probes for cell biology, Nat Rev Mol Cell Bio, 3 (2002) 906-918.

[22] Y.S. Guo, X.M. Li, S.J. Ye, S.S. Zhang, Modern optical techniques provide a bright outlook for cell analysis, Trac-Trend Anal Chem, 42 (2013) 168-185.

[23] A.P. Alivisatos, Semiconductor clusters, nanocrystals, and quantum dots, Science, 271 (1996) 933-937.

[24] C. Burda, X.B. Chen, S.M. Halasz, J.V. Mankus, Development of novel nanostructure-based solar cells, Abstr Pap Am Chem S, 229 (2005) U452-U452.

[25] M. Ohlson, J. Sorensson, B. Haraldsson, A gel-membrane model of glomerular charge and size selectivity in series, Am J Physiol-Renal, 280 (2001) F396-F405.

[26] T.W. Kim, H.Y. Yoon, J.H. Park, O.H. Kwon, D.J. Jang, J.I. Hong, Molecular tripods showing fluorescence enhancement upon binding to streptavidin, Org. Lett., 7 (2005) 111-114.

[27] P. Venkatraman, T.T. Nguyen, M. Sainlos, O. Bilsel, S. Chitta, B. Imperiali, L.J. Stern, Fluorogenic probes for monitoring peptide binding to class II MHC proteins in living cells, Nat Chem Biol, 3 (2007) 222-228.

[28] M.E. Vazquez, M. Nitz, J. Stehn, M.B. Yaffe, B. Imperiali, Fluorescent caged phosphoserine peptides as probes to investigate phosphorylation-dependent protein associations, J. Am. Chem. Soc., 125 (2003) 10150-10151.

[29] A. Baruch, D.A. Jeffery, M. Bogyo, Enzyme activity--it's all about image, Trends Cell Biol, 14 (2004) 29-35.

[30] A. Miyawaki, Visualization of the spatial and temporal dynamics of intracellular signaling, Dev Cell, 4 (2003) 295-305.

[31] N.P. Mahajan, D.C. Harrison-Shostak, J. Michaux, B. Herman, Novel

mutant green fluorescent protein protease substrates reveal the activation of specific caspases during apoptosis, Chem Biol, 6 (1999) 401-409.

[32] A.Y. Ting, K.H. Kain, R.L. Klemke, R.Y. Tsien, Genetically encoded fluorescent reporters of protein tyrosine kinase activities in living cells, Proc. Natl. Acad. Sci. USA, 98 (2001) 15003-15008.

[33] B. Laxman, D.E. Hall, M.S. Bhojani, D.A. Hamstra, T.L. Chenevert, B.D. Ross, A. Rehemtulla, Noninvasive real-time imaging of apoptosis, P Natl Acad Sci USA, 99 (2002) 16551-16555.

[34] A.G. Vorobyeva, M. Stanton, A. Godinat, K.B. Lund, G.G. Karateev, K.P. Francis, E. Allen, J.G. Gelovani, E. McCormack, M. Tangney, E.A. Dubikovskaya, Development of a Bioluminescent Nitroreductase Probe for Preclinical Imaging, Plos One, 10 (2015).

[35] L.M. Wysocki, L.D. Lavis, Advances in the chemistry of small molecule fluorescent probes, Curr Opin Chem Biol, 15 (2011) 752-759.

[36] X.H. Li, X.H. Gao, W. Shi, H.M. Ma, Design Strategies for Water-Soluble Small Molecular Chromogenic and Fluorogenic Probes, Chem. Rev., 114 (2014) 590-659.

[37] J.S. Wu, W.M. Liu, J.C. Ge, H.Y. Zhang, P.F. Wang, New sensing mechanisms for design of fluorescent chemosensors emerging in recent years, Chem. Soc. Rev., 40 (2011) 3483-3495.

[38] S.J. Lord, N.R. Conley, H.L.D. Lee, S.Y. Nishimura, A.K. Pomerantz, K.A. Willets, Z.K. Lu, H. Wang, N. Liu, R. Samuel, R. Weber, A. Semyonov, M. He, R.J. Twieg, W.E. Moerner, DCDHF Fluorophores for Single-Molecule Imaging in Cells, Chemphyschem, 10 (2009) 55-65.

[39] Z. Li, X.H. Li, X.H. Gao, Y.Y. Zhang, W. Shi, H.M. Ma, Nitroreductase Detection and Hypoxic Tumor Cell Imaging by a Designed Sensitive and

Selective Fluorescent Probe, 7-[(5-Nitrofuran-2-yl)methoxy]-3H-phenoxazin-3-one, Anal. Chem., 85 (2013) 3926-3932.

[40] S. Park, S.Y. Lim, S.M. Bae, S.Y. Kim, S.J. Myung, H.J. Kim, Indocyanine-Based Activatable Fluorescence Turn-On Probe for gamma-Glutamyltranspeptidase and Its Application to the Mouse Model of Colon Cancer, Acs Sensors, 1 (2016) 579-583.

[41] K.Z. Gu, Y.J. Liu, Z.Q. Guo, C. Lian, C.X. Yan, P. Shi, H. Tian, W.H. Zhu, In Situ Ratiometric Quantitative Tracing of Intracellular Leucine Aminopeptidase Activity via an Activatable Near-Infrared Fluorescent. Probe, Acs Appl Mater Inter, 8 (2016) 26622-26629.

[42] H. Takakusa, K. Kikuchi, Y. Urano, S. Sakamoto, K. Yamaguchi, T. Nagano, Design and synthesis of an enzyme-cleavable sensor molecule for phosphodiesterase activity based on fluorescence resonance energy transfer, J. Am. Chem. Soc., 124 (2002) 1653-1657.

[43] A. Cobos-Correa, J.B. Trojanek, S. Diemer, M.A. Mall, C. Schultz, Membrane-bound FRET probe visualizes MMP12 activity in pulmonary inflammation, Nat Chem Biol, 5 (2009) 628-630.

[44] T. Terai, K. Kikuchi, Y. Urano, H. Kojima, T. Nagano, A long-lived luminescent probe to sensitively detect arylamine N-acetyltransferase (NAT) activity of cells, Chem. Commun., 48 (2012) 2234-2236.

[45] Y.H. Li, Y. Sun, J.C. Li, Q.Q. Su, W. Yuan, Y. Dai, C.M. Han, Q.H. Wang, W. Feng, F.Y. Li, Ultrasensitive Near-Infrared Fluorescence-Enhanced Probe for in Vivo Nitroreductase Imaging, J. Am. Chem. Soc., 137 (2015) 6407-6416.

[46] T.I. Kim, H.J. Kang, G. Han, S.J. Chung, Y. Kim, A highly selective fluorescent ESIPT probe for the dual specificity phosphatase MKP-6, Chem.

Commun., (2009) 5895-5897.

[47] G. Chen, D.J. Yee, N.G. Gubernator, D. Sames, Design of optical switches as metabolic indicators: New fluorogenic probes for monoamine oxidases (MAO A and B), J. Am. Chem. Soc., 127 (2005) 4544-4545.

[48] T.I. Kim, H. Kim, Y. Choi, Y. Kim, A fluorescent turn-on probe for the detection of alkaline phosphatase activity in living cells, Chem Commun (Camb), 47 (2011) 9825-9827.

[49] J. Chen, D.L. Liao, Y. Wang, H.P. Zhou, W.Y. Li, C. Yu, Real-Time Fluorometric Assay for Acetylcholinesterase Activity and Inhibitor Screening through the Pyrene Probe Monomer-Excimer Transition, Org. Lett., 15 (2013) 2132-2135.

[50] G.L. Liang, H.J. Ren, J.H. Rao, A biocompatible condensation reaction for controlled assembly of nanostructures in living cells (vol 2, pg 54, 2009), Nat Chem, 2 (2010) 239-239.

[51] M. Buono, M.P. Cosma, Sulfatase activities towards the regulation of cell metabolism and signaling in mammals, Cell. Mol. Life. Sci., 67 (2010) 769-780.

[52] G. Diez-Roux, A. Ballabio, Sulfatases and human disease, Annu. Rev. Genomics. Hum. Genet., 6 (2005) 355-379.

[53] S.R. Hanson, M.D. Best, C.H. Wong, Sulfatases: structure, mechanism, biological activity, inhibition, and synthetic utility, Angew. Chem. Int. Ed., 43 (2004) 5736-5763.

[54] S. Bhattacharyya, J.K. Tobacman, Steroid sulfatase, arylsulfatases A and B, galactose-6-sulfatase, and iduronate sulfatase in mammary cells and effects of sulfated and non-sulfated estrogens on sulfatase activity, J. Steroid Biochem. Mol. Biol., 103 (2007) 20-34.

[55] T. Suzuki, T. Nakata, Y. Miki, C. Kaneko, T. Moriya, T. Ishida, S. Akinaga, H. Hirakawa, M. Kimura, H. Sasano, Estrogen sulfotransferase and steroid sulfatase in human breast carcinoma, Cancer Res., 63 (2003) 2762-2770.

[56] S.G. Gibby, J.M. Younker, A.C. Hengge, Investigation of the sulfuryl transfer step from substrate to enzyme by arylsulfatases, J. Phys. Org. Chem., 17 (2004) 541-547.

[57] J.M. Grange, K. Clark, Use of umbelliferone derivatives in the study of enzyme activities of mycobacteria, J. Clin. Pathol., 30 (1977) 151-153.

[58] A.B. Roy, E.A. Williams, The Sulfatase of Helix-Pomatia - Purification and Kinetic-Properties, Comp. Biochem. Phys. B, 93 (1989) 229-237.

[59] H.J. Park, H.W. Rhee, J.I. Hong, Activity-based fluorescent probes for monitoring sulfatase activity, Bioorg. Med. Chem. Lett., 22 (2012) 4939-4941.

[60] J.S. Rush, K.E. Beatty, C.R. Bertozzi, Bioluminescent probes of sulfatase activity, Chembiochem, 11 (2010) 2096-2099.

[61] E.L. Smith, C.R. Bertozzi, K.E. Beatty, An expanded set of fluorogenic sulfatase activity probes, Chembiochem, 15 (2014) 1101-1105.

[62] I. Stawoska, S. Gaweda, M. Bielak-Lakomska, M. Brindell, K. Lewinski, P. Laidler, G. Stochel, Mechanistic studies of the hydrolysis of p-nitrophenyl sulfate catalyzed by arylsulfatase from Helix pomatia, J. Coord. Chem., 63 (2010) 2472-2487.

[63] K.E. Beatty, M. Williams, B.L. Carlson, B.M. Swarts, R.M. Warren, P.D. van Helden, C.R. Bertozzi, Sulfatase-activated fluorophores for rapid discrimination of mycobacterial species and strains, Proc. Natl. Acad. Sci. USA, 110 (2013) 12911-12916.

[64] Formation of isoindole derivatives from O-phthaldialdehyde has been

widely used for detection of primary amines including amino acids and an enzyme activities producing ammonium or amines; (a) C. Qin, S.Y. Lin, W.S. Lang, A. Goutopoulos, S. Pavlopoulos, F. Mauri, A. Makriyannis, Determination of anandamide amidase activity using ultraviolet-active amine derivatives and reverse-phase high-performance liquid chromatography, Anal. Biochem., 261 (1998) 8-15, (b) A. Banerjee, R. Sharma, U.C. Banerjee, A rapid and sensitive fluorometric assay method for the determination of nitrilase activity, Biotechnol. Appl. Biochem., 37 (2003) 289-293, (c) A. Garras, R. Djurhuus, B. Christensen, J.R. Lillehaug, P.M. Ueland, A Nonradioactive Assay for N5-Methyltetrahydrofolate-Homocysteine Methyltransferase (Methionine Synthase) Based on O-Phthaldialdehyde Derivatization of Methionine and Fluorescence Detection, Anal. Biochem., 199 (1991) 112-118.

[65] J.F. Stobaugh, A.J. Repta, L.A. Sternson, Autoxidation of 1-(Tert-Butylthio)-2-(N-Propyl)Isoindole, J. Org. Chem., 49 (1984) 4306-4309.

[66] M.C.G. Alvarezcoque, M.J.M. Hernandez, R.M.V. Camanas, C.M. Fernandez, Formation and Instability of Ortho-Phthalaldehyde Derivatives of Amino-Acids, Anal. Biochem., 178 (1989) 1-7.

[67] R. Bonnett, R.F. Brown, R.G. Smith, Isoindole, J. Chem. Soc. Perkin. Trans. 1, 13 (1973) 1432-1436.

[68] W. Rettig, J. Wirz, Electronic-Structure and Photophysical Properties of Isoindole and It Benzo[F]-Derivatives and Dibenzo[E,G]-Derivatives, Helv. Chim. Acta, 59 (1976) 1054-1074.

[69] M.H. Palmer, S.M.F. Kennedy, Electronic-Structure of Heteroaromatic Molecules - Abinito Calculations and Photoelectron-Spectra for Aza Derivatives of Benzo(C)Furan, Benzo[C]Thiophen, N-Methyl Isoindole and

Related Compounds, J. Mol. Struct., 43 (1978) 33-48.

[70] J.K. Kochi, Singleto.Ea, Autoxidation of N-Alkylisoindolines - Solvent Effects and Mechanisms, Tetrahedron, 24 (1968) 4649-&.

[71] P. Bojarova, E. Denehy, I. Walker, K. Loft, D.P. De Souza, L.W.L. Woo, B.V.L. Potter, M.J. McConville, S.J. Williams, Direct evidence for ArO-S bond cleavage upon inactivation of Pseudomonas aeruginosa arylsulfamates by aryl sulfatase, Chembiochem, 9 (2008) 613-623.

[72] C.H. Tai, C.P. Lu, S.H. Wu, L.C. Lo, Synthesis and evaluation of turn-on fluorescent probes for imaging steroid sulfatase activities in cells, Chem. Commun., 50 (2014) 6116-6119.

[73] A. Purohit, G.J. Williams, N.M. Howarth, B.V. Potter, M.J. Reed, Inactivation of steroid sulfatase by an active site-directed inhibitor, estrone-3-O-sulfamate, Biochemistry, 34 (1995) 11508-11514.

[74] N.M. Howarth, A. Purohit, M.J. Reed, B.V. Potter, Estrone sulfamates: potent inhibitors of estrone sulfatase with therapeutic potential, J. Med. Chem., 37 (1994) 219-221.

[75] H. Lee, J. Torres, L. Truong, R. Chaudhuri, A. Mittal, M.E. Johnson, Reducing agents affect inhibitory activities of compounds: results from multiple drug targets, Anal. Biochem., 423 (2012) 46-53.

[76] L.S. Simpson, T.S. Widlanski, A comprehensive approach to the synthesis of sulfate esters, J. Am. Chem. Soc., 128 (2006) 1605-1610.

[77] A. Warnecke, F. Kratz, 2,4-Bis(hydroxymethyl)aniline as a building block for oligomers with self-eliminating and multiple release properties, J. Org. Chem., 73 (2008) 1546-1552.

[78] M.A. Kertesz, Riding the sulfur cycle – metabolism of sulfonates and sulfate esters in Gram-negative bacteria, FEMS Microbiol. Rev., 24 (2000)

135-175.

[79] M.H. Stipanuk, Metabolism of Sulfur-Containing Amino-Acids, Annu. Rev. Nutr., 6 (1986) 179-209.

[80] T. Stressler, I. Seitl, A. Kuhn, L. Fischer, Detection, production, and application of microbial arylsulfatases, Appl. Microbiol. Biotechnol., 100 (2016) 9053-9067.

[81] J.H. Kim, D.S. Byun, J.S. Godber, J.S. Choi, W.C. Choi, H.R. Kim, Purification and characterization of arylsulfatase from Sphingomonas sp AS6330, Appl. Microbiol. Biotechnol., 63 (2004) 553-559.

[82] X.Y. Wang, D.L. Duan, J.C. Xu, X. Gao, X.T. Fu, Characterization of a novel alkaline arylsulfatase from Marinomonas sp FW-1 and its application in the desulfation of red seaweed agar, J Ind Microbiol Biot, 42 (2015) 1353-1362.

[83] J.M. Lim, Y.H. Jang, H.R. Kim, Y.T. Kim, T.J. Choi, J.K. Kim, S.W. Nam, Overexpression of arylsulfatase in E-coli and its application to desulfatation of agar, J. Microbiol. Biotechnol., 14 (2004) 777-782.

[84] S. Klose, J.M. Moore, M.A. Tabatabai, Arylsulfatase activity of microbial biomass in soils as affected by cropping systems, Biol Fert Soils, 29 (1999) 46-54.

[85] M. Garcia-Sanchez, M. Klouza, Z. Holeckova, P. Tlustos, J. Szakova, Organic and inorganic amendment application on mercury-polluted soils: effects on soil chemical and biochemical properties, Environ Sci Pollut R, 23 (2016) 14254-14268.

[86] C.P. Narkhede, A.R. Patil, S. Koli, R. Suryawanshi, N.D. Wagh, B.K. Salunke, S.V. Patil, Studies on endosulfan degradation by local isolate Pseudomonas aeruginosa, Biocatal Agric Biote, 4 (2015) 259-265.

[87] S.S. Kalyani, J. Sharma, S. Singh, D. Prem, Lata, Enrichment and isolation of endosulfan-degrading microorganism from tropical acid soil, J Environ Sci Heal B, 44 (2009) 663-672.

[88] C.A. Hickey, K.A. Kuhn, D.L. Donermeyer, N.T. Porter, C.S. Jin, E.A. Cameron, H. Jung, G.E. Kaiko, M. Wegorzewska, N.P. Malvin, R.W.P. Glowacki, G.C. Hansson, P.M. Allen, E.C. Martens, T.S. Stappenbeck, Colitogenic Bacteroides thetaiotaomicron Antigens Access Host Immune Cells in a Sulfatase-Dependent Manner via Outer Membrane Vesicles, Cell Host Microbe, 17 (2015) 672-680.

[89] V.L.N. Murty, J. Piotrowski, M. Morita, A. Slomiany, B.L. Slomiany, Inhibition of Helicobacter-Pylori Glycosulfatase Activity toward Gastric Sulfomucin by Nitecapone, Biochem Int, 26 (1992) 1091-1099.

[90] J.D. Mougous, R.E. Green, S.J. Williams, S.E. Brenner, C.R. Bertozzi, Sulfotransferases and sulfatases in mycobacteria, Chem Biol, 9 (2002) 767-776.

[91] A. Knaust, B. Schmidt, T. Dierks, R. von Bulow, K. von Figura, Residues critical for formylglycine formation and/or catalytic activity of arylsulfatase A, Biochemistry, 37 (1998) 13941-13946.

[92] T. Dierks, B. Schmidt, L.V. Borissenko, J.H. Peng, A. Preusser, M. Mariappan, K. von Figura, Multiple sulfatase deficiency is caused by mutations in the gene encoding the human C-alpha-formylglycine generating enzyme, Cell, 113 (2003) 435-444.

[93] T. Dierks, C. Miech, J. Hummerjohann, B. Schmidt, M.A. Kertesz, K. von Figura, Posttranslational formation of formylglycine in prokaryotic sulfatases by modification of either cysteine or serine, J. Biol. Chem., 273 (1998) 25560-25564.

[94] C. Miech, T. Dierks, T. Selmer, K. von Figura, B. Schmidt, Arylsulfatase from Klebsiella pneumoniae carries a formylglycine generated from a serine, J. Biol. Chem., 273 (1998) 4835-4837.

[95] C. Marquordt, Q.H. Fang, E. Will, J.H. Peng, K. von Figura, T. Dierks, Posttranslational modification of serine to formylglycine in bacterial sulfatases - Recognition of the modification motif by the iron-sulfur protein AtsB, J. Biol. Chem., 278 (2003) 2212-2218.

[96] C. Szameit, C. Miech, M. Balleininger, B. Schmidt, K. von Figura, T. Dierks, The iron sulfur protein AtsB is required for posttranslational formation of formylglycine in the Klebsiella sulfatase, J. Biol. Chem., 274 (1999) 15375-15381.

[97] Q.H. Fang, J.H. Peng, T. Dierks, Post-translational formylglycine modification of bacterial sulfatases by the radical S-adenosylmethionine protein AtsB, J. Biol. Chem., 279 (2004) 14570-14578.

[98] O. Berteau, A. Guillot, A. Benjdia, S. Rabot, A new type of bacterial sulfatase reveals a novel maturation pathway in prokaryotes, J. Biol. Chem., 281 (2006) 22464-22470.

[99] T.L. Grove, J.H. Ahlum, R.M. Qin, N.D. Lanz, M.I. Radle, C. Krebs, S.J. Booker, Further Characterization of Cys-Type and Ser-Type Anaerobic Sulfatase Maturating Enzymes Suggests a Commonality in the Mechanism of Catalysis, Biochemistry, 52 (2013) 2874-2887.

[100] B. Soufi, K. Krug, A. Harst, B. Macek, Characterization of the E-coli proteome and its modifications during growth and ethanol stress, Frontiers in Microbiology, 6 (2015).

[101] M.S. Weiss, I.V. Pavlidis, C. Vickers, M. Hohne, U.T. Bornscheuer, Glycine Oxidase Based High-Throughput Solid-Phase Assay for Substrate

Profiling and Directed Evolution of (R)- and (S)-Selective Amine Transaminases, Anal. Chem., 86 (2014) 11847-11853.

[102] A.P. Green, N.J. Turner, E. O'Reilly, Chiral Amine Synthesis Using omega-Transaminases: An Amine Donor that Displaces Equilibria and Enables High-Throughput Screening, Angew. Chem. Int. Ed., 53 (2014) 10714-10717.

[103] D. Baud, N. Ladkau, T.S. Moody, J.M. Ward, H.C. Hailes, A rapid, sensitive colorimetric assay for the high-throughput screening of transaminases in liquid or solid-phase, Chem. Commun., 51 (2015) 17225-17228.

[104] J.M. Bric, R.M. Bostock, S.E. Silverstone, Rapid Insitu Assay for Indoleacetic-Acid Production by Bacteria Immobilized on a Nitrocellulose Membrane, Appl Environ Microb, 57 (1991) 535-538.

[105] R.C. Kasana, R. Salwan, H. Dhar, S. Dutt, A. Gulati, A Rapid and Easy Method for the Detection of Microbial Cellulases on Agar Plates Using Gram's Iodine, Curr Microbiol, 57 (2008) 503-507.

[106] W.P. Heal, T.H.T. Dang, E.W. Tate, Activity-based probes: discovering new biology and new drug targets, Chem. Soc. Rev., 40 (2011) 246-257.

[107] H.Y. Yoon, J.I. Hong, Sulfatase activity assay using an activity-based probe by generation of N-methyl isoindole under reducing conditions, Anal. Biochem., 526 (2017) 33-38.

[108] M. Cregut, S. Piutti, S. Slezack-Deschaumes, E. Benizri, Compartmentalization and regulation of arylsulfatase activities in Streptomyces sp., Microbacterium sp. and Rhodococcus sp. soil isolates in response to inorganic sulfate limitation, Microbiol. Res., 168 (2013) 12-21.

[109] M. Sardiello, I. Annunziata, G. Roma, A. Ballabio, Sulfatases and

sulfatase modifying factors: an exclusive and promiscuous relationship, Hum Mol Genet, 14 (2005) 3203-3217.

[110] T. Adachi, H. Okamura, Y. Murooka, T. Harada, Catabolite Repression and Derepression of Arylsulfatase Synthesis in Klebsiella-Aerogenes, J. Bacteriol., 120 (1974) 880-885.

[111] T. Adachi, Y. Murooka, T. Harada, Regulation of Arylsulfatase Synthesis by Sulfur-Compounds in Klebsiella-Aerogenes, J. Bacteriol., 121 (1975) 29-35.

[112] S. Beil, H. Kehrli, P. James, W. Staudenmann, A.M. Cook, T. Leisinger, M.A. Kertesz, Purification and Characterization of the Arylsulfatase Synthesized by Pseudomonas-Aeruginosa Pao during Growth in Sulfate-Free Medium and Cloning of the Arylsulfatase Gene (Atsa), Eur. J. Biochem., 229 (1995) 385-394.

[113] T. Harada, Formation of Sulphatases by Pseudomonas Aeruginosa, Biochim. Biophys. Acta, 81 (1964) 193-&.

[114] H. Okamura, T. Yamada, Y. Murooka, T. Harada, Purification and Properties of Arylsulfatase of Klebsiella-Aerogenes Identity of Enzymes Formed by Non-Repressed and De-Repressed Synthesis, Agr. Biol. Chem. Tokyo, 40 (1976) 2071-2076.

[115] B.L. Wang, X.F. Zhang, C. Wang, L.C. Chen, Y. Xiao, Y. Pang, Bipolar and fixable probe targeting mitochondria to trace local depolarization via two-photon fluorescence lifetime imaging, Analyst, 140 (2015) 5488-5494.

[116] E.B. Veale, T. Gunnlaugsson, Bidirectional photoinduced electron-transfer quenching is observed in 4-amino-1,8-naphthalimide-based fluorescent anion sensors, J. Org. Chem., 73 (2008) 8073-8076.

[117] H.Y. Zhang, S.L. Zhang, L. Liu, G.S. Luo, W.H. Duan, W. Wang,

Synthesis of Chiral 3-Substituted Phthalides by a Sequential Organocatalytic Enantioselective Aldol-Lactonization Reaction. Three-Step Synthesis of (S)-(-)-3-Butylphthalide, J. Org. Chem., 75 (2010) 368-374.

[118] Y.W. He, C.Y. Cheng, B. Chen, K. Duan, Y. Zhuang, B. Yuan, M.S. Zhang, Y.G. Zhou, Z.H. Zhou, Y.J. Su, R.H. Cao, L.Q. Qiu, Highly Enantioselective Synthesis of 2,3-Dihydro-1H-imidazo[2,1-a]isoindol-5(9bH)-ones via Catalytic Asymmetric Intramolecular Cascade Imidization-Nucleophilic Addition-Lactamization, Org. Lett., 16 (2014) 6366-6369.

[119] H.Z. Huang, H. Tanaka, B.D. Hammock, C. Morisseau, Novel and highly sensitive fluorescent assay for leucine aminopeptidases, Anal. Biochem., 391 (2009) 11-16.

[120] M. Matsui, J.H. Fowler, L.L. Walling, Leucine aminopeptidases: diversity in structure and function, Biol. Chem., 387 (2006) 1535-1544.

[121] S. Mizutani, K. Shibata, F. Kikkawa, A. Hattori, M. Tsujimoto, M. Ishii, H. Kobayashi, Essential role of placental leucine aminopeptidase in gynecologic malignancy, Expert Opin Ther Tar, 11 (2007) 453-461.

[122] M. Tsujimoto, Y. Goto, M. Maruyama, A. Hattori, Biochemical and enzymatic properties of the M1 family of aminopeptidases involved in the regulation of blood pressure, Heart Fail Rev, 13 (2008) 285-291.

[123] L.W. Dong, M.T. Martin, Enzyme-triggered formation of electrochemiluminescent ruthenium complexes, Anal. Biochem., 236 (1996) 344-347.

[124] M. Roth, Une Ultramicro-Methode Fluorimetrique Pour Le Dosage De La Leucine-Aminopeptidase Dans Les Liquides Biologiques, Clin. Chim. Acta, 9 (1964) 448-&.

[125] K. Saifuku, T. Sekine, T. Namihisa, T. Takahashi, Y. Kanaoka, Novel

Fluorometric Ultramicro Determination of Serum Leucine Aminopeptidase Using a Coumarin Derivative, Clin. Chim. Acta, 84 (1978) 85-91.

[126] X. Xiong, A. Barathi, R.W. Beuerman, D.T.H. Tan, Assay of leucine aminopeptidase activity in vitro using large-pore reversed-phase chromatography with fluorescence detection, Journal of Chromatography B-Analytical Technologies in the Biomedical and Life Sciences, 796 (2003) 63-70.

[127] J. Grembecka, A. Mucha, T. Cierpicki, P. Kafarski, The most potent organophosphorus inhibitors of leucine aminopeptidase. Structure-based design, chemistry, and activity, J. Med. Chem., 46 (2003) 2641-2655.

[128] S.J. Lord, Z.K. Lu, H. Wang, K.A. Willetst, P.J. Schuck, H.L.D. Lee, S.Y. Nishimura, R.J. Twieg, W.E. Moerner, Photophysical properties of acene DCDHF fluorophores: Long-wavelength single-molecule emitters designed for cellular Imaging, J. Phys. Chem. A, 111 (2007) 8934-8941.

[129] J.S. Yount, L.K. Tsou, P.D. Dossa, A.L. Kullas, A.W.M. van der Velden, H.C. Hang, Visible Fluorescence Detection of Type III Protein Secretion from Bacterial Pathogens, J. Am. Chem. Soc., 132 (2010) 8244-+.

[130] L.K. Tsou, M.Z.M. Zhang, H.C. Hang, Clickable fluorescent dyes for multimodal bioorthogonal imaging, Org Biomol Chem, 7 (2009) 5055-5058.

[131] C.C. Stamper, D.L. Bienvenue, B. Bennett, D. Ringe, G.A. Petsko, R.C. Holz, Spectroscopic and X-ray crystallographic characterization of bestatin bound to the aminopeptidase from Aeromonas (Vibrio) proteolytica, Biochemistry, 43 (2004) 9620-9628.

[132] A. Stockel-Maschek, B. Stiebitz, R.K. Koelsch, K. Neubert, Novel 3-amino-2-hydroxy acids containing protease inhibitors. Part 1: Synthesis and kinetic characterization as aminopeptidase P inhibitors, Biorg. Med. Chem.,

13 (2005) 4806-4820.

[133] D.H. Rich, B.J. Moon, S. Harbeson, Inhibition of Aminopeptidases by Amastatin and Bestatin Derivatives - Effect of Inhibitor Structure on Slow-Binding Processes, J. Med. Chem., 27 (1984) 417-422.

[134] P. Gopalan, H.E. Katz, D.J. McGee, C. Erben, T. Zielinski, D. Bousquet, D. Muller, J. Grazul, Y. Olsson, Star-shaped azo-based dipolar chromophores: Design, synthesis, matrix compatibility, and electro-optic activity, J. Am. Chem. Soc., 126 (2004) 1741-1747.

[135] R. Hobkirk, Steroid Sulfation - Current Concepts, Trends Endocrin Met, 4 (1993) 69-74.

[136] C.R. Scriver, The metabolic and molecular bases of inherited disease, 8th ed., McGraw-Hill, Place Published, 2001.

[137] M. Morimoto-Tomita, K. Uchimura, Z. Werb, S. Hemmerich, S.D. Rosen, Cloning and characterization of two extracellular heparin-degrading endosulfatases in mice and humans, J. Biol. Chem., 277 (2002) 49175-49185.

[138] C.R. Scriver, The metabolic and molecular bases of inherited disease, 7. ed., McGraw-Hill, Place Published, 1995.

[139] M.J. Reed, A. Purohit, L.W.L. Woo, S.P. Newman, B.V.L. Potter, Steroid sulfatase: Molecular biology, regulation, and inhibition, Endocr Rev, 26 (2005) 171-202.

[140] L. Bernstein, R.K. Ross, Endogenous Hormones and Breast-Cancer Risk, Epidemiol Rev, 15 (1993) 48-65.

[141] A.B. Roy, Aryl Sulfatases - Colorimetric and Fluorometric Assays, Methods Enzymol., 143 (1987) 207-217.

[142] M. Ipuy, C. Billon, G. Micouin, J. Samarut, C. Andraud, Y. Bretonniere, Fluorescent push-pull pH-responsive probes for ratiometric detection of

intracellular pH, Org Biomol Chem, 12 (2014) 3641-3648.

[143] P. Nussbaumer, D. Geyl, A. Horvath, P. Lehr, B. Wolff, A. Billich, Nortropinyl-arylsulfonylureas as novel, reversible inhibitors of human steroid sulfatase, Bioorg. Med. Chem. Lett., 13 (2003) 3673-3677.

[144] N.M. Howarth, A. Purohit, M.J. Reed, B.V.L. Potter, Estrone Sulfamates - Potent Inhibitors of Estrone Sulfatase with Therapeutic Potential, J. Med. Chem., 37 (1994) 219-221.

국문 초록 **(Abstract in Korean)**

효소활성의 탐지는 생명시스템의 자연 성질과 생분자간의 관계를 이해하는데 많은 정보를 제공한다. 효소반응은 많은 생명 현상에 관여하는 기능을 조절하기 위하여 효소 기질의 화학적 변화를 유도한다. 효소 활성 측정을 위한 대부분의 접근 방법은 효소 기질의 화학적 변환을 이용하는 반응기반 전략이다. 지금까지 개발된 수많은 효소 활성 측정 탐침은 효소 반응을 바탕으로 다양한 신호 발생 방법을 도입하였다. 여기서는 두 가지 신호 발생 전략을 이용한 탐침을 제안한다.

첫번째는 효소 활성 반응을 통하여 일어나는 탐침의 화학적 변화가 분자내 고리화가 일어나 형광을 내는 N-methylisoindole을 생성하는 전략이다.

Sulfatase는 생체 분자의 sulfate를 가수분해하는 효소이다. Sulfatase에 의해 가수분해되면 N-methylisoindole을 생성하는 반응기반 탐침을 개발하였다. N-methylisoindole은 자체 산화가 쉽게 일어나기 때문에 glutathione (GSH)나 tri(2-carboxyethyl)phosphine (TCEP)와 같은 환원제를 이용하여 환원가능한 환경에서 sulfatase의 활성을 측정하였다. 이같은 환원 가능한 환경에서 probe 1은 일반적인 환경에서 일어나는 효소 반응과 비슷한 속도로 가수분해 되지만, 형광은 더욱 강하게 나타난다. 또한 probe 1dl sulfatase와 반응하여 생성하는 N-methyisoindole은 산성환경에서보다 중성환경에서 더욱 강한 형광을 나타내지만, 특별한 sulfatase에 대하여 선택성에 대해 한계가 있다. 그럼에도 불구하고, probe1 은 sulfatase와 반응하여

생성되는 N-methylisoindole의 형광증가는 고속대량스크리닝이 가능한 sulfatase의 활성 측정법을 새로이 제시할 수 있다.

Bacterial arylsulfatase는 aromatic sulfate ester를 분해해 황을 공급함으로써 많은 미생물 내의 생합성에 관여하고 있다. 또한 arylsulfatase는 감염성 질병의 발병에 관여할 뿐 아니라, 생촉매 생산같은 산업 분야에도 이용되고 있다. Probe 1dl sulfatasedp 의하여 가수분해되면 N-methylisoindole의 형광이 증가하고 N-methyisoindoledml 고분자화로 인하여 어두운 색의 침전물이 생성된다. 이는 액체상태 혹은 고체상태에서 bacterial colony 상태로 aylsulfatase의 활성을 볼 수 있을 뿐 아니라. 원형질막내의 sulfatase와 원형질막과 외막 사이에 존재하는 sulfatase를 구별할 수 있다.

생물 영상화를 하기에는 probe 1과 sulfatase의 활성에 의해 생성되는 N-methylisoindole의 형광 파장이 짧다. 이문제를 해결하기 위하여, fluorescence resonance energy transfer (FRET), aggregation-induced emission (AIE), 그리고 excimer형성을 이용한 전략을 도입하였다. FRET를 기반으로 하는 탐침은 N-methyisoindole을 에너지 주개로, naphthalimide를 에너지 받개로 이용하였으나, naphthalimide의 형광변화는 나타나지 않았다. 계산 결과에 의한 두 분자간의 거리가 6.6 Å으로 FRET가 일어난다고 알려져 있는 10~100 Å을 벗어나므로 FRET가 일어나지 않았다고 생각할 수 있다. AIE 기반 탐침은 sulfatase에 의하여 오히려 형광이 감소하고 색변화가 있었다. 이는 sulfatase의 활성에 의해 생성된 N-methylisoindole과 그 고분자화는 AIE 과정에 영향을 주지 않는다고 할 수 있다. Excimer 형성을 기반으로 한 탐침은 sulfatase 반응에 의하여 excimer의 형광은

감소하는 반면, monomer의 형광은 증가하였고, 침전물도 생성되었다. 이를 박테리아 실험에 응용하였으나, 형광 변화에는 경향성이 보이지 않았고, 침전물만 형성되었다. 그러므로 excimer기반 탐침은 원형질막과 외막 사이에 있는 sulfatase를 발현하는 박테리아를 염색하는데 이용할 수 있다.

효소 활성 탐침을 고안하기 위한 다음의 전략은 분자내 전하 이동(ICT)을 기반으로 하였다. 기본 구조 골격은 2-dicyanomethylene-3-cyano-2,5-dihydrofuran (DCDHF)를 전자받개부분으로 이용하고 이에 전자주개 부분을 다양하게 변화시켜 π-conjugation을 한 것이다.

Leucine aminopeptidase는 다양한 생물체에 분포하고 있으며, 세포 유지와 세포성장에 관여하기 때문에 LAP의 활성측정과 잠재적인 억제제의 screenning은 필요하다. 여기서 DCDHF에 leucine을 결합시켜 소분자 탐침을 개발하여 색과 형광 변화로 ㅣ메의 활성을 측정하였다.

Human steroid sulfatase (STS)는 estrogen receptor (ER)에 결합하는 steroiddml 활성을 조절하는데 중요한 역할을 한다. DCDHF에 phenyl sulfate ester를 도입한 탐침은 pH에 영향을 받아 발광하므로 중성 환경에서 활성을 보이는 STS를 선택적으로 검출할 수 있다. DCDHF에 phenyl sulfate ester를 자가희생 연결부로 도입하여 ratiometric 탐침을 개발하고 이를 이용하여 복잡한 환경에서도 sulfatase의 활성을 관찰할 수 있다.

주요어: 생물 영상화, 반응기반 탐침, 효소 활성 측정, 광학적 신호 변화